

High Temperature Corrosion – Shrier's  
Corrosion VOL 1: Types of High  
Temperature Corrosion: High  
Temperature Tribocorrosion

I.A. Inman, P.S. Datta, H.L. Du, C. Kübel and P.D. Wood



Published in 2010 by Elsevier

# Contents

<b>Abstract .....</b>	<b>iv</b>
<b>1.0 Introduction .....</b>	<b>1</b>
<b>2.0 Wear Theory.....</b>	<b>2</b>
2.1 Early Wear Theory .....	2
2.1.1 Archard and Hirst – Distinction between Mild and Severe Wear.....	2
2.1.2 Classification by Mechanism .....	4
2.2 ‘Two and Three Body’ Wear.....	5
2.2.1 Overview .....	5
2.2.2 Surface Films and Preoxidation – Third Body or Not? .....	9
2.2.3 Behaviour of Particles at the Interface.....	9
2.2.4 The Effect of Forces of Attraction between Third Bodies.....	12
2.3 Mild Wear and Mechanisms of Compact Oxide Formation .....	14
2.3.1 Introduction to Compacted Oxides or ‘Glazes’ .....	14
2.3.2 Quinn’s Oxidational Wear Model .....	16
2.3.3 Modification of Quinn’s Oxidational Wear Model for Discontinuous Contact.....	19
2.4 Effect of Load and Sliding Speed.....	20
2.4.1 Early Work .....	20
2.4.2 Wear of Cobalt-Based Alloys.....	23
2.4.3 The Effect of Load and Sliding Speed – Stellite 6 .....	25
2.4.3.1 The Presence of Carbides in Stellite 6 .....	28
2.5 Effect of a Second Phase on Wear .....	29
<b>3.0 High Temperature Wear Behaviour of Advanced Materials.....</b>	<b>31</b>
3.1 Oxide Dispersion Strengthened (ODS) Alloys.....	31
3.1.1 Introduction .....	31
3.1.2 Observations on High Temperature Wear Behaviour of Some ODS Alloys .....	32
3.1.2.1 Incoloy 800HT Counterface.....	32
3.1.2.2 Stellite 6 Counterface.....	33
3.1.3 Effects of Load .....	34
3.2 Intermetallics.....	34
3.2.1 Introduction .....	34

3.2.2	Wear of TiAl – Metallic Counterfaces.....	35
3.2.3	Wear of TiAl - Ceramic Counterfaces .....	36
<b>3.3</b>	<b>Nimonic Alloys .....</b>	<b>37</b>
3.3.1	Incoloy 800HT Counterface.....	37
3.3.1.1	Effects of Load .....	38
3.3.2	Stellite 6 Counterface.....	38
3.3.2.1	Effects of Load .....	40
3.3.3	Effect of Nimonic Material Processing Route on Wear .....	40
3.3.4	Nimonic 80A Sliding Wear – Comparisons between Various Wear Rig Configurations .....	40
3.3.5	Si <sub>3</sub> N <sub>4</sub> Counterface.....	41
<b>3.4</b>	<b>Effects of Environmental Variables .....</b>	<b>41</b>
3.4.1	Oxygen Levels and Partial Pressure .....	41
3.4.2	Effect of Water Vapour and Relative Humidity.....	42
3.4.3	Other Atmospheres .....	43
<b>3.5</b>	<b>Effects of Pre-treatment of Sliding Surfaces .....</b>	<b>44</b>
3.5.1	Pre-oxidation .....	44
3.5.2	Pre-sliding .....	45
3.5.3	Ion Implantation .....	45
<b>4.0</b>	<b>‘Glaze’ Formation – Micro-scale and Nano-Scale Investigations ...</b>	<b>46</b>
4.1	Introduction .....	46
4.2	Micro-scale Studies of ‘Glaze’ Formation.....	47
4.3	Third Body Interaction in Relation to Compact Oxide Formation .	49
4.4	Nano-scale Investigations of ‘Glaze’ Formation .....	52
4.4.1	Wear Data.....	53
4.4.2	Studies of Wear-affected Surfaces Produced during Sliding of Nimonic 80A against Stellite 6 at 20°C .....	53
4.4.2.1	Scanning Electron Microscopy (SEM).....	53
4.4.2.2	Transmission Electron Microscopy (TEM).....	54
4.4.3	Nano-scale Microscopy of ‘Glazed’ Layers Formed during High Temperature Sliding Wear at 750°C .....	58
4.4.4	Other Systems.....	59
<b>5.0</b>	<b>Wear Maps: A Useful Design Aid for Selecting Wear Resistant Materials and Surfaces .....</b>	<b>60</b>

5.1	Introduction .....	60
5.2	Work by Lim .....	60
5.3	Dissimilar Interfaces .....	61
5.3.1	Oxide Chemistry .....	63
<b>6.0</b>	<b>Summary .....</b>	<b>63</b>
	<b>Glossary .....</b>	<b>64</b>
	<b>List of Symbols Used .....</b>	<b>71</b>
	<b>References .....</b>	<b>73</b>
	Withdrawn References .....	80
	<b>Tables .....</b>	<b>81</b>
	<b>Figures .....</b>	<b>84</b>
	<b>APPENDIX 1: Withdrawn Data .....</b>	<b>134</b>
	A1.1 Second Phases in Some Key Alloys in This Study .....	134
	A1.2 Alternative Wear-resistant Alloys .....	135
	A1.3 Hall-Petch Effects .....	136
	<b>Withdrawn Tables .....</b>	<b>137</b>
	<b>Withdrawn Figures .....</b>	<b>138</b>

## **Abstract**

A review of High Temperature Tribocorrosion is presented focussing attention on those contributions that illustrate the general principles, modelling and scientific theories of the processes of high temperature wear. A significant aspect of this chapter is the inclusion of new information on glaze formation, generated at the sub-microscopic and nano-scale level.

# High Temperature Corrosion – VOL 1: Types of High Temperature Corrosion: High Temperature Tribocorrosion

I.A. Inman<sup>a\*</sup>, P.S. Datta<sup>a</sup>, H.L. Du<sup>a</sup>, C. Kübel<sup>b</sup> and P.D. Wood<sup>c</sup>

*a. Northumbria University, Newcastle upon Tyne, NE1 8ST, UK*

*b. Forschungszentrum Karlsruhe, Institute for Nanotechnology, Postfach 3640, 76021 Karlsruhe, Germany*

*c. Ricardo plc, Shoreham Technical Centre, Shoreham-by-Sea, West Sussex, BN43 5FG, UK*

---

## 1.0 Introduction

High temperature wear is a serious problem in many situations, examples including power generation, transport, materials processing and turbine engines [1-5]. Such wear is accentuated by faster surface oxidation kinetics, loss of mechanical hardness and strength of materials forming the contacting surfaces and changes in adhesion between these surfaces caused by the joint action of temperature and tribological parameters. Efforts to prevent wear have included the use of oxidation resistant and thermally stable materials, coatings and materials with pre-oxidised surfaces [1-8]. However, the choices of coatings and materials are severely restricted by high temperature environmental conditions [1-3].

An alternative method of generating wear resistant surfaces on coated and uncoated materials is to take advantage of certain events that accompany the high temperature wear process, such as oxidation, debris generation and elemental transfer between contacting surfaces [1-3, 9]. These events under certain conditions of temperature, pressure and speed can lead to ‘glaze’ formation on contacting surfaces, enhancing resistance to further wear [1-3, 9-29]. Although ‘glaze’ formation and the general issues relating to wear at elevated temperatures have been extensively studied [1-3, 9-29], it is still difficult to predict the precise conditions which promote ‘glazed’ surface formation. Many aspects of high temperature wear, including debris generation, debris oxidation, material transfer between surfaces and enhanced elemental diffusion, still need clarification. At present, there is incomplete understanding of the formation, nature, microstructure and defect structure of high temperature wear resistant surface ‘glaze’.

This chapter is not intended to catalogue all previous work. Instead, the objective is to concentrate on generic principles, modelling and scientific theories, which where possible will facilitate understanding of the high temperature wear process. There is

---

\*e-mail: beefnetuk@yahoo.co.uk

a heavy reliance on the information generated in the authors' own laboratory, where extensive use has been made of current microscopical techniques.

The chapter is structured as follows; section 2 deals with some general principles of wear, sections 3 and 4 consider published research while section 5 discusses some results of nano-scale investigations of 'glaze' formation; section 6 concludes with some final remarks.

## **2.0 Wear Theory**

### **2.1 Early Wear Theory**

#### ***2.1.1 Archard and Hirst – Distinction between Mild and Severe Wear***

In 1956, Archard and Hirst [30,31] categorised wear into two groups: mild wear and severe wear.

'Mild wear' occurs when the debris produced (generally oxide) prevents direct metal-to-metal contact. Although Quinn [32] does not specifically mention the oxidation reaction in his review of oxidational wear when discussing the definition of mild wear, the majority of studies into sliding wear have concentrated on the oxidation reaction. Debris produced is of very small size (less than 1  $\mu\text{m}$ ) and complete coverage is not necessarily achieved, with oxide in many cases only forming on load-bearing areas such as asperities. Electrical contact resistance is high, due to the presence of the oxide on the wear surfaces.

The absence of such oxides allows contact between the metallic interfaces, with adhesion, plastic deformation and, to varying degrees, material transfer between the surfaces. This is typical of the 'severe wear' situation, examples of which have already been observed in the lower temperature sliding wear of Incoloy MA956 against Incoloy 800HT in the work of Wood [1] and Rose [2] (these authors refer to these alloys as MA956 and Incoloy 800); the 270°C case shown in Fig. 1 is one such example. Debris particles tend to be large, flat and angular, up to 0.1 mm or greater. Contact resistance on surfaces that have undergone severe wear tends to be very low, due to the exposure of the metallic surface.

Temperature affects the nature of wear as it influences the kinetics of oxidation. Other factors such as relative humidity [33] and partial pressure of oxygen also affect the nature of wear as explained by Lancaster [25] and Stott *et al.* [12,34]. Fig. 2

shows a smaller range of severe wear in an oxygen atmosphere at 300°C, compared to that in air.

The model that Archard and Hirst [30] proposed assumes a true area of contact, occurring between a small number of asperities on the contacting surfaces. The true area of contact can be calculated by equation {2.1}:

$$A = P/H \quad \{2.1\}$$

where  $P$  is the applied load and  $H$  is the materials indentation hardness.

If  $W$  is the worn volume and  $L$  is the sliding distance producing the wear, then  $W/L$  is dependent on and is therefore proportional to the area of the friction junctions or true area of contact.

$$W/L \propto A \quad \text{or} \quad W/L = K_a A \quad \{2.2\}$$

This gives:

$$W/L = K_a P/H \quad \text{or} \quad W = K_a PL/H \quad \{2.3\}$$

the dimensionless parameter  $K_a$  being the constant of proportionality and also the probability of a wear particle being generated. It is also referred to as the “wear coefficient”. An alternative form ( $K_l = K_a/H$ ) is:

$$W = K_l PL \quad \{2.4\}$$

$K_l$  being referred to as the “ $K$  factor” [30]. Taking equation 2.1 and rearranging allows  $K_a$  to be expressed in terms of wear depth, sliding velocity and pressure. Dividing by the apparent area of contact gives:

$$d/L = p(K_d/H) \quad \{2.5\}$$

where  $d$  is the depth of wear (volume divided by area) and  $p$  is the mean pressure (load over area). If  $v$  is sliding speed and  $t$  is the time of sliding,  $L=vt$ , then



$$d/vt = p(K_a/H) \quad \text{or} \quad t = dH/K_a pv \quad \{2.6\}$$

$$K_a = dH/pvt \quad \{2.7\}$$

The above implies that the level of wear is proportional to the sliding distance and applied load; Archard and Hirst showed this to be true over a limited range [30] (Fig. 3).

The Archard model [30] is effective assuming that there are no changes in the wear surface as a result of the sliding process. However, changes do occur in many cases, leading to changes in wear rate resulting from little or no variation in experimental or operational parameters [26,27,35,36] and thus changes in  $K_a$  value may be observed. Previous experimental work [1-3] has demonstrated that such changes can occur, with changes in friction being coincident with a switch from early severe wear to mild oxidational wear, without any alteration of experimental parameters. This was usually denoted by decreases in the mean coefficient of friction and also in the variability of the coefficient of friction versus time trace. For example, during early severe wear at 750°C, mean values typically between 0.7 and 1 could be obtained for Nimonic 80A versus Incoloy 800HT. On reaching the mild wear stage, values of between 0.4 and 0.5 were typically obtained.

A direct link between hardness and wear rate is not always observed. Archard and Hirst proposed the theory of mild and severe wear discussed in this section, to resolve these difficulties [30].

### **2.1.2 Classification by Mechanism**

Many approaches to classifying wear have been attempted; Quinn's 1983 review [32] lists a number of these and tries to classify them under Archard and Hirst's mild and severe wear [30] headings (Table 1). For example, Burwell and Strang [37] propose seven different classifications of mild and severe wear, which Quinn argues are actually special cases of Archard and Hirst's mild and severe wear (with many of their classifications including elements of both) [30]. Ludema [38] talks in terms of "scuffing" ('roughening of surfaces by plastic flow, whether or not there is material loss or transfer') and "run-in", Quinn seeing "scuffing" as a form of adhesive wear and "run-in" as corrosive or mild wear (due to the generation of oxides on the wear surface). Finally, Tabor [39] does not distinguish between adhesive and corrosive

wear, preferring to classify both as adhesive wear, with Burwell and Strang's remaining mechanisms being referred to as "non-adhesive wear" (surface fatigue, abrasion and fretting) or a mixture of both (cavitation and erosion).

The classification of wear mechanisms clearly remains a matter of debate, although Quinn [32] proposes that each of the forms of wear described should be considered in terms of either mild or severe wear in any given situation. However, it is the view of the current authors that it is not possible to talk simply in terms of mild and severe wear. For example, when material is lost by abrasion, the loss of material by the ploughing action of asperities on a wear surface does not necessarily require adhesion or corrosion to remove material. Also, loss of material by delamination wear is a fatigue-related process, caused by repeated loading and unloading of surface layers as asperities of the opposite surface pass over it, assisting the propagation of sub-surface cracks, eventually leading to material loss. Although adhesion or reaction with a corrosive environment may accelerate the process, again neither is necessary for fatigue and crack propagation to occur.

The different behaviours of oxide debris are not accounted for either. Inman *et al.* [3,20-23] observed that during sliding wear, an oxide could either be protective or abrasive or even in limited quantities affect the severe wear process. It was thus suggested that mild and severe wear could be sub-categorised into '*standard severe wear*' (no oxide present, adhesion and delamination dominating), '*abrasion-assisted severe wear*' (oxide abrasively assists the adhesion / delamination dominated wear process), '*protective mild wear*' (oxide prevents metallic contact and forms a protective layer as loose debris or 'glaze') and '*abrasive mild wear*' (oxide debris prevents metallic contact, but remains loose and promotes wear by abrasion) [23].

Another suggested classification system is that of Rabinowicz [40], who, as well as adhesive and corrosive wear, identifies abrasive and fatigue wear as distinct categories of wear in their own right. Each of these four categories of wear is now discussed.

## **2.2 'Two and Three Body' Wear**

### **2.2.1 Overview**

Much of the discussion so far has been concerned with what happens when two surfaces move relative to one another, generating wear debris. The consideration of

wear without the interaction of debris is referred to as ‘two body’ wear. However, the generation of debris particles introduces a ‘third body’ into the sliding process, which can then go on to have a significant effect on the wear process.

This debris may be retained within the interface area, where it may become an ‘active’ participant [41] in the wear process or may be ejected immediately after its formation, in which case, it is referred to as ‘passive’ debris. Active debris tends to be fine and may be a mixture of metallic and oxide particles. On the other hand, ‘passive’ debris particles are in general much larger and, due to their immediate removal from the wear interface on formation, may retain much of their original form and structure. In metallic wear, ‘passive debris’ is more likely to be metallic.

The work of Rose [2] and Inman *et al.* [3, 20-22] clearly illustrates this difference. For sliding of Nimonic 80A and Incoloy MA956 versus Stellite 6, at lower temperatures (390°C and lower at 0.654 m.s<sup>-1</sup>, 270°C and lower at 0.905 m.s<sup>-1</sup>), debris particles tended to be of a fine nature; these were largely retained at the interface, commuted and converted to a layer of loose, discrete (usually) oxide particles. The retention of this debris as a ‘third body’ then acted to keep the interfaces separated and wear values low. This is an example of ‘active’ debris.

At intermediate temperatures up to 630°C for Nimonic 80A versus Stellite 6 and 510°C for Incoloy MA956 versus Stellite 6, debris was ejected as larger metallic particles that did not remain at the wear interface and thus did not separate the two wear surfaces. This is an example of ‘passive’ debris.

At higher temperatures, larger amounts of fine oxide debris were generated; in the case of Incoloy MA956 versus Stellite 6, this again separated the interfaces and also formed protective compacted oxide or ‘glaze’ layers. Nimonic 80A slid against Stellite 6 also formed protective layers at 0.314 m.s<sup>-1</sup>, however, at 0.654 and 0.905 m.s<sup>-1</sup>, wear levels increased due to oxide debris acting abrasively against the Nimonic 80A surface. These latter observations are once again examples of ‘active’ debris.

As well as promoting mild wear, the negative effect of abrasion has also been noted; as with hard and soft surfaces in the two body wear models already discussed, for a third body to have an abrasive effect at the wear interface possibly leading to

increased wear, it is normally expected that the hardness of the third body will be at least 1.3 times greater than that of either of the contacting materials [32].

Active participation of third bodies has been noted by other researchers, notably Iwabuchi *et al.* [42-44], who studied the effects of the introduction of iron oxide ( $\text{Fe}_2\text{O}_3$ ) particles to the wear interface, noting that, where the particles were supplied under fretting test conditions, the severe running-in wear volume for a standard carbon steel (S45C), was decreased ten-fold [44]. Increased surface roughness also proved to be a positive factor in that the particles were more effectively retained. Introduction of a large enough quantity of  $\text{Fe}_2\text{O}_3$  particles eliminated the severe wear running in stage.

Iwabuchi also studied the effects of particle size [42] and found that with a surface roughness of maximum asperity height  $20\mu\text{m}$ , a particle size of  $0.3\mu\text{m}$ , the smallest studied, was found to give the lowest wear rate during mild wear. However, particle sizes of  $1\mu\text{m}$  were observed to decrease the wear rate in the severe wear stage the most. Ideally, the same size particle would result in both; for practical use to be made of such observations, a compromise needs to be made. It is also to be noted that Iwabuchi expressed uncertainty as to whether the  $0.3\mu\text{m}$  particle size is the most effective only for the  $20\mu\text{m}$  maximum asperity height or for other asperity heights as well.

The current authors suggest that the optimum size will vary and also change as the wear test proceeds, for the simple reason that, as the larger asperities are removed, until such time as an oxide layer forms, the particle size that can be contained in the recesses will also decrease. Conversely, during severe wear, roughening of the wear surface may allow for a larger particle size to be retained. A limiting factor is that there will probably be an upper limit of particle size, partially due to comminution and ejection of larger debris and also a limit to the size of particle that can convert from metal to oxide.

Iwabuchi also points out that the tendency to form a protective compacted layer of oxide is affected by other parameters; varying test parameters such as load and sliding speed showed that, for certain conditions, the oxide particles acted as an abrasive and increased the wear rate. Fig. 4 is a wear map of load versus amplitude, where different combinations of load and amplitude produce different outcomes as regards

the influence of the introduced oxide particles [41]. For very low loads and amplitudes, the introduction of the oxide particles has a positive effect, lowering the level of wear. For medium loads and amplitudes, the oxides have a negative effect and wear levels are higher due to the abrasive action of the oxides. Moreover, increasing load for moderate amplitude or amplitude for moderately high load again results in a positive influence and wear levels are low.

Leheup and Pendlebury [45] took a different approach, by the use of an interfacial air flow in a like-on-like 'cup-on-flat surface' sliding test at various temperatures for Fe-18% Cr-9% Ni stainless steel. The effect of temperature was quite marked, with removal of the debris at room temperature leading to increased wear. At temperatures of 400°C and 500°C, formation of compacted oxide layers did still occur; this was considered to be due to the ready sintering and adherence of the loose oxide particles at these temperatures. The attractive effects of Van der Waals' forces (acting to retain smaller particles between the wear surfaces) were also considered, as detailed in Sections 2.2.3 and 2.2.4. Colombie *et al.* [46] obtained similar results with increased wear on blowing nitrogen through the wear interface at frequent intervals, the more frequent the intervals, the greater the observed wear. Magnetic fields can also have an effect with ferromagnetic materials; Hiratsukam *et al.* [47] showed that the field direction could influence whether debris was retained (thus decreasing wear) or ejected (thus increasing wear).

Rigney [48] also questioned the validity of the traditional models of wear if they do not take into account third bodies resulting from transfer and mixing; as well as separating or screening 'first bodies' (sample and counterface), third bodies can have other effects as they are able to flow and transmit load, accommodate velocity gradients and are also created, destroyed and regenerated during sliding. Resulting behaviour can depend on dimensions, compositions (may be the same as either of the 'first body' materials or a mixture of both), properties (the materials may undergo stresses close to their mechanical limits) and hardness. Chemical composition is a key to the observed properties of the third body.

Despite the evidence, it is still the case that many models of wear do not take into account the action of the third body, with debris assumed to be ejected on formation. Much work has been done using experimental rigs in which debris is retained at the wear interface, including fretting wear and much of the pin-on-disk work [4, 8, 12,

15-18, 32, 34, 42, 45, 49-71]. Even in situations where ejection is favoured, such as the block-on-cylinder approach [1,2], debris has remained at the interface and has played a significant part in the promotion of mild wear.

### ***2.2.2 Surface Films and Preoxidation – Third Body or Not?***

Also absent from the traditional models, is consideration of the effect of any surface films, adsorbed gases or other volatile species that may be present in most situations. Clearly, the wear process will be affected by the nature of the surfaces [72,73].

This is also true for pre-oxidised films [1,47,48,51], where early metal-to-metal contact has been decreased or eliminated to varying degrees, followed by earlier formation of compacted oxides in a number of cases. Although not a ‘third body’ in their own right (they are directly attached to one or both ‘first body’ surfaces at the beginning of sliding), the sliding action will create extra loose material from the surface oxide layer, which will proceed to act as a third body where retention is preferred over ejection.

### ***2.2.3 Behaviour of Particles at the Interface***

The behaviour of third body material at the wear interface goes beyond just acting as an agent for separation of the sliding surfaces or removing material from them. Rigney’s observations [48] on load transmission, velocity gradients and debris particle creation, destruction and regeneration are one example of this.

In addition, the particles may undergo varying degrees of motion at the interface due to the movement of the sliding surfaces. Halliday and Hirst [52] noted accumulation and ‘rolling’ of debris particles during fretting corrosion tests on mild steel specimens, which they commented as being responsible for the decrease in friction during testing. They also noted that some sliding debris must be present, as the observed coefficient of friction would have been in the region of 0.002 for rolling alone, rather than the values near or below 0.05 observed after the run-in phase was completed. Halliday and Hirst also established that the presence of the oxide particles prevented wear due to welding (adhesion) of the surfaces together.

Conversely, Suh and Sin [74] noted an increase in friction and wear by ploughing due to the presence of debris particles; this was confirmed by the removal of the debris, after which the coefficient of friction fell from a high ‘steady-state’ value and

gradually rose again as further debris was generated. It is to be commented here, that Suh and Sin used a unidirectional crossed rotating-cylinder-on-stationary-cylinder-configuration, whilst Halliday and Hirst conducted tests with an ‘oscillatory-cylinder-on-two-block-fretting-wear’ configuration. Thus, it would have been likely that debris retention in Halliday and Hirst’s work would have been much greater, allowing for the observed generation of Fe<sub>2</sub>O<sub>3</sub> oxide particles.

Also, Suh and Sin’s work [74] largely describes a metal-metal interaction, with most testing being carried out in a purified argon atmosphere. Even where an inert atmosphere is not used (as with AISI 1020 steel), there was nothing to suggest the generation of oxide debris and thus all interactions can be assumed to be metal-metal in their case. Hence, a direct comparison between their work and that of Halliday and Hirst may not be wholly appropriate. However, Rose [2] and Inman *et al.* [3,20,21,23] report high levels of wear for Nimonic 80A versus Stellite 6 at elevated temperature, where only oxide debris was generated during all but the earliest part of the sliding process. Here, it is the oxide debris that acts as a third body and aids material removal [3,20,21,23].

Rice *et al.* [75] showed that the effects of debris parameters on coefficient of friction are more important than asperity parameters. On modelling and comparing the influence of variations in density and size of particles at the interface with that of asperities on coefficient of friction, the sensitivity of coefficient of friction to changes in particle density and size was much the greater.

When particle parameters alone were considered, it was observed that increases in density lead to a much faster increase in coefficient of friction to a high steady state value. Increased particle sizes also lead to increases in coefficient of friction values, or conversely, smaller particle sizes are preferred for a lower friction regime. Of most interest in the work of Rice *et al.* [75], was the observation that, if particle density was increased whilst particle size was decreased (which could be regarded as analogous to particle break-down early in the wear process), then there was a sharp increase in friction, followed by a steady decrease with time.

It is to be noted that, as Suh and Sin [74], Rice *et al.* [75] did not consider the movement of debris, as the debris was ‘entrapped’. However, their approach [75]

does allow for estimation of friction where particle size means that movement is not a primary consideration; Hesmat [76] proposes a lower size limit of 20  $\mu\text{m}$  for debris to be a contributor to abrasive wear. At higher values, the results of Suh and Sin [74] and Rice *et al.* [75] are, therefore, more applicable.

Debris movement for smaller particles is clearly a key consideration, as the fall in friction due to, for instance, rolling, invalidates any models that fail to consider it. Jiang, Stott and Stack [18] proposed the following series of mechanisms for wear debris movement under sliding conditions, each mechanism accounting for a different mode of perceived particle movement (Fig. 5).

1. **Rotating:** a particle is entrapped in front of another fixed or immovable particle or object. It cannot move from its current position when impacted by an asperity from the opposite surface and is only able to rotate around its own centre.
2. **Relative skidding:** a fixed or locked grain in one half of the sliding pair slides or 'skids' against a fixed grain attached to the opposite surface.
3. **Rolling:** the particles are able to freely move or roll along with the opposite sliding surface (and are not entrapped by it as with the 'rotation' mechanism).
4. **Adhesion or sintering affected rolling mechanism:** adhesion developing between adjacent particles hinders rolling of particles, affecting (increasing) friction compared to the 'free' rolling mechanism.

The mechanisms of movement can change and any particle may be subject to a different mechanism at different times. It is also possible that a particle will become 'interlocked' or 'entrapped' [53] and be unable to move and thus be liable to fracture, due to a build-up of stress upon it. Further appraisal of these mechanisms [53] does not specifically mention the fourth mechanism, with adhesion and sintering general factors affecting the resulting particle layer as a whole.

It is also possible that for a given range of particle sizes, powder 'flow' may occur. Hesmat [76] observes that particles of an intermediate size, between 5  $\mu\text{m}$  and 20  $\mu\text{m}$ , may undergo '*quasi-hydrodynamic flow*' under sliding conditions. Larger particles will behave as in-situ elastic bodies and contribute to abrasive wear, whilst smaller particles will compact and behave as a nearly solid body, moving along with the 'first



body' interface and protecting it. At these smaller sizes, Van der Waals' forces and other attractive forces will become important factors and inhibit the flow process.

However, it is to be pointed out that the debris particles produced using the block-on-cylinder configuration [1,2], in the 5 µm to 20 µm size range specified by Hesmat for flow, were noted to be highly irregular in shape, being 'flat and angular' as the result of delamination wear. Also, they were metallic, meaning that adhesion between metallic surfaces would also be a major influence; Hesmat's work was with oxide particles. The combination of these influences would thus inhibit any flow process and eliminate the '*quasi-hydrodynamic flow*' region; high levels of metallic wear were observed [1,2] during the 'severe wear' stages, with associated high levels of adhesion due to transfer and back-transfer of material between metallic interfaces. Where oxidational wear did occur, particles were 5 µm in size or less, when, as Hesmat points out, Van der Waals' and other attractive forces and compaction come into play. This means that '*quasi-hydrodynamic flow*' cannot play a significant part in the sliding wear process, as observed between the selected test alloys in the current configuration, favouring ejection of material from the wear interface. Hesmat's lower limit of 20 µm for abrasive wear could, therefore, be revised downwards to the 5 µm upper limit for forces of attraction and compaction.

#### **2.2.4 The Effect of Forces of Attraction between Third Bodies**

As already noted [76], attractive forces such as Van der Waals' forces become a factor when considering very small particles (for oxides, 5 µm or less). Electrostatic forces between particles, and between particles and tribosurfaces, also exist, but these are only about 1% of Van der Waals' forces for non-conductive solids [77].

If ' $F$ ' is the force of attraction and assuming the particle is spherical, this can be directly related to particle size by:

$$F = \frac{AR}{6r^2} \quad \{2.8\}$$

where:

- $A$  - Hamaker constant;
- $R$  - radius of the particle or sphere;
- $r$  - equilibrium separation.

The Hamaker constant [49] is dependent on the surface energy of the sphere:

$$A = 9\pi r^2 \gamma \quad \{2.9\}$$

where:

- $r$  - distance affecting mutual action of Van der Waals' forces  
(which can be estimated at 0.3  $\mu\text{m}$  to 0.5  $\mu\text{m}$ );
- $\gamma$  - surface energy.

Van der Waals' forces are extremely short range in nature, produced by dipole induction between neighbouring bodies. This accounts for the attraction observed between the smaller wear particles (less than 5 $\mu\text{m}$  [76]) and the wear surfaces [78].

Surface energy is temperature-dependent, thus making the Hamaker 'constant' and the force of attachment  $F$  temperature-dependent. An Arrhenius relationship exists between surface energy and temperature:

$$\gamma = \gamma_o \cdot \exp\left(-\frac{E}{RT}\right) \quad \{2.10\}$$

where:

- $R$  - gas constant;
- $E$  - activation energy for 'bonding';
- $T$  - absolute temperature.

The amount of work done in relationship to wear is fairly minimal, compared to the formation of compacted oxides and 'glazes' as discussed in Section 2.3, with the work of Hesmat [76] being one of the more comprehensive studies of the potential behaviour of debris and particles at the wear interface in relation to their size. It is suggested, here, that the role of Van der Waals' forces in the accumulation and grouping together of particles is perhaps more important, especially at more elevated temperatures. For sintering and fusion of finer oxide particles to form glazes, an attractive force must be present to hold the particles in position long enough to allow significant sintering reactions to occur.

The importance of sintering in the formation of debris layers in itself cannot be ignored. Zhou *et al.* [79] showed that for iron, nickel and iron-25% nickel powders, significant sintering can occur on raising the temperature above room temperature (denoted by the significant shrinkage of specially prepared compacts), where the particle size is defined as ‘ultra-fine’, in this case, 30 to 40 nm. In comparison, more traditional fine particles of around 5  $\mu\text{m}$  did not show a significant response (in terms of shrinkage) until above 500°C. This doesn’t mean that sintering didn’t occur with the larger particles; it is more that a greater response was obtained for the smaller particles due to their greater relative surface area and, therefore, contact area. With particles of 300 to 400 nm, a ready sintering response may be detectable in a wear situation.

The effect of shrinkage of the compacts, as occurs in all powder compacts on sintering, is worth noting. As sintering and thus shrinkage undoubtedly occur in accumulations of wear debris at not necessarily greatly elevated temperatures, this will no doubt have an influence on the formation of compacted oxide layers during the wear process. To date, no attempt has been made to address this issue or its importance on the sliding wear process.

## **2.3 Mild Wear and Mechanisms of Compact Oxide Formation**

### ***2.3.1 Introduction to Compacted Oxides or ‘Glazes’***

As stated in Section 2.1, Archard and Hirst [30,31] defined mild wear as that occurring where the surface is extremely smooth and consisting partially or wholly of the product of reaction between the material under sliding and the surrounding atmosphere or fluid. An oxidation reaction is required for the creation of the corrosion product, although, as already stated, the corrosion product itself need not necessarily be an oxide.

The term ‘glaze’ is misleading, as it implies a glassy amorphous material, which was thought to be the case until Lin, Stott and Wood [4] proved it to be crystalline by means of electron diffraction; the term ‘compacted oxide layer’ is a more accurate description. ‘Glaze’ and ‘compacted oxide’ tend to be used fairly interchangeably throughout literature and despite the crystalline nature of these surfaces, the term ‘glaze’ has remained in common use. More recently Datta *et al.* [13,80] have demonstrated that the compacted oxide layers formed in some systems and under

certain conditions have a nano-crystalline structure and are highly disordered as discussed further in Section 4.3.

Compacted oxide layers tend to form under conditions of moderately high temperature, low loading and usually low sliding speed. For a compacted oxide layer to form and a resultant decrease in wear to occur, many researchers specify that a minimum temperature that is dependent on conditions and alloy composition, must be exceeded. With increasing temperature, the formation of these compacted oxides becomes more rapid, with a consequent decrease in the ‘severe wear’ running in period, the debris from which can be a major source of material needed for the formation of the compacted oxide layers. Compacted oxide formation is not restricted to low sliding speed, as the effect of frictional heating due to high sliding speed can raise the temperature above the critical temperature required for the formation of the compacted oxide layers.

Many researchers have extensively studied the decrease in wear by the formation of compacted oxides at high temperatures. As well as Archard and Hirst [30, 31], others such as Lancaster [25], Bhansali [81], Razavizadeh and Eyre [82], Stott *et al.* [4, 8, 12, 18, 15-17, 34, 49, 54-60], Quinn [32, 61-64] and Garcia [83], have contributed to the knowledge base on compacted oxide formation. Recent work [1-3,19-24] has additionally concentrated on the sliding of dissimilar interfaces and their effects on the mode of wear. The key issues on oxide formation are discussed below.

Wear that is dependent on the tendency to oxidation is highly dependent on temperature. The tendency to oxidation with respect to temperature can be described by the following Arrhenius type equation:

$$K_p = A_p e^{Q_p/RT_o} \quad \{2.11\}$$

where  $K_p$  is the oxidation rate,  $A_p$  is the Arrhenius constant,  $Q_p$  is the activation energy (for oxidation),  $R$  is the gas constant and  $T_o$  is the absolute temperature in Kelvin.

Stott in conjunction with Lin and Wood [4, 54-58], and later Glascott and Wood [8, 49, 53, 59, 60] proposed various modes and mechanisms of ‘glaze’ formation based

on the generation and behaviour of oxide debris at the sliding interface. Jiang *et al.* building on studies of third body interactions [18] (later revised by Stott [53]) and adhesive processes between particles [15], proposed a descriptive model for debris behaviour at the sliding interface [17], based on their generation, commutation, sintering to form 'glaze' layers (above a critical temperature), layer break-up and debris removal. These mechanisms and modes of formation are discussed in more detail in Section 4.

### 2.3.2 *Quinn's Oxidational Wear Model*

Quinn's model of wear [61] assumes a dependence upon the wear rate of oxide film formation on the wear interface. At a critical thickness  $\xi$  the oxide layers are no longer able to withstand the forces acting tangentially on them, and suffer failure and break away. Combining Quinn's and Archard's models [30] allows the critical thickness to be used to relate wear rate to material oxidation rate, showing an increase in wear rate with temperature.

From Archard's wear equation {2.3}, the wear volume  $W$  is related to the applied load  $P$  and the total sliding distance  $L$ , giving:

$$W = \frac{K_a PL}{H} \quad \text{or} \quad W = K_a AL \quad \left( A = \frac{P}{H} \right)$$

$K_a$  can be regarded as the probability of a wear particle being generated in any given encounter (assuming unit sliding distance in the following derivation, making  $W$  the wear rate). Thus,  $1/K_a$  is the number of encounters required to produce a wear particle.

In oxidational wear, a wear particle cannot be produced until the critical thickness for mechanical stability  $\xi$  is reached; thus  $1/K_a$  is the number of encounters required to generate an oxide layer of this thickness. If  $t$  is the time required to grow the layer and  $\tau$  is the length of time of each encounter, then:

$$t = \frac{\tau}{K_a} \quad \{2.12\}$$

If  $V$  is the sliding speed and  $d$  is the distance along which the sliding contact is maintained, then:

$$\tau = \frac{d}{V} \quad \{2.13\}$$

and equation {2.12} can be modified to:

$$t = \frac{d}{VK_a} \quad \{2.14\}$$

In a given time period  $t$ , the growth of oxide per unit area will be  $\Delta m$ . Assuming parabolic oxidation:

$$\Delta m^2 = K_p t \quad \{2.15\}$$

where  $K_p$  is the parabolic rate constant. If  $f$  is the mass fraction of oxide that is oxygen and  $\rho$  is the oxide average density, then:

$$\Delta m = f\xi\rho \quad \{2.16\}$$

and:

$$f^2 \xi^2 \rho^2 = K_p t \quad \{2.17\}$$

Substituting {2.17} into {2.14} gives:

$$K_a = \frac{dK_p}{Vf^2 \xi^2 \rho^2} \quad \{2.18\}$$

The rate constant can normally be calculated using an Arrhenius relationship, as described by equation {2.11}:

$$K_p = A_p e^{-Q_p/RT_o}$$

where  $A_p$  is the Arrhenius constant,  $Q_p$  is the activation energy (in this case for oxidation),  $R$  is the gas constant and  $T_o$  is the absolute temperature of reaction. Thus:

$$K_a = \frac{dA_p e^{-Q_p/RT_o}}{Vf^2 \xi^2 \rho^2} \quad \{2.19\}$$

Substituting into Archard's equation [30] gives a final expression for wear rate:

$$W = \frac{dAA_p e^{-Q_p/RT_o}}{Vf^2 \xi^2 \rho^2} \quad \{2.20\}$$

This expression relates directly to the oxidational properties of the materials, plus the critical environmental variables affecting the wear process, such as temperature at the interface at the time of contact and sliding speed relative to the opposing interface, as well as the critical thickness of the oxide. Knowing the critical thickness of the oxide [61] and the static oxidation properties of the wearing materials, wear rate prediction can be easily achieved.

However, there are many complications that can prevent accurate prediction of the wear rate:

- The difficulty in estimating the wear interface temperature, particularly in the presence of oxides;
- The slower heat flow from the wear interface and thus higher interface temperature, caused by lower thermal conductivity of the oxides;
- The presence of multi-layer scales (formed particularly at high temperature, for example, with iron), preventing the calculation of the temperature based on the oxide type generated [32];
- The expected presence of increased levels of surface defects at the contacting surfaces, increasing the oxidation rate constant;
- The continued removal of oxides leading to exposure of fresh surfaces and decrease in oxide thickness (hence diffusion distance), thereby enhancing the tribo-oxidation rate; and

- The presence of defects such as cracks and grain boundaries, allowing ingress of oxygen (in ion and molecular form) leading to an enhanced oxidation rate.

A schematic presentation of Quinn's models [84] is shown in Fig. 6.

### 2.3.3 *Modification of Quinn's Oxidational Wear Model for Discontinuous*

#### *Contact*

The validity of Quinn's model [63] is conditional upon the maintenance of contact between the two surfaces, which is clearly often not the case. Quinn's model was further modified by Garcia *et al.* [83] to take into account discontinuous contacts between the contacting surfaces.

For this modified model, it is assumed that  $1/K_a$  contact events are required for  $\xi$ , the critical oxide thickness, to be achieved; this is the same as for Quinn's model. However, in this case, the time required to reach this critical thickness depends on the contact frequency  $F$ , which is the inverse of the elapsed time between two contacts at a given point between the contacting surfaces; whilst this can clearly be related to sliding speed, the frequency of contact can also be changed by varying the length of the wear track without any need to vary sliding speed. It is clear that each asperity will not make contact each time the disk rotates; however, Garcia [83] comments that the probability of a contact (and hence a wear particle being generated) is included in the statistical meaning of the wear coefficient,  $K_a$ .

Therefore:

$$t = \frac{1/K_a}{F} = \frac{1}{FK_a} \quad \{2.21\}$$

The constant of proportionality  $K_a$  in Archard and Hirst's model [30] is thus defined by:

$$K_a = \frac{K_p}{Ff^2\xi^2\rho^2} \quad \{2.22\}$$

and substituting the rate constant, as defined by equation {2.9}, gives:



$$K_a = \frac{A_p e^{-Q_p/RT_o}}{Ff^2 \xi^2 \rho^2} \quad \{2.23\}$$

Substituting into Archard's equation {2.3}:

$$W = \frac{K_a PL}{H} \quad \text{or} \quad W = K_a AL \quad \left( A = \frac{P}{H} \right)$$

gives a final expression for wear rate (again as sliding distance  $L$  is assumed to be 1, the wear volume  $W$  can be taken to represent the wear rate), with the frequency of contact events being the determining parameter for the input of energy for oxide growth, rather than sliding speed:

$$W = \frac{AA_p e^{-Q_p/RT_o}}{Ff^2 \xi^2 \rho^2} \quad \{2.24\}$$

The validity of Garcia's model [83] is dependent upon a wear particle being generated on any given contact. For this to work, it is necessary for a wear particle to be generated each time a contact is made; this in itself is highly improbable. However, the lower level of data scatter achieved by Garcia's discontinuous contact model, indicates that this alternative frequency-based approach provides a good approximation in circumstances where Quinn's model is less effective in predicting wear rates (i.e. where contact is not maintained).

## 2.4 Effect of Load and Sliding Speed

### 2.4.1 Early Work

A significant contribution on the effects of load and sliding speed came from Welsh's work [26,27] on low carbon steels using a pin-on-rotating-ring (cylinder) configuration with applied loads of up to 2 kg.f and sliding speeds of up to 2.66 m.s<sup>-1</sup>. The wear process was characterised by two transitions; T<sub>1</sub> being mild-to-severe at low load and sliding speed and T<sub>2</sub> being severe-to-mild at high load and sliding speed. Increasing the sliding speed decreased the critical load at which these transitions occurred (Fig. 7), with the lower transition being eliminated in some cases, leaving only the severe wear to mild wear transition. In extreme cases, these transitions could be decreased enough to be eliminated from the experimental data – mild wear

could be observed over the whole range. The variation in the upper transition from the intermediate severe wear back to higher speed mild wear, was observed to be the more sensitive to sliding speed.

Low speed, low load mild wear was attributed to the presence of loose oxide debris at the sliding interface and intermediate severe wear to direct metal-to-metal wear. The mild wear encountered at high speed and high load was attributed to hardening, accompanied by the development of an adherent oxide film, as a result of frictional heating. The hardening came about as a result of the low carbon steels undergoing phase changes, due to high localised temperatures around points of contact being sufficient to produce a transformation to austenite, followed by rapid cooling by conduction of heat into the bulk metal producing a structure at the surface not too dissimilar to martensite.

A critical hardness had to be exceeded by these phase changes for mild wear to be re-established under high speed, high load conditions; the transition back from severe wear to mild wear is in fact a two part transition, with  $T_2$  referring to the point where sufficient phase hardening occurs to suppress severe wear without the intervention of an oxide film (the development of which further acts to protect the wear surface) and a  $T_3$  transition approximately matching the point where permanent phase change hardening occurs.

Subramanian [85] conducted a series of sliding tests of an Al-12.3 wt. % Si alloy in pin form against various rotating 'ring' counterfaces, including mild steel in the rolled condition, quenched and tempered die steel and copper with varying levels of aluminium, during which the sliding speed was increased at various times. The wear rate of the Al-12.3 wt. % Si alloy pin (Fig. 8) decreased with increased sliding speed up to a critical value of usually  $1 \text{ m}\cdot\text{s}^{-1}$ , regardless of counterface material or applied pressure used. Further increases in speed above this critical value led to progressive increases in wear.

Subramanian explains the decrease in wear with increasing sliding speed due to increasing strain rates and due to increased hardness and flow strength of the wear surface. The true area of contact is thus and with a lower level of contacts between the wearing surfaces, a lower wear rate results. In competition with this is the effect of increased temperature due to frictional heating (which was observed to occur),

softening the material at the wear interface. This results in an increase in the true area of contact and thus an increase in the wear rate. Subramanian does not go into detail with his reasoning, however, the softening of the material must allow for deformation and ‘spreading’ of asperities and also increased contact at other points.

Changes in wear mechanism were observed at Subramanian’s ‘1 m.s<sup>-1</sup>’ transition, with equiaxed particles produced below this critical or ‘transition’ speed, compaction of these particles and delamination of the compacted particles around the transition speed and delamination or plastically deformed material at higher speeds. It is not stated whether the particles produced at any particular speed are metallic or oxide.

The critical speed was observed to be dependent on counterface material and a higher transition was noted for harder, more thermally conductive alloys. Decreased mutual solubility also led to a higher transition speed.

Welsh [26,27] discusses the existence of lower limits of load and speed, marking the transition from mild to severe wear and also an upper limit, marking the transition back to mild wear. So [86] on the other hand only discusses a single limit or critical value for both load and speed for the transition from mild wear at low speeds and loads, to severe wear at high speeds and loads. Comparison with the work of Welsh would make So’s transition equivalent to the lower transition, with no mention of an upper transition despite the use of higher sliding speeds. So quotes values of 400°C and 5 MPa contact pressure as being limiting conditions for mild wear for many steels. In one test of note, a high carbon steel sample underwent a mild-to-severe wear transition at a contact pressure of 4.43 MPa, on raising the sliding speed from 3 to 4 m.s<sup>-1</sup>. A Stellite sample remained in the mild wear state at a contact pressure of 8.85 MPa (just under twice as much pressure) under similar conditions. As So used a pin-on-disk configuration, compared to the pin-on-rotating-cylinder configuration of Welsh, this may account for the differences in results; the pin-on-disk configuration may not have generated sufficiently severe conditions for the upper transition to occur.

Most load and sliding speed work done to date has concentrated on what happens at room temperature, with little work at elevated temperature. One example is the work of Rose [2], where a series of experiments was conducted at 750°C with loads between 7 and 25 N, during which an apparent transition from mild-to-severe wear

was noted at 15 N, when Nimonic 80A was worn against Incoloy 800HT. Also, when Incoloy MA956 was worn against Stellite 6 or Incoloy 800HT, at 25 N, the 'glaze' layer formed on the Incoloy MA956 was beginning to show signs of breaking away (as described later).

#### ***2.4.2 Wear of Cobalt-Based Alloys***

Valuable information can be gleaned from work on cobalt-based alloys. Amongst the most comprehensive work carried out on the sliding wear of cobalt was that by Buckley [87], who compared the sliding wear in vacuum of cobalt with that of copper. Lower friction and adhesion levels noted for cobalt were attributed to its hexagonal close-packed structure, compared to copper's face-centred cubic structure.

The observed increase in friction and cohesion for cobalt tested at temperatures greater than or equal to 300°C, with complete welding at 450°C, was considered to result from a phase change from hexagonal close-packed to face-centred cubic due to increased temperature (to above 417°C; the phase change temperature for cobalt) caused by frictional heating.

The differences between the sliding behaviour of metals in hexagonal close-packed phase and face-centred cubic phase are due to the greater number of active slip systems available in face-centred cubic structures. There are twelve primary slip systems within a typical face-centred cubic metal (4 slip planes each with three slip directions), which are all crystallographically similar, compared to only three primary slip systems in cobalt, these being based on the basal plane with the highest atomic density (i.e. 1 slip plane with 3 slip directions). Cross slip is also more difficult, as with hexagonal close-packed structures such as cobalt, screw dislocations are required to move out of the primary basal glide plane onto planes that unlike face-centred cubic structures, are crystallographically different. Hexagonal close-packed materials are thus less deformable.

The effect of these hexagonal close-packed structures on wear was further elaborated on by Persson [88,89] on studying the low friction tribological properties of Stellite 21 and Stellite 6. Persson comments that although a metastable face-centred cubic structure may be retained in both Stellite alloys down to room temperature, transformation to a hexagonal close-packed structure can be induced by application of

sufficiently high shear stresses (i.e. during sliding). A thin, easily sheared layer can develop at the sliding surface due to the shear-induced alignment of the hexagonal close-packed basal plane parallel to the direction of sliding [89]. This alignment significantly reduces friction and improves galling resistance, with shear and adhesive transfer restricted to this layer. This sliding regime persists even as this layer is removed, as it is easily regenerated. Also, the removal of material in such thin sections may at least in part explain the ready generation of fine Stellite 6-sourced Co-based oxide debris observed elsewhere [1-3, 19-24]. These sections may be more easily commutable to a small size and oxidised, providing a ready supply of material for 'glaze' formation.

The formation of compacted oxide layers during like-on-like fretting wear tests of cobalt-based Stellite 31 between room temperature and 800°C (293 K to 1,074 K) was observed by Stott, Stevenson and Wood [90]. The formation of these oxides was by a similar route to that observed for iron-based and nickel-based alloys, with alloying components present in the oxides to roughly the same proportions as the original alloy.

At temperatures between room temperature and 300°C, Stellite 31 undergoes a much lower level of wear than various nickel- and iron-based alloys, which Stott also attributes to the smaller number of slip planes in the hexagonal close-packed structure of cobalt. He specifies an initial period of low wear for up to an hour, followed by the production of a bright, rough metallic wear scars showing characteristics of abrasion and evidence of material transfer. This he attributes to a probable change in phase from hexagonal close-packed to face-centred cubic and thus a loss in wear resistance. Later, the bright worn surface is lost with increasing amounts of oxide being produced, although the load-bearing areas remain metallic.

Both the 'phase changes' and oxide production have been attributed to temperature increases at the wear interface. However, the phase transformation temperature for cobalt is 417°C; Stellite 31 contains 26% chromium, which has the effect of significantly raising the hexagonal close-packed to face-centred cubic transition temperature; 20% Cr is estimated to raise the transition temperature to 847°C (expressing uncertainty as to the effects of the other alloying components). This suggests a far greater influence due to frictional heating and localised flash temperatures due to asperity interactions; for a phase change to readily occur, the

temperature at the immediate interface would have to reach 500°C above ambient. In a fretting wear situation, it is difficult to see how this could occur.

However, the level of alteration of temperature for any phase transitions will also depend on the effects of other alloying components in cobalt-based alloys. As already stated, chromium will raise the transition temperature quite dramatically. Other references [68, 87-89] suggest that tungsten and molybdenum also raise this transition, whilst nickel and iron (also, magnesium and carbon [88,89]) have the effect of stabilising the higher temperature face-centred cubic structure (due to increases in stacking fault energy [88,89]) and suppressing this transition. It is possible that the presence of nickel to 10.5% and iron to 2% may be sufficient to retard the effect of the chromium and 7.5% tungsten to a much lower level. Thus a much smaller increment in temperature due to frictional heating and flash temperatures may be needed to effect any phase transition, confirming the conclusion that the damage observed can be attributed to phase changes and hence a decrease in resistance to deformation.

At elevated temperatures, Stott *et al.* [90] observed that compacted oxide formation was not accompanied by any decreases in friction observed during similar experimentation with nickel-based alloys. With friction levels already low due to the hexagonal close-packed structure, it is possible that no significant difference between the friction levels before and after elimination of metallic contact by higher temperature ‘glaze’ formation may be discerned.

The face-centred cubic to hexagonal close-packed transformation observed in Co-based alloys is considered a martensitic transformation [91]. Attempts to utilise Co-free hard wearing alternatives making similar use of the austenite-martensite transition in Fe-based alloys, have been limited by typical upper useful temperatures of ~180°C [88,89] (not discussed in the current work).

#### **2.4.3 The Effect of Load and Sliding Speed – Stellite 6**

Following on from previously discussed work (Section 2.4.1) with a Stellite material [86], So *et al.* went on to test Stellite 6 clad mild steel against AISI 4140 and 4340 steels in the martensitic phase, first as the pin material (4.75 mm in diameter) then the disk material [29]. Measured hardness values were 580 VHN (Vickers Hardness Number) for the Stellite 6 layer and 750 VHN for the steels, increasing to 970 VHN

after an unspecified heat treatment followed by water quenching, with test loads of up to 156.8 N and sliding speeds of up to 4 m.s<sup>-1</sup> used. After sliding for up to 10,000 m, the Stellite 6 layer was observed to be mostly covered by an oxide layer reported to consist of W<sub>3</sub>O, CrO and Co<sub>2</sub>O<sub>3</sub>. Where this oxide layer spalled, a new oxide film was observed to replace it readily. This applied for all combinations of loads (19.6, 39.2, 78.4 and 156.8 N) and sliding speeds (1, 2, 3 and 4 m.s<sup>-1</sup>), with the exception of the most severe tested combination, 156.8 N and 4 m.s<sup>-1</sup>, when severe wear was observed for the Stellite 6 as the pin material. The experimental data obtained from these tests are presented in Fig. 9.

The steels underwent increased wear compared to the Stellite 6, despite being of much greater hardness and So *et al.* concluded that the oxide layer formed on the Stellite 6 must be tougher than that formed on the steels. When used as a disk material, only a thin layer of oxide material was formed on the AISI 4340, compared to the thicker layer formed on the Stellite 6; the wear rate of the steel was seven times that of the Stellite 6 laser-clad pin. As the pin material, severe wear was observed for the AISI 4140 steel, the rate of wear being 10 times higher than that of the Stellite 6 laser-clad disk. For all but the highest load, the wear rate of the Stellite 6 pin actually decreased when the sliding speed was increased from 1 to 2 m.s<sup>-1</sup>, with only a slight increase at intermediate loads on raising the sliding speed to 4 m.s<sup>-1</sup> (Fig. 9). At the lowest load used, the decrease in wear continued up to 4 m.s<sup>-1</sup>.

The increasing wear rate for specimens under a load of 156.8 N was ascribed to softening of material due to the higher flash temperatures encountered, especially at higher sliding speed. The higher flash temperatures also led to changes in the oxide phases that were reported to form on the respective wear surfaces. A shift was noted from Fe<sub>2</sub>O<sub>3</sub> to FeO on the steels and from W<sub>3</sub>O, through Co<sub>2</sub>O<sub>3</sub>, CrO, Cr<sub>2</sub>O<sub>3</sub> to Cr<sub>5</sub>O<sub>12</sub> on the laser-clad Stellite 6 layer with increasing temperature; this was accompanied by a decrease in friction. So does not offer an explanation for the change in oxide with temperature, though as for the oxidation of iron, it appears that this can be attributed to changes in oxidation state of the chromium in Stellite 6, with preferential oxidation of tungsten and cobalt respectively at lower temperatures. It is curious to note here that, in the work of Wood [1] and Rose [2], no such shift was observed for Stellite 6, with Cr<sub>2</sub>O<sub>3</sub>, Co<sub>3</sub>O<sub>4</sub> or a combined oxide of the two being consistently observed from XRD results. No evidence of tungsten phases was found, although

this could be attributed to the sensitivity of the measurement and characterisation equipment.

Also of note was the fact that the oxide layers formed in So's work were more reminiscent of those created at higher ambient temperature in the work of Wood and Rose (510°C plus), indicating extremely high temperatures at the points of contact. So's measurements indicate a rapid rise in temperature with increasing load and speed (speed having less of an effect than load). So comments that, under the most severe conditions (156.8 N and 4 m.s<sup>-1</sup>), the mean surface temperature at the point of contact reaches over 700°C and, because of this, wear becomes severe due to softening. This may be more to do with the load and speed conditions than to temperature (even accounting for phase transitions), as Wood and Rose tested Incoloy MA956 and Nimonic 80A against Stellite 6 at an ambient temperature of 750°C, with oxide layers being obtained in both cases on the Stellite 6 counterface.

This implies that So has underestimated the temperature at the sliding interface in this case. The softening may again be attributable to phase changes from hexagonal close-packed to face-centred cubic. In the case of Stellite 6, there are far fewer alloying additions to offset the effects of chromium (present at 27%) and tungsten (5%) on this transition. The transition between the two phases for 27% chromium is approximately 880°C to 900°C [3,92], almost 200°C higher than So's 700°C estimate.

Crook and Li [69] carried out a comparative 'like-on-like' sliding study of Stellite 6 and a number of other hard-facing alloys of various cobalt contents, including Stellite 1 (with higher levels of carbon, chromium and tungsten than Stellite 6), Stellite 2006 (a 33% cobalt-iron-chromium alloy), Haynes No. 716 (a nickel-iron-chromium alloy with 11% cobalt) and Haynes No. 6 (a nickel-chromium alloy with no cobalt). They observed that in general the higher the cobalt content, the better was the resistance to metal-metal wear at temperatures up to 750°C. Where no cobalt was present within the alloy, wear rates were observed to be highest. Above this temperature (at 1,000°C), all alloys exhibited low wear with a protective oxide layer forming across the wear surface. Increases in wear were observed for all combinations with increased contact pressure, though at high load, increases became less severe for cobalt-chromium and cobalt-iron-chromium alloys. Of particular note is the response to increasing the sliding speed by an order of ten from the 7.06 x 10<sup>-4</sup> m.s<sup>-1</sup> used for all their other tests, to 7.88 x 10<sup>-3</sup> m.s<sup>-1</sup>, carried out at 500°C



and 20.69 MPa. For the high cobalt-chromium alloys including Stellite 1 and Stellite 6, there was a slight decrease in the observed wear rate. Where cobalt levels were low or non-existent, the converse was true and increases in wear were observed.

Crook and Li [69] attributed the superior wear resistance of the cobalt-chromium alloys, firstly to the superior galling resistance and secondly to the tendency of alloys when in the face-centred cubic form to undergo phase changes and become hexagonal close-packed, which as discussed earlier is less prone to deformation, due to a smaller number of available slip planes. Conversely, they point out that high nickel alloys have a poor galling resistance, yet specifically quote the work of Stott *et al.* [54,55,57] as examples of nickel-chromium alloys in particular exhibiting low levels of wear and developing 'glaze' during the wear process at high temperature.

In both experimental programmes, a low amplitude 'button-on-disk' system suitable for fretting wear studies was used. However, Stott *et al.* concentrated solely on one material (Nimonic 80A), whereas Crook and Li's comparative work on a range of alloys showed that, although wear was still low for nickel-chromium alloys, the wear resistances were inferior to those of cobalt-containing alloys. In both cases, it is not possible to say that in an extreme high wear environment (e.g. high speed, high load) similar observations of low wear would be made. In the case of Stellite 6, So's work [29] does indicate continued low wear rates during moderately high speed, high load uni-directional sliding wear (up to 156.8 N and 4 m.s<sup>-1</sup>, with frictional temperatures of up to 700°C being generated); however, if the works of Wood [1] and Rose [2] are considered, high rates of wear are observed with Nimonic 80A at elevated temperature (750°C, 0.654 m.s<sup>-1</sup>, 7N, 9,418 m sliding distance) when undergoing uni-directional wear against a Stellite 6 counterface. Even in a like-on-like situation, wear properties of Nimonic 80A are inferior to those of Stellite 6 [2,93].

#### ***2.4.3.1 The Presence of Carbides in Stellite 6***

In both the work of Stott [90] and So [86], no mention was made of the effect of carbides that would have formed with both Stellite 31 and especially Stellite 6, carbon being present to 0.5% and 1.1% respectively. In the cast form, carbon combines with chromium to form a chromium carbide phase at the grain boundaries; in Stellite alloys, these are of the form M<sub>7</sub>C<sub>3</sub> and M<sub>23</sub>C<sub>6</sub> [29]. In the wrought and hot isostatically pressed forms, these carbides instead form discrete particles dispersed

evenly in the microstructure (the effect of Stellite processing or carbide position on sliding wear has not, to the knowledge of the authors, been investigated).

The presence of these hard, difficult-to-deform carbides may have had a number of effects on both sets of experimental work. Firstly, they may have further inhibited deformation of the mainly cobalt matrix during sliding wear, over and above the effect expected from the hexagonal close-packed structure, blocking the operation of the fewer slip planes present. Secondly, the removal of material from the Stellite alloys may have released some of these carbides into the sliding interface, increasing the levels of wear observed due to increased abrasion effects. The enhanced wear of the AISI 4140 and 4340 steels, when worn against Stellite 6 clad mild steel in So's work [29] may have in addition been partially attributable to this.

There is also the possibility that the carbides (up to 30 $\mu$ m in size) within the Stellite 6 may affect the formation of 'glaze' (only a few  $\mu$ m thick) on opposing wear surfaces [2] as the Stellite 6 is worn down and the carbides are exposed; Inman [3], however, suggested that the exposed carbides are not hard enough to do this. The possible effects of carbides are discussed in more detail in Sections 2.5 and 3.3.2.

## **2.5 Effect of a Second Phase on Wear**

The role of second phases in the wear process is often neglected in wear studies. In many, experimentation has concentrated only on single-phase alloys. However, second phases are used in many alloys for various reasons, including enhancement of strength and creep resistance, especially in high temperature systems where the properties of the metallic matrix can become less robust.

During the wear process, where second phases are harder than the matrix material, it is not sufficient to assume that their presence will have no effect on the wear process and that they will simply be 'worn away' with the matrix as sliding proceeds; this only occurs if the second phase is of similar or lesser hardness. Vardavoulias [94] studied a number of steels into which hard ceramic phases of various sizes were introduced; these included titanium carbide (modified to a much finer carbon nitride phase by nitrogen annealing), copper phosphide and alumina. It is assumed following that the substrate metal is oxidised and is the main source of compacted oxide or oxide debris and, thus, the oxide / metal interface is effectively moving into the metal.

If the sizes of the second phase particles are less than the critical oxide thickness ( $\xi$  from Quinn's oxidational wear theory [61]), then these particles pass into the oxide layer as the metal is oxidised. They may not protrude above the surface of the oxide layer and thus cannot directly protect the matrix or impinge on the counterface material. The particles are lost as the oxide layer breaks up at the critical thickness to form debris. The only contribution may be to enhance the load-carrying capacity of the metallic matrix in supporting the oxide film.

Where the second phase particle size is only slightly greater than the critical oxide thickness (between  $\xi$  and  $3\xi$ ), there is a transition in the wear mechanism; this is referred to as the 'first stage'. Whilst a small quantity of the second phase may be removed with the oxide, as it breaks up, most will remain embedded in the substrate or matrix. These particles protrude above the nominal surface of the interface and the counterface slides over them. This continues until the oxide layer can reform and during this stage of wear, the matrix cannot influence the wear process; this is the 'second stage'.

The mechanical properties of the second phase particles influence what happens next during the 'second stage'. If the particles are able to resist the sliding action, then the matrix will be protected for a prolonged period and the 'second stage' is extended. Enhanced wear of the counterface material by abrasion may occur in this stage. If they are unable to resist the sliding process and fail under the load from the counterface, then contact between matrix and counterface is quickly restored and the 'first stage' of wear will be repeated. A further possibility is detachment of second phase particles as the oxide breaks up, with these particles acting as third body abrasives; this occurs where cohesion between matrix and second phase is poor.

If the mean particle size is much greater than the critical oxide thickness, the particles show increased efficiency in providing oxidational wear protection to the material subject to wear. After break up of the oxide layer (end of the 'first stage'), the harder second phase particles remain embedded in the matrix. Again, the main interaction is between the particles and the counterface and this process controls the wear mechanism; the matrix plays no direct part. The majority of the particles are surrounded by the matrix, thus break up is more difficult and detachment is almost impossible. Whilst this means that the matrix is well protected against wear, the counterface may undergo high rates of wear and thus become the main source of

debris. The inference here is that the first stage cannot resume until these larger particles wear to near to the level of the rest of the sample surface; as other particles will continue to be exposed elsewhere on the surface, first stage wear with protective oxide layer formation cannot readily happen and severe wear will continue.

Based on the apparent failure of carbides in Stellite 6 to disrupt 'glaze' formation for certain wear combinations, Inman [3] suggested that the second phase particles must also be harder than the generated 'glaze' on the opposing sliding surface (Section 3.3.2). If this is not so, the second phase particles may wear in preference to the 'glaze' layer and not promote its break-up. This may prove beneficial, with a harder second phase conferring wear resistance but allowing protective 'glazes' to form. Tribaloy alloys, consisting of a hard Laves intermetallic second phase in a Ni-based or more notably a Co-based matrix [95] are possible examples (not discussed in the current work).

## **3.0 High Temperature Wear Behaviour of Advanced Materials**

### **3.1 Oxide Dispersion Strengthened (ODS) Alloys**

#### **3.1.1 Introduction**

This section discusses the HT wear behaviour of ferritic ODS alloys, Incoloy MA956 and its variants. The section starts with a brief introduction to ODS alloys to provide a context and facilitate interpretation of the experimental observations on their HT wear characteristics.

Ni-base-Inconel alloys MA 6000, MA754, MA758 and MA760, and Fe-base Incoloy MA956, PM2000 and PM2000SD are well known examples of ODS Superalloys. Such ODS alloys possess good high temperature strength and resistance to HT corrosion and oxidation. They derive their strength from the insoluble, deformation resistant and thermally stable dispersoids such as  $Y_2O_3$  (as used in Incoloy MA956 [96]) introduced during fabrication by mechanical alloying. This process offers great opportunities in the selection of dispersoids-matrix combination. Strengthening by insoluble, deformation resistant and inert dispersoids is far more effective than other methods such as solid solution and precipitation hardening as thermodynamics imposes limitation on their continued effectiveness. At certain critical temperatures,

solubility limits may be exceeded, leading to the onset of precipitation and eventually Oswald ripening of the precipitates.

During high temperature deformation, most ODS alloys exhibit a threshold stress  $\sigma_0$  below which creep becomes negligible; the threshold stress  $\sigma_0$  is less than Orowan stress  $\sigma_{or}$ . Several models such as dislocation climb, dislocation detachment (local climb) have been advanced to explain the existence of the threshold stress. None of these models have been universally accepted.

To increase the temperature capability of ODS alloys, the powder produced by mechanical alloying is subjected to hot extrusion and the fine grained extruded structure is then subjected to a high temperature secondary recrystallisation anneal.

The overall enhancement of HT capability may be associated with:

- Large grain size produced by secondary recrystallisation;
- High GAR (Grain Aspect Ratio) produced by recrystallisation under a high temperature gradient and minimising the detrimental effect of transverse grain boundary effect;
- Formation of serrated grain boundaries allowing grain inter-locking; and
- Minimum grain boundary hardening.

### ***3.1.2 Observations on High Temperature Wear Behaviour of Some ODS Alloys***

There is no evidence to suggest any improved wear resistance conferred by alloy pre-treatment for the three near identical ODS alloys, Incoloy MA956, PM2000 and PM2000SD [1] (Fig. 10). Testing against various counterfaces (Stellite 6 and  $\text{Si}_3\text{N}_4$ ) and at various temperatures (room temperature to 750°C) does not indicate a definitive trend in relation to grain size and hardness.

#### ***3.1.2.1 Incoloy 800HT Counterface***

Only on sliding against Incoloy 800HT is there an apparently strong preference towards lower grain size and increased hardness (Table 2) favouring higher wear [1]. The severity of wear was of the order 'PM2000SD', 'PM2000' and 'Incoloy MA956'.

Poor wear resistance and high friction coefficient characterise the wear behaviour of the ODS alloys worn against Incoloy 800HT at 750°C (reciprocating rig, 0.314, 0.654

and 0.905 m.s<sup>-1</sup> sliding speed, 7N load) as indicated by higher weight losses compared to that at room temperature (Fig. 10 – 0.654 m.s<sup>-1</sup> [1]). The apparent improved wear resistance observed at room temperature is attributable to transfer [1-3] and work hardening of a layer of Incoloy 800HT or back-transferred Incoloy MA956 [3], protecting the ODS alloy surface from sustained wear (Fig. 11a – 0.654 m.s<sup>-1</sup>).

The loss of strength and hardness suffered by the ODS alloys at higher temperatures [8-10] (Fig. 12) probably undermines the ability of the alloy to support the process of ‘glaze’ development. Severe wear continues (Fig. 11b – 0.654 m.s<sup>-1</sup>) and the low levels of oxide produced act only to inhibit metallic adhesion, preventing the formation of the protective metallic transfer layer seen at room temperature [3] and wear thus increases with temperature. Some transfer of Incoloy 800HT material still occurs at high temperature; however, continued sliding removes this layer [1,3]. Such transfer tends to be greater at higher sliding speeds and, hence, the weight loss is lower at 0.905 m.s<sup>-1</sup> than at 0.314 m.s<sup>-1</sup> [3]. Only at 690°C and 750°C (Fig. 11c – 0.654 m.s<sup>-1</sup> example shown) is an oxide [1] or ‘glaze’ [2,3] layer able to develop on the Incoloy MA956 surface (sourced from the Incoloy MA956) after an initial period of severe wear [3].

### ***3.1.2.2 Stellite 6 Counterface***

The improved wear resistance of ODS alloys when worn against Stellite 6 coincides with rapid oxide development; such oxide is sourced from both sample and counterface. At low temperature, this debris remains loose and does not readily form ‘glaze’ (Figs. 13a and 14a). At high temperature, it sinters rapidly to form more extensive ‘glaze’ layers (Figs. 13c and 14c) [1-3]. The relative contributions of sample- and counterface-sourced debris (at least for Incoloy MA956 versus Stellite 6) have been observed to depend on sliding speed [3,22]. A slow sliding speed (0.314 m.s<sup>-1</sup> [3]) favours greater Stellite 6 wear and thus higher levels of Co-based oxide debris. Faster sliding speeds (0.654 m.s<sup>-1</sup> [2] and especially 0.905 m.s<sup>-1</sup> [3]) encourage greater Incoloy MA956 wear and thus higher levels of Fe and Cr oxide contribution. At 750°C, the presence of Co in the debris promotes more rapid ‘glaze’ formation [22] and prevents continued early wear.

Only at intermediate temperatures (390°C and 450°C) [2,3] and at 0.654 and 0.905 m.s<sup>-1</sup>, does the oxide fail to separate wear surfaces and allow severe wear to

occur (Fig. 14b). Below these temperatures, the oxide separates the surfaces even in the form of the aforementioned loose debris. At progressively higher temperatures, severe wear is increasingly restricted to only the initial sliding period as continued sliding promotes debris sintering and ‘glaze’ formation. Above 630°C, ‘glaze’ development is so rapid that severe wear is all but eliminated. No severe wear is observed at 0.314 m.s<sup>-1</sup>, with the loose debris progressively developing into ‘glaze’ as sliding temperature is increased [3] (Fig. 13 shows the debris (a) loose at room temperature, (b) partially forming a ‘glaze’ layer at 510°C and (c) forming a comprehensive ‘glaze’ layer at 750°C).

### ***3.1.3 Effects of Load***

Rose [2] also examined the effect of load (7 to 25 N, 0.654 m.s<sup>-1</sup> only) on the sliding behaviour of Incoloy MA956 when slid against Incoloy 800HT and Stellite 6 counterfaces at 750°C (Fig. 16). ‘Glaze’ layers were observed for all loads up to 20N for both counterfaces and no change in oxide behaviour was observed with increasing load (although greater material working was reported as being necessary to provide material for ‘glaze’ when an Incoloy 800HT counterface was used). No significant increases in weight loss were observed with increasing load up to 20N load (Fig. 17). These observations were irrespective of whether the ‘glaze’ was primarily Stellite 6-counterface-sourced or Incoloy MA956-sample sourced (when the counterface was Incoloy 800HT). Higher losses were reported at 25N (most noticeably with an Incoloy 800HT counterface – Fig. 17) and, although ‘glaze’ layers still formed, the Incoloy MA956 sample substrate was unable to provide sufficient support for the ‘glaze’ layer to remain protective.

## **3.2 Intermetallics**

### ***3.2.1 Introduction***

Strong, predominantly metallic bonding between unlike atoms leads to the formation of intermetallics and intermetallic compound phases. From such bonding comes crystal structure, ordering, high strength at low and high temperature, low ductility and low  $K_{1c}$ , particularly at low temperature.

The low ductility, low  $K_{1c}$  and high strength of intermetallics stem from such critical factors as complex crystal structures, the large Burgers Vector, high lattice stress, the in-adequate slip systems and the inability to cross slip. The complex interplay

between these parameters makes the prediction of intermetallic wear behaviour difficult.

The expected improvement in wear resistance from high strength, ordering and an adequate slip system may be off set by low  $K_{Ic}$  and low fracture strain. The advantage in providing high wear resistance due to ordering may eventually be lost by the destruction of this ordering due to elemental diffusion from the counterface into the intermetallic lattice. At elevated temperature, increased  $K_{Ic}$  and fracture strain are likely to improve the wear resistance, however, some of the effects of these parameters may be masked by the formation of wear resistance surface ‘glaze’ layers.

### **3.2.2 Wear of TiAl – Metallic Counterfaces**

In discussing intermetallic wear resistance, attention is focussed on TiAl and TiAl-based intermetallics because of increasing interest in using these materials in many industrial applications, including automotive, aerospace and power generation.

TiAl when worn against Incoloy 800HT at room temperature (‘reciprocating-block-on-rotating-cylinder’ rig, load 7 N, sliding speed  $0.654 \text{ m.s}^{-1}$ ) shows a similar wear pattern to the ODS and Nimonic alloys, and involves a similar mechanism [1]; the transfer of Incoloy 800 to the TiAl surface, followed by work hardening of the transferred layer and formation of a wear resistant oxide layer ( $\text{NiCr}_2\text{O}_4/\text{Fe}_2\text{O}_3$ ). The development of this hardened, wear resistant layer causes some improvement in wear resistance without any observable ‘glaze’ formation (Fig. 18a).

In contrast, ‘glaze’ formation has been observed in the same system at  $750^\circ\text{C}$  (7N,  $0.654 \text{ m.s}^{-1}$ ), the ‘glaze’ (Fig. 18b) containing mainly oxidised Fe/Ni/Cr material from Incoloy 800 with little Ti and Al [1]. These observations are in conflict with other work where the ‘glaze’ contained the elements of TiAl. It is believed that the use of a different test system (‘pin-on-disk’ rather than ‘block-on-cylinder’) in the latter work accounts for this difference. The role of TiAl is considered to provide a deformation and wear resistant substrate for the ‘glaze’ to develop, to reside and be sustained.

When worn against Stellite 6 (7N,  $0.654 \text{ m.s}^{-1}$  [1]), initial transfer of Stellite 6-based material on the TiAl surface results initially in a like-on-like sliding regime, with the Stellite 6 counterface sliding against this transferred layer. At room temperature



(Fig. 18c), instability of this layer leads to a continual process of transfer and removal from both surfaces and a loose oxide containing Ti and Al from the TiAl, and Co and Cr from the Stellite 6 is generated. Only at 750°C (at 0.314 m.s<sup>-1</sup> [97] as well as 0.654 m.s<sup>-1</sup> [1]) does the transferred Stellite 6 material form a primarily Co-Cr-oxide 'glaze' layer on the TiAl surface (Figs. 18d and 19a), this layer being thinner than that created when sliding against Incoloy 800HT.

### **3.2.3 Wear of TiAl - Ceramic Counterfaces**

TiAl suffers moderate wear when slid against a silicon nitride interface at room temperature (0.654 m.s<sup>-1</sup>). Whilst the debris generated (sourced from both sample and counterface) forms loose oxide platforms (or 'plateaux' – Fig. 20a), these are formed and removed as sliding continues and do not form a wear protective layer. The high TiAl wear has been attributed to the elements of the counterface material interfering with the ordered structure of the intermetallic, as small atomic radii Si and N enter the lattice and increase its susceptibility to wear. A mixture of abrasive and adhesive wear with some evidence of stick-slip, possibly due to high mutual chemical compatibility between the Si<sub>3</sub>N<sub>4</sub> and the TiAl, has been reported [98] (Si<sub>3</sub>N<sub>4</sub> has been previously observed to have high mutual chemical compatibility with both Ti and Al [99]), leading to moderate wear of the TiAl and high wear of the Si<sub>3</sub>N<sub>4</sub>. In contrast, TiAl undergoes lower wear when slid against silicon nitride at 750°C (at 0.314 m.s<sup>-1</sup> [97] and 0.654 m.s<sup>-1</sup> [1]), due to the rapid formation of a thin wear-resistant oxide layer (Figs. 19b and 20b). The formation of this layer, sourced from both the TiAl and Si<sub>3</sub>N<sub>4</sub>, prevents substantial wear. It is suggested that any high mutual compatibility enhances the very early stages of wear, providing the necessary material for the wear-resistant layer.

TiAl undergoes higher wear when worn against Al<sub>2</sub>O<sub>3</sub> at room temperature [97] with enhanced material removal by abrasion, the debris from which does not form a protective layer. The material generated from an initial period of high TiAl-wear against Al<sub>2</sub>O<sub>3</sub> at 750°C [97], however, readily forms a 'glaze' layer (Fig. 19c) which provides some protection for the TiAl surface and prevents excessive wear. However, despite the 'glaze' layer, the abrasive nature of the oxide generated (a mixture of Ti and Al oxides) still promotes continued material removal. In contrast, the Al<sub>2</sub>O<sub>3</sub> undergoes little wear at both room temperature [99] and 750°C [97], with it

having no potential chemical compatibility with TiAl; hence no adhesive mechanism can occur.

### **3.3 Nimonic Alloys**

#### **3.3.1 Incoloy 800HT Counterface**

Wood [1] reported a correlation between Nimonic 80A cast, Nimonic 80A HIPped and Nimonic 90 when tested against different counterfaces at various temperatures ( $0.654 \text{ m.s}^{-1}$ , 7N load and reciprocating-block/sample-on-rotating-cylinder/counterface configuration). The results of room temperature tests seemed to be greatly influenced by the degree of material transfer to the Nimonic surface, this transfer itself being influenced by counterface hardness; the softer was the counterface the higher was the amount of transfer.

Metallic transfer readily occurred from the relatively soft Incoloy 800HT counterface onto the surfaces of each of the Nimonic materials at room temperature. The transferred material formed a wear resistant layer which protected the Nimonic material surfaces and led to very small weight changes. Inman [3] later reported the development of metallic transfer layers at  $0.314$  and  $0.905 \text{ m.s}^{-1}$  (Figs 21 and 22 - greater transfer was observed at  $0.905 \text{ m.s}^{-1}$ ) when Nimonic 80A was slid against Incoloy 800HT; these layers were work hardened.

At  $750^\circ\text{C}$ , the Nimonic alloys showed a large range of behaviours when tested against the same three counterfaces [1]. When slid against Incoloy 800HT, mainly Incoloy 800HT-sourced layers that protected the Nimonic alloys against wear, together with low weight changes, were observed. Rose [2] and Inman [3] additionally reported 'glaze' overlying any transferred material when Nimonic 80A was worn against Incoloy 800HT at this temperature.

Rose ( $0.654 \text{ m.s}^{-1}$  [2]) and Inman ( $0.314$  and  $0.905 \text{ m.s}^{-1}$  [3]) examined temperatures between room temperature and  $750^\circ\text{C}$  (Figs. 21 and 22), with Rose [2] noting that Incoloy 800HT-sourced transfer layers continued to be observed up to  $570^\circ\text{C}$ . Inman [3] reported the development of transfer layers up to  $750^\circ\text{C}$ , observing an increase in transfer with sliding speed. At  $0.314 \text{ m.s}^{-1}$ , transfer was less, due to increased amounts of oxide that interfered with metallic adhesion, but did not form 'glaze'. At  $0.905 \text{ m.s}^{-1}$ , transfer was greater than at either  $0.314$  or  $0.654 \text{ m.s}^{-1}$ ; any surface

oxidation was more readily removed, allowing greater adhesion of transferred material.

'Glaze' layers were observed only between 630°C and 750°C [2,3], with its formation being favoured by increased test temperature [2,3] and lower sliding speed (due to decreased material removal) [3]. These 'glaze' layers were reported to form after transfer from the Incoloy 800HT counterface to the Nimonic 80A surface [3]; effectively, the 'glaze' was generated by 'like-on-like' sliding of the transfer layer against the Incoloy 800HT counterface.

### ***3.3.1.1 Effects of Load***

Rose [2] also examined the effect of load (7 to 25 N, 0.654 m.s<sup>-1</sup> only) on sliding behaviour for Nimonic 80A when slid against Incoloy 800HT at 750°C. Limited compacted oxide layers formed at 7N (Fig 23a) and 10N load, protecting the Nimonic 80A surface. At loads between 15N to 25N (Fig. 23b), an abrasive, oxidational wear regime dominated, with no debris build-up or layer formation; the behaviour of the oxide changed from protective to abrasive due to the increased load. This was reflected by a rapid increase in weight loss above 15N (Fig. 17).

### ***3.3.2 Stellite 6 Counterface***

Wood (0.654 m.s<sup>-1</sup>, 7N load) [1] reported only limited material transfer from the harder Stellite 6 counterface to the Nimonic material surfaces at room temperature. Thin mixed oxide layers were formed on the Nimonic surfaces; these contained material from both the Nimonic and Stellite 6 wear surfaces and provided only limited protection. Testing of Nimonic 80A against a Stellite 6 counterface at 0.654 m.s<sup>-1</sup> [2] and at 0.314 and 0.905 m.s<sup>-1</sup> [3,20,21] (Figs. 24a and 25a) resulted in preferential wear of the Stellite 6 counterface, generating loose Co-Cr-based oxides. This debris separated the wear surfaces, preventing metallic contact; a low temperature mild wear regime resulted.

Behaviour at intermediate and high temperature depended significantly on sliding speed. At 0.314 m.s<sup>-1</sup> [3,20,21], the loose debris mild wear regime (Fig. 24a) continued up to 450°C. Increased sintering was observed at 390°C, isolated 'glaze' at 450°C, with increasingly comprehensive 'glaze' formation above 510°C (Fig. 24b) and most notably between 630 to 750°C (Fig. 24c) [3,20,21,23].

The loose debris mild wear regime was observed up to 390°C at 0.654 m.s<sup>-1</sup> [2] and 270°C at 0.905 m.s<sup>-1</sup> [3,20,21]; at higher temperatures, there was a transition to intermediate severe wear. Such severe wear was observed at 0.654 m.s<sup>-1</sup> up to 570°C [2], without any evidence of oxide (Fig 25b); only metallic debris sourced from the Nimonic 80A was generated by delamination wear. At 630°C, however, oxide was observed and this assisted severe wear by abrasion [3,20,21,23]. A similar pattern was observed at 0.905 m.s<sup>-1</sup> [3,20,21], though enhanced frictional heating led to oxide generation at 570°C as well as 630°C.

On increasing temperature to 690 and 750°C, further increases in oxide production were sufficient to separate completely the Nimonic 80A sample and Stellite 6 counterface; a mild wear regime was thus established. However, high wear rates continued; although technically a mild wear regime, the high wear rates indicated that the oxide was not protective. Two slightly different forms of oxidational behaviour were observed, depending on researcher. At 0.654 m.s<sup>-1</sup>, Wood [1] reported the formation of a poorly adherent ‘glaze’ that was continuously removed. In contrast, Rose [2] reported no ‘glaze’ formation on Nimonic 80A and the generation of only loose oxides that acted abrasively (NiO and Cr<sub>2</sub>O<sub>3</sub>), thereby enhancing removal from the Nimonic 80A surface. These latter observations were confirmed by Inman [3,21,23] at both 0.654 m.s<sup>-1</sup> (Fig. 25c) and 0.905 m.s<sup>-1</sup>, who observed greater oxide generation at 0.905 m.s<sup>-1</sup> but still without ‘glaze’ layer formation.

Rose [2] stated that layers were unable to form due to insufficient debris adhesion to the Nimonic 80A sample surfaces and lack of debris cohesion, caused by the ploughing of sample surfaces by hard carbide particles in the Stellite 6 counterface. However, Inman [3] argued that the carbides were not hard enough to have this ploughing effect and inhibit the development of oxide layers; it was possible that the carbides were softer than the ‘glaze’ layers and wore in preference to them. This inability of the Nimonic 80A-sourced NiO and Cr<sub>2</sub>O<sub>3</sub> oxides to form a ‘glaze’ was instead attributed to their relatively poor sinterability. If this failure to form ‘glaze’ layers had been due to carbide ploughing, then these layers would not have formed in other systems involving Stellite 6. For example, Stellite 6-sourced Co-Cr layers formed in the Nimonic 80A / Stellite 6 (counterface) system at 0.314 m.s<sup>-1</sup> [3, 21, 23]. Also, Incoloy MA956-sourced Fe-Cr-based layers formed at 0.905 m.s<sup>-1</sup> in the Incoloy MA956 / Stellite 6 (counterface) system [3, 22].

Inman, Rose and Datta [21] collated the available data to create a temperature versus sliding speed wear map for the Nimonic 80A versus Stellite 6 (counterface) system (later further developed by Inman and Datta [23]), covering a variety of different modes of wear behaviour that are dependant on load / sliding speed combination. This is discussed further in Section 5.3.

### ***3.3.2.1 Effects of Load***

Rose also studied the effect of load on sliding behaviour for Nimonic 80A worn against Stellite 6 at 750°C [2]. At all loads (7N to 25N), the wear mechanism remained predominantly oxidational, with elements of abrasive wear, regardless of applied load (Fig. 23c and d); no compacted debris layers were formed across the range of loads (7 to 25N) at 750°C. There was no evidence that changing load had any significant effect on wear regime in this case; however, the grooves on the damaged surface became more pronounced at high load. This was reflected by increased weight loss at high load (Fig. 17).

### ***3.3.3 Effect of Nimonic Material Processing Route on Wear***

Very similar wear properties were observed for Nimonic 80A (cast) and Nimonic 80A (HIPped) [1] and it was not possible to conclude that processing route affected wear resistance. Wear behaviour was also similar for Nimonic 90, the only exception being the enhanced wear resistance of Nimonic 90 over Nimonic 80A (cast) at 750°C.

### ***3.3.4 Nimonic 80A Sliding Wear – Comparisons between Various Wear Rig Configurations***

The apparently poor sintering and ‘glaze’ forming characteristics of NiO and Cr<sub>2</sub>O<sub>3</sub> generated from Nimonic 80A (at 0.654 m.s<sup>-1</sup> and 0.905 m.s<sup>-1</sup>) [2,3,20,21,23] at first seems to contradict the extensive studies carried out into ‘glaze’ formation with Nimonic 80A-based systems by Jiang *et al.* [14-18]. However, the last group used lower sliding speeds with a like-on-like reciprocating ‘pin-on-disk’ configuration (mean sliding speed 83 mm.s<sup>-1</sup>); such systems have a higher degree of debris retention, providing greater opportunity for the oxide debris to sinter together to form ‘glaze’ layers. The ‘block-on-cylinder’ configuration used by Rose [2] and Inman *et al.* [3,20,21,23] is a unidirectional sliding wear system that promotes debris mobility and ejection over retention, especially at higher sliding speeds. The decreased

residency and greater mobility of the debris do not allow sufficient contact time between debris particles for sintering and welding processes to occur, as is necessary for 'glaze' formation.

### **3.3.5 $Si_3N_4$ Counterface**

Wood (0.654 m.s<sup>-1</sup>, 7N load) [1] reported limited material transfer from the harder  $Si_3N_4$  counterface to the Nimonic material surfaces at room temperature. Thin mixed oxide layers were formed on the Nimonic surfaces; these contained material from both wear surfaces that provided only limited protection.

Wood [1] observed a very different wear resistance when Nimonic 80A (cast) and Nimonic 90 were worn against  $Si_3N_4$  at 750°C. Nimonic 80A (cast) showed very poor resistance, with no 'glaze' formation in contrast to Nimonic 90 where 'glaze' formation and very low weight losses were observed. Wood attributed the difference to the presence of Co in the Nimonic 90, which somehow improved 'glaze' adhesion and/or strength on the Nimonic 90 surface.

## **3.4 Effects of Environmental Variables**

### **3.4.1 Oxygen Levels and Partial Pressure**

Even in environments with low oxygen partial pressure [18,100] (effectively removing much of the oxygen from the system), stable oxide layers are still able to form. Under vacuum, increasing pressure from high vacuum conditions to 10<sup>-2</sup> Pa was enough to result in a decrease in friction in sliding of an iron-chromium alloy. Buckley [101] noted during the like-on-like sliding of clean iron that a pressure of 400 Pa (or 3 Torr) was sufficient to prevent seizure. Lancaster [25] noted that, at 300°C, the range of sliding speeds over which severe wear was observed when a 60/40 brass was slid against tool steel was greatly in an oxygen atmosphere compared to the level of wear observed in air (Fig. 2).

Barnes *et al.* [100,102,103] investigated the effects of partial pressure on iron-chromium alloys, ranging from pure iron to iron-40% chromium (Fig. 27). Initial work in a normal atmosphere indicated high friction and seizure at 450°C for iron and between 500-600°C (rising slightly with chromium content) for various iron-chromium alloys; the only exception to this was Fe-40%Cr where there was no seizure up to the maximum test temperature of 850°C.

Adhesive wear and seizure (here defined as the coefficient of friction rising above a nominal value of 3.5) were dominant at oxygen partial pressures of  $10^{-6}$  and  $10^{-5}$  Pa, despite there apparently being sufficient oxygen present to prevent this. On raising the partial pressure to  $10^{-4}$  Pa, however, significant amounts of oxide were observed and areas of compacted debris had developed. These 'islands' were specified as the reason for the switch from severe to mild wear, with even more rapid development of these oxides on raising the partial pressure to  $10^{-1}$  Pa. The compacted debris was either completely oxidised or oxide-covered metallic debris; its formation was accompanied by decreases in friction (Fig. 27). However, despite the presence of this oxide debris, the wear rate remained high until the oxygen partial pressure reached 1 Pa or above.

Changes in partial pressure were also made during sliding tests [100], with oxygen in some cases being removed from the wear system (the pressure was from  $10^{-1}$  Pa to  $10^{-6}$  Pa). When this occurred, the oxide debris and the compacted oxide layers remained at the wear interface, showing continued stability and wear resistance even without a continued supply of oxygen.

#### ***3.4.2 Effect of Water Vapour and Relative Humidity***

The presence of water vapour in the atmosphere can have a positive or negative effect on oxide development, depending on relative humidity levels and materials. For mild steel a decrease in wear was observed with increasing relative humidity under fretting conditions [104,105] and similarly with carbon steel under sliding wear conditions [15]. It has been suggested that adsorbed moisture might have a dual effect [106], in that on the debris surface, it might act as a lubricant, promoting speedier debris dispersal and, thus, less abrasive wear. From this, it was proposed that the hydrated form of the iron oxide that develops in the presence of the moisture might be a less abrasive medium. Such debris does, however, have the potential to enhance interface contact and bring about adhesive wear.

Experimental work by Bill [107] demonstrated that this could be the case, with the relationship between relative humidity and wear rates becoming quite complex. Iron showed a significant increase in wear rate on raising the relative humidity from 0 to 10%, followed by a rapid decrease and minimum values in the region of 50 to 70%, then by a small increase towards atmospheric saturation. Increasing wear was

demonstrated for titanium at up to 30% relative humidity, followed by an erratic decline in wear values up to saturation levels. Nickel showed a sharp decrease in wear levels between 0 and 10% relative humidity, followed by increasing wear with relative humidity up to saturation.

Oh *et al.* [15] suggested a transition from severe to mild wear with increasing relative humidity for carbon steels. At low relative humidity, severe wear was encountered, with total losses amounting to between 0.130g and 0.190g. This remained the case up to 50% relative humidity. The level of wear dropped rapidly after this ‘transition point’, with mild wear being observed at relative humidity levels of 70% and losses totalling no more than 0.002g. The amounts of carbon in the steel were observed to affect this transition, which occurred at higher values with increasing carbon content. Friction was also observed to fall rapidly, from between 0.62 and 0.68 at 35% relative humidity to between 0.44 and 0.48 at 70% relative humidity.

### 3.4.3 Other Atmospheres

The wear process in atmospheres other than air or oxygen will depend on whether the atmosphere is oxidising or reducing. In most practical situations, corrosion product will not form in a reducing (non-oxidising) atmosphere and, thus, the formation of wear protective layers is not possible. Only the presence of adsorbed gases or other volatiles will act to separate the wear surfaces, adhesion and, therefore, levels of wear and friction [108].

In other oxidising atmospheres, only carbon dioxide has been examined to any significant extent. Sullivan and Granville [50] showed that a compacted oxide layer was formed when a Fe-9%Cr steel was tested in a pin-on-disk rig in carbon dioxide, between 200 and 550°C. Smith [109] observed the formation of compacted oxides on wear testing of 316 stainless steel in carbon dioxide at temperatures between 20°C and 600°C. The carbon dioxide acted as the oxidising agent in each case:



with the wear mechanisms being very similar to those in air.

Research in other environments is extremely limited. Bill [107] obtained ‘prodigious amounts of black debris’ on testing titanium in supposedly pure dry nitrogen. It may



be that this is removed oxide that was present prior to sliding (or formed during sliding by reaction with the trace oxygen invariably present in bottled gases) or even a mixture of metallic titanium and oxide. The possibility of titanium nitride is extremely unlikely, if not impossible, due to the tests being carried out at room temperature. However, no attempt was made to analyse the debris or explain the result.

### **3.5 Effects of Pre-treatment of Sliding Surfaces**

#### **3.5.1 Pre-oxidation**

Stott and Mitchell [51] carried out pre-oxidation (oxidation prior to commencement of sliding) on Jethete M152 (a high chromium steel) and 321 stainless steel. Elimination of metal-to-metal contact was observed immediately on commencement of sliding in the case of Jethete M152 and also the immediate establishment of compacted oxide in the case of the 321 stainless steel. They concluded that the pre-oxidation provided an extra supply of oxide debris that led to the more rapid establishment of 'glaze' surfaces.

Iwabuchi *et al.* [65] studied the effects of pre-oxidation of a number of samples of S45C carbon steel; for each sliding test, a moving disk specimen was rotated against a fixed ring specimen, with both pre-oxidised samples and non-oxidised samples undergoing unidirectional sliding for 1,000 m at room temperature. The pre-oxidation treatment was carried out at 300°C for 5 minutes, 1 hour or 3 hours. Times of 5 minutes and 1 hour did result in progressive decreases in wear (Fig. 28); however, increasing the time to 3 hours produced no further improvement. The observed decreases in wear occurred because of break-down of the oxide layer to form debris, the presence of which prevented metal contact and adhesion.

Iwabuchi *et al.* conducted similar experiments with 304 stainless steel specimens [65], with specimen configurations identical to those for S45C plain carbon steel. Pre-oxidation was carried out at 300°C for times of up to 10 hours. Although there was some scatter in the data after 300 m of sliding, there was no evidence of any effect of pre-oxidation on overall wear, regardless of the time of pre-oxidation and it was concluded that pre-oxidation had no effect under the prescribed test conditions.

This was due to ‘selective oxidation’ of chromium at the surface; this decreased the level of oxidation of the stainless steel, with the result that there was insufficient oxide to decrease the severe wear rate by debris generation from this layer.

Thus, although pre-oxidation can decrease or eliminate early metal-metal contact, this cannot be guaranteed. Under certain circumstances, possibly due to the effects of variations in alloy composition on the nature of the surface oxidation, the production of suitable surface oxide required for the promotion of early ‘glaze’ formation may not occur.

### **3.5.2 Pre-sliding**

Iwabuchi *et al.* [65] additionally looked at samples of S45C carbon steel that had undergone pre-sliding for 300 m at 300°C; this was sufficient to create an accumulated loose oxide layer. Subsequent tests indicated the complete elimination of the severe wear regime (Fig. 28), with only mild wear being observed, regardless of test temperature. In the case of pre-oxidation, the oxide layer served at best only to reduce (dependent on combination) the severe wear “run-in” period (Section 3.5.1).

A decrease in severe wear was also observed when 304 stainless steel underwent pre-sliding for 100 m at room temperature, due again to the presence of an accumulated loose oxide layer. In both cases, the availability of pre-existing oxide debris acted to prevent contact between the metallic interfaces.

Pre-sliding was additionally carried out for 304 stainless steel over a distance of 300 m at room temperature, 200°C and 400°C (at which temperature the oxide layer formed was a ‘glaze’), with the severe wear stage being eliminated in each case during subsequent sliding. The presence of accumulated oxide from pre-sliding did not, however, lead to a decrease in the rate of wear during mild wear.

### **3.5.3 Ion Implantation**

Langguth *et al.* [66] carried out oxygen ion implantation on a series of chromium and carbon steels (AISI 52100, AISI 440B, AISI M2) and 321 stainless steel, followed by a series of sliding experiments using a pin-on-disk rig. A sliding speed of  $28 \times 10^{-3} \text{ m.s}^{-1}$  was used over a sliding distance of 400 m, with relative humidity at 30% or 80%.

In general, recorded levels of wear for the ion-implanted samples were much lower than for their untreated equivalents (Table 3). This was due to the oxygen in the surface layers assisting the formation of oxidised debris and, thus, decreasing the initial severe wear period. Certain aspects of heat treatment of the alloys and the sliding conditions were observed to affect this. For example, in the case of the chromium and carbon steels, the improvement in wear resulting from oxygen ion implantation was noticeably less for AISI 52100 and AISI 440B in the annealed form compared to the martensitic form; this can be seen from the data in Tables 3 and 4. Relative humidity has a marked effect, as in the case of AISI 52100 steel, where the oxygen ion implanted material actually undergoes a higher level of wear than the untreated material. These observations were attributed to the higher plasticity of the annealed samples.

A change in the form of the debris was also observed, from a smooth oxide layer for the martensitic samples to loose debris for the annealed samples. The one exception was for AISI 440B steel, where the decrease was greater in the annealed state and sliding was accompanied by a change in the state of the oxide debris from the loose form to the oxide layer form.

In comparison to standard pre-oxidation treatment (Table 4), wear tended to be less, with the exception of annealed AISI 52100, where the pre-oxidised samples produced superior results, regardless of the levels of relative humidity.

Langguth *et al.* note also that implantation has been tried using different ions, including nitrogen, carbon and boron, with varying degrees of success, though not to the same extent as oxygen, as these alternatives do not promote wear track oxidation.

## **4.0 ‘Glaze’ Formation – Micro-scale and Nano-Scale Investigations**

### **4.1 Introduction**

It is clearly recognised that ‘glaze’ formation on the contacting surfaces affords significant protection against wear damage and degradation. The generation of HT wear resistant surfaces in situ overcomes the serious limitations on materials and coatings imposed by HT wear conditions. ‘Glaze’ formation is very useful as it takes advantage of important events that accompany the processes of HT wear, such as

oxidation, debris generation and elemental transfer between the contacting surfaces [1-4,12,110]. These events, under certain conditions of temperature, pressure and speed [1-4,12,19-21,23,24,111] lead to the formation of surfaces with self functionalised HT wear resistance. Although the phenomenon of ‘glaze’ formation and related general issues of HT wear have been extensively studied, it is still not possible to predict the precise conditions which promote ‘glazed’ surfaces.

Here, it has been recognised that a step forward would be to gain detailed knowledge of ‘glaze’ layer micro-structure and nano-scale structure evolution so that the precise mechanisms of ‘glaze’ formation can be established. This section summarises and updates the studies carried out on ‘glaze’ formation during wear of various systems. It has been written with emphasis on generic principles and wear systems have been selected that facilitate the mechanistic understanding of the ‘glaze’ formation process.

#### **4.2 Micro-scale Studies of ‘Glaze’ Formation**

From a study of mainly nickel- or nickel-iron-based alloys containing significant quantities of chromium in like-on-like sliding, and in some cases, cobalt, it was established by Stott *et al.* [4] that the oxides formed have elemental ratios that differ little from the original base alloys. It was thus concluded that the observed low wear and friction arise from the physical properties and condition of the glaze, rather than their chemical compositions.

Further research [4,49,54-58] allowed the identification of the following modes of compacted layer formation.

- The first mode is characterised by the formation of transient oxides, followed by the oxide thickening by continued oxidation by oxygen diffusion to the substrate-oxide interface and through physical defects.
- The second mode of formation is characterised by two stages. Stage one involves the formation of an insufficiently thick layer due to unfavourable temperature and low alloy strength, possibly involving an extended pre-glaze or severe run-in period. Stage two involves the formation of a sufficiently thick oxide layer through continued break-up and consolidation of ‘glaze’ debris produced in stage one.

- In the third mode, the ‘glaze’ does not remain stable during sliding and areas of compacted oxide continually break down and reform.

Stott *et al.* [8,49,59,60,112] later produced a further set of three modified mechanisms, based on their studies of the elevated temperature (200-600°C) fretting wear of iron-based alloys. These mechanisms [49] were seen as limiting cases for oxide debris generation, after which the build-up of oxide to form compacted layers continued:

- **Oxidation – scrape – reoxidation:** This involves a two-stage process. In the first step, oxide generation takes place in the areas of contact between the two sliding surfaces, with general oxidation over the apparent sliding area of contact and, also, at asperity contacts where temperatures exceed the general temperature in the region of the sliding area of contact. In the second stage, this oxide is removed by subsequent traversals of the sliding interfaces, exposing fresh metal for further oxidation. The debris formed may then be either completely removed from the interface, act as a third body abrasive, thereby contributing to the wear process or be compacted to form a wear-protective oxide layer.
- **Total oxidation:** Under certain conditions, particularly high ambient temperatures, oxide generated during sliding or even present prior to the commencement of sliding, is not completely removed by subsequent traversals of the sliding interfaces, allowing the oxide to thicken with time. Provided this layer is coherent and adherent to the metal substrate and can withstand the stresses of sliding, a plastically deformed wear-protective oxide layer can develop.
- **Metal debris:** Debris particles generated during the early stages of wear are broken up by the sliding action, with any fresh areas of exposed metal being subject to further oxidation. There may be a high level of oxidation of the debris surfaces, due to the relatively large exposed surface area of metal.

Enhanced oxidation is promoted by heat of deformation and increased energy of the particles due to increased defect density and surface energy (the exposed surface area of debris material will increase as particle size decreases). There is

also an input due to the heat of oxidation, promoting oxidation of the metallic particles, the finer particles undergoing complete and spontaneous oxidation. The resulting oxide can later develop into a wear-protective layer.

The formation of compacted layers has also been observed by Wood *et al.* [1,10], Rose [2], Inman *et al.* [3,20-24], Datta *et al.* [19] and Du *et al.* [110].

The third mechanism proposed in Stott's original work is similar to that of Lin and Wood [4], both depending on the generation of larger debris from the wear substrate and the comminution of this debris to fine oxide particles as the wear process continues to develop.

The one major difficulty with these mechanisms is that they were developed from work on low speed reciprocating sliding wear, where frictional heating is not such an important factor [60]. At sliding speeds of greater than  $1 \text{ m.s}^{-1}$  [104], frictional heating increasingly becomes an issue.

### **4.3 Third Body Interaction in Relation to Compact Oxide Formation**

In Section 2.2.3, a brief discussion was made of four mechanisms of particle behaviour at the sliding interface, as proposed by Jiang *et al.* [18] – these included *(1) rotation, (2) skidding, (3) rolling* and *(4) adhesion/sintering affected rolling* (Fig. 5). Jiang *et al.* observed that the friction levels for mechanism (4) are highly dependent on the adhesion force between particles in the sliding system. While this adhesion force is weak, friction levels for mechanism (4) are lower than those for mechanism (2); however, increasing this adhesion force above a critical level results in a situation where the reverse is the case. Skidding then becomes the dominant mechanism, with no relative movement between neighbouring particles – an increase in adhesion force locks them in place. A stable compact layer can result and, at higher temperatures, a wear resistant 'glaze type' layer is possible (with the particles locked together, there is sufficient time for sintering). Stott's later modification of this approach [111] (the inclusion of adhesion and sintering effects in rotation, skidding and rolling mechanisms) better recognises the fact that adhesion and sintering has a more general effect on the various particles making up the particle layer, regardless of whether they are entrapped or in relative motion.

Adhesive forces and sintering tend to take effect at more elevated temperatures, as demonstrated by experimental work carried out by Jiang *et al.* [15] on the sliding wear of Nimonic 80A at 20, 150 and 250°C. At 20°C, a thick layer of compacted, fine wear debris was formed, with some evidence of solidification and sintering in some areas; however, these layers were found to be predominantly particulate in nature. There is a transition from metal-metal wear to contact between these primarily oxide particle layers, at which point increases in contact resistance and decreases in levels of wear are coincident. At 250°C, sintering becomes a significant factor and there is a tendency to form smooth ‘glaze’ layers on top of these compacted oxide layers. The 150°C case was intermediate, with some development of smooth load-bearing areas between the particulate layers. Removal of this more loosely compacted material by ultrasonic cleaning in acetone left behind the more compacted debris, load-bearing areas.

These observations clearly indicate that temperature is a major driving force for adhesion between particles and formation of load-bearing compacted debris layers. This was demonstrated further [15] by a heat treatment of 90 minutes at 600°C, for samples pre-slid at 20°C. The compacted layers formed during the sliding phase of the test became solidly sintered together as a result of the subsequent heating of the samples. The effect of a very small particle size would be to increase the available surface energy, due to the resultant increase in relative surface area. This would act to drive the adhesion and sintering processes and allow for observable sintering at temperatures where sintering of the larger particles used in powder technology applications would not be noticeable. As adhesion itself is temperature-dependent, increases in temperature due to ambient or frictional heating would accelerate the adhesion and, therefore, the sintering process. An Arrhenius relationship [63] influences the process ( $K_p = A_p e^{-Q_p/RT_o}$ ). Shrinkage and thermal stress-induced cracks were, however, observed on layers sintered at 600°C.

From experimental observations, Jiang *et al.* proposed a descriptive model of the sliding wear process [17,112]. Fig. 29 shows this diagrammatically, with possible modifications to it for the re-incorporation of debris for broken-down compacted oxide and ‘glaze’ layers:

1. Generation of wear particles due to the relative movement of the metal surfaces;
2. Removal of some particles from the wear tracks to form loose wear particles;
3. Retention of other particles within the wear track;
4. Comminution of the retained particles by repeated plastic deformation and fracture, with particles freely moving between the rubbing surfaces and undergoing partial or even complete oxidation, due to continued exposure of fresh metallic surfaces during comminution;
5. Continued fragmentation and agglomeration at various sites on the wear surfaces, due to adhesion forces between solid surfaces originating from surface energy and the formation of relatively stable compact layers.

This has two effects, viz:

- i. Firstly, material loss is reduced by a material recycling effect of the wear debris particles. Material breaking away from the compacted debris may rejoin it.
- ii. Secondly, due to heavy deformation and oxidation of the wear debris particles, the layers formed are hard and wear-protective.

Two competitive processes then occur during subsequent sliding, i.e.:

- a. The compacted layers are continually broken down, the debris generated promoting wear (though, again, reincorporation may occur).
- b. Continuing sintering and cold welding between particles within the layers, leading to further consolidation.

For the latter case to predominate, the temperature must be high enough (in excess of a critical temperature) to encourage the sintering processes required to ensure the formation of a solid wear-protective layer on top of the compacted particle layers before the layers are broken-down. The effects of this can be seen in the experimental work of Jiang *et al.* – at 20°C, this critical temperature was not reached and the debris, although undergoing compaction, did not sinter to form a ‘glaze’ layer. At 250°C, ‘glaze’ was clearly visible, whilst at 150°C, closer to and possibly just



above the critical temperature, more limited sintering meant although some 'glaze' areas were formed, there were also substantial areas of loose debris still present.

Also of note is the formation of compacted debris layers close to the centre of the wear scars, the location of highest debris retention [16], where coverage by high resistance compacted layers was estimated to be 20 to 50%.

Jiang estimated also that, to cause a transition from severe to mild wear, only 20% of the surface needed to be covered by 'glaze'-type layers, compared to a value of greater than 30% for non-glaze compacted layers, demonstrating that 'glaze' layers offer more physical protection.

Jiang's model is based on experimental work done on fretting wear systems and Rose [2] questioned the applicability of Jiang's model in a low debris retention system. However, Jiang does account for debris removal from the system leading to wear as would occur in, for example, high speed unidirectional sliding [1-3,19-24,110] or debris removed by introduced interfacial airflow [45]. Also, in Rose's own 'reciprocating-block-on-rotating-cylinder' experimental work (a higher speed unidirectional sliding configuration), examples of debris retention with 'glaze' formation and compacted layers do occur (i.e. Incoloy MA956 versus Stellite 6), despite the more adverse sliding conditions. However, as Rose points out, there are examples where compacted oxide layers do form and there is no significant third body debris retention [1-3,22,57], thus suggesting that Jiang's model requires further modification to account for this; Fig. 29 includes some suggestions by Inman [3] to cover these points.

#### **4.4 Nano-scale Investigations of 'Glaze' Formation**

This section reports recent findings on the evolution of structures and sub-structures of 'glaze' layers at the nano-scale level [19,24,113], from extensive research carried out in the authors' laboratory. Data relating to transmission electron microscopy (TEM) and scanning tunneling microscopy (STM) studies are presented in Figs. 30 to 44. Scanning tunneling spectroscopy (STS) and current imaging tunneling spectroscopy (CITS) data are not shown here.

The work presented here is generic in nature, but refers to a particular system in order to facilitate understanding of the underlying mechanisms for nano-structure evolution

in the surface ‘glaze’ layers and their improved HT wear resistance. In this case, the ‘Nimonic 80A (sample) versus Stellite 6 (counterface)’ system is considered, using a counterface surface sliding speed of  $0.314 \text{ m.s}^{-1}$ , with a 7N applied load and total sliding distance of 4,522 m [3,22-24]. The sample also underwent a reciprocating action against the counterface for a distance of 12 mm, 3 times a minute, thereby limiting debris retention to between 20 and 30% (most of the debris was allowed to escape).

#### **4.4.1 Wear Data**

Fig. 30 displays the wear data for the Nimonic 80A / Stellite 6 system as a function of temperature at  $0.314 \text{ m.s}^{-1}$ . Weight changes after 4,522 m of sliding were extremely low for all temperatures, with the largest mean change being 0.002(4) g at 270°C. Slight gains were observed for all test temperatures between 450°C and 750°C, with maxima in the mean values at 510°C and 630°C of 0.001(1) g and 0.001(4) g respectively. It should be noted that the wear data at 570°C show a departure from the general trend and repeated experiments indicate the 570°C situation needs further attention. The following discussion focuses on the situation at room temperature and 750°C.

The coefficient of friction values measured during the tests showed an initial period of rapid change, before, in many cases, settling down into a ‘steady state’ situation with less variation. The data in Fig. 31 show no significant changes with time after an initial peak at the very beginning of the test. This indicates the rapid onset of debris generation (up to 450°C) or ‘glaze’ layer formation (~450°C and above, almost immediate at 750°C), with the lack of frictional variation during the “steady state” stage being due to the continued presence of debris or ‘glaze’ on the worn surfaces (Fig. 24). Coefficient of friction levels (Fig. 31) are significantly lower for ‘glaze’ covered surfaces (i.e. 750°C) than for loose debris covered surfaces (i.e. room temperature).

#### **4.4.2 Studies of Wear-affected Surfaces Produced during Sliding of Nimonic 80A against Stellite 6 at 20°C**

##### **4.4.2.1 Scanning Electron Microscopy (SEM)**

The top layer of the wear surface after sliding at 20°C (Fig. 24) consisted of a loosely bound non-compacted oxide that was easily detachable by brushing or light polishing.

Underneath this layer, there was a more compacted layer that was not clearly apparent using optical and scanning electron microscopy [113].

Analysis of the surfaces reveals the presence of oxygen and elements from Nimonic 80A (typically Ni/Cr) and Stellite 6 (Co/Cr). The results indicate elemental transfer from the counterface to the specimen and mixing of the transferred and host element oxides. In this section, attention is focussed on the surface layers produced at 20°C [113].

#### ***4.4.2.2 Transmission Electron Microscopy (TEM)***

Fig. 32a shows a cross-sectional TEM image of the wear-affected Nimonic 80A surface, revealing the interface between the Nimonic 80A substrate and the compact 'glaze' layer (the loosely bound uncompacted oxide debris layer was not visible in this area) [113]. The associated selected area diffraction (SAD) pattern (Fig. 32c) is dominated by Debye rings and some well-defined Bragg reflections. Dark-field images (Fig. 32e,f) reveal that the latter correspond to irregular shaped Nimonic 80A crystals of several hundred nanometres diameter, in a layer up to 1 µm from the 'glaze' layer / substrate interface. The 'glaze' layer shows a very different morphology, consisting of small and misoriented crystals produced by fragmentation (Fig. 32b, e), of typical diameter of 5 to 20 nm. Although the adhesion between the 'glaze' layer and Nimonic 80A substrate was generally good, cracks were visible in some areas.

Fig. 33 shows a HAADF-STEM overview image of the FIB prepared cross-section described in the previous paragraph [113]. This is consistent with the structural variations observed by TEM. Two different areas are revealed for the substrate: a uniform "bulk" area and a large grained structure about one micron below the interface with the 'glaze' layer. The latter exhibits a fine-grained structure (5 - 20 nm) with irregular shaped grain boundaries. The particles are larger close to the interface (up to about 50 nm). Furthermore, the strong Z-dependence of the HAADF-STEM image reveals several metal particles in the (oxidised) 'glaze' layer as well as low-density material at the interface.

Fig. 34 shows examples from a STEM line trace of nano-diffraction patterns, taken using a ~30 nm probe [113]. As previously, only small randomly oriented crystals are observed in the 'glaze' layer and at the interface. The larger grains in the alloy

exhibit various crystallographic orientations; some of them well defined and similar to those expected for Nimonic 80A.

Fig. 35 shows EDX analyses of the 'glaze' layers, together with their reference areas [113]. The quantification is based on theoretical k-factors and uses a thickness correction for an estimated 150 nm sample thickness (EELS thickness measurements indicate a thickness of 2-3 nm mean free path). Quantitative analysis of the Nimonic 80A layer (Area 1) gives the characteristic composition of the bulk alloy (Table 5), apart from a slightly higher silicon concentration and a small amount of cobalt.

Analysis of the 'glaze' layer shows that it is essentially oxidised Stellite 6, with a significant contribution of between 15-20% Ni from the Nimonic 80A.

The interface layer consists of a mixture of Nimonic 80A and Stellite 6, with a higher than average titanium concentration [113]. HAADF-STEM EELS/EDX line traces across the interface (Fig. 36) show the transition between the 'glaze' layer and the Nimonic 80A substrate, based on the cobalt and nickel concentrations; the composition of the 'glaze' layer is locally inhomogeneous (Figs. 36 and 37). There are some variations in the chromium, cobalt and oxygen concentrations as well as a few distinct particles with a high nickel concentration. Nevertheless, the overall concentrations are relatively uniform throughout the 'glaze' layer, e.g. no nickel concentration gradient was observed. The line traces further reveal the preferential formation of titanium and aluminium oxides in a ~100 nm thick layer at the interface. Slight chromium depletion is observed in the substrate close to the interface, with a corresponding chromium enrichment in the first ~300 nm of the 'glaze' layer.

Similar areas of enrichment / depletion have been found at other locations along the interface; an example is given at a higher spatial resolution in Fig. 37 [113]. Furthermore, this line trace also confirms aluminium enrichment at the interface; moreover, this Al<sub>2</sub>O<sub>3</sub> layer is between the TiO<sub>2</sub> layer and the Nimonic 80A substrate. Aluminium (in Al<sub>2</sub>O<sub>3</sub>) enrichment is further responsible for the dark areas in the HAADF-STEM image, leading from the interface into the substrate (Fig. 26).

The atomic numbers of chromium (24), cobalt (27) and nickel (28) are similar and compositional variations of these main elements do not explain the strong contrast observed in the HAADF-STEM image (Fig. 38) [113]. However, the EDX/EELS

line traces reveal a low oxygen concentration for the bright areas, indicating that the image mostly reflects the oxidation state. Furthermore, a low oxygen concentration coincides with a low chromium concentration; local EDX analysis shows a low chromium and oxygen concentration for the particles that appear bright in the image. This implies that some of the nickel and cobalt particles are not completely oxidised.

EDX line traces in an area up to about one micron below the interface reveal the preferential segregation of light elements, especially aluminium and in some cases titanium (Fig. 39) [113]. This segregation is also visible in the HAADF-STEM images as thin lines (<10 nm diameter) oriented parallel to the interface (Figs. 33, 38 and 39). It is noted that the peaks of Ti and Al are overlapped away from the interface, which indicates the presence of sub-microscopic  $\gamma'$ -phase,  $\text{Ni}_3\text{Al}$  or  $\text{Ni}_3(\text{TiAl})$  particles, as expected following ageing [113].

These results clearly indicate the formation of a wear resistant nanostructured surface during sliding wear of Nimonic 80A against Stellite 6 at 20°C using a speed of  $0.314 \text{ m}\cdot\text{s}^{-1}$  under a load of 7N [113]. The analyses reveal the complex structure of this surface, which consists of multiple layers:

- 1) A loose, uncompacted, highly oxidised layer.
- 2) A nano-crystalline (5-20 nm grain diameter) compacted layer mostly consisting of oxides of elements originating both from Stellite 6 and Nimonic 80A. The nickel concentration (from the Nimonic 80A) is uniform throughout the whole layer, except for the presence of several larger non-oxidised particles that were randomly dispersed in the glaze.
- 3) Larger particles with a diameter of up to 50 nm were observed in a layer of about 300 nm at the base of the 'glaze' layer. The compositions indicate the presence of elements from both Stellite 6 and Nimonic 80A, but chromium-enriched.
- 4) The chromium-rich phase gradually gave way to a titanium (oxide)-rich phase of about 100 nm thickness, followed by an aluminium (oxide)-rich phase of about 50 nm thickness, at the interface with the Nimonic 80A substrate.
- 5) Adjacent to the interface with the 'glaze' layer, the Nimonic 80A substrate exhibited a large-grained structure (of diameter of several hundred

nanometres). Slight chromium depletion was observed. The precipitation lines (diameter <10 nm) indicated that aluminium-, and in some cases titanium-, enriched phases formed near the large-grained structures. The larger dark areas perpendicular to the interface were also due to aluminium enrichment.

- 6) A uniform “bulk” Nimonic 80A composition was observed at depths greater than one micron below the interface.

The first key process in the development of nano-structured ‘glaze’ layers involves oxidation of the contacting surface/particles subjected to high mechanical stress due to rotation of the counterface. The ‘glaze’ layer, consisting mainly of the oxides of the elements originating from the contacting surfaces, acted as a barrier that separated the substrate from the environment. Although the mechanical effect would continue to influence the ‘glaze’ layer and subsurface deformation, the subsequent oxidation process is controlled by oxygen species and substrate element diffusion, and the thermodynamic nature of the relevant oxides. The observed sequential existence of the oxides  $\text{Cr}_2\text{O}_3/\text{TiO}_2/\text{Al}_2\text{O}_3/\text{substrate}$  at the interface can be understood in terms of thermodynamics. Fig. 40a indicates the oxidation tendencies of relevant elements [113]. The dissociation partial pressures for  $\text{Al}_2\text{O}_3$ ,  $\text{TiO}_2$ ,  $\text{Cr}_2\text{O}_3$ ,  $\text{NiO}$  and  $\text{Co}_3\text{O}_4$  follow the same trend in the range of temperatures  $25^\circ\text{C}$ - $1000^\circ\text{C}$ .  $\text{Al}_2\text{O}_3$ ,  $\text{TiO}_2$  and  $\text{Cr}_2\text{O}_3$  are more likely to develop with increasing temperatures. Although the temperature generated was not measured, the relatively fast kinetics of oxidation, as evidenced by the rapid formation of the ‘glaze’ layer, indicates the generation of relatively high temperatures, sufficient for such oxidation to occur.

Additionally, it is apparent that the high Cr activity in both counterface and sample materials leads to the formation of  $\text{Cr}_2\text{O}_3$  preferentially in the early stages of the process. When oxygen diffuses inwards, Ti in the  $\gamma'$  phase is favourably oxidised. The formation of  $\text{TiO}_2$  gives rise to a decrease in Ti activity and, correspondingly, the Al activity in the  $\gamma'$  phase increases and  $\text{Al}_2\text{O}_3$  becomes a favourable product, as described for oxidation of TiAl in air [114,115].  $\text{NiO}$  and  $\text{Co}_3\text{O}_4$  are much less stable than  $\text{TiO}_2$  and  $\text{Al}_2\text{O}_3$ , which is the reason why some particles of Ni and Co have not been oxidised in the wear process. These oxides ( $\text{TiO}_2$  and  $\text{Al}_2\text{O}_3$ ) formed beneath the ‘glaze’ layer, play an important role in providing support additional to that

provided by the substrate, to sustain the 'glaze' layer and prevent it from collapsing [2].

#### ***4.4.3 Nano-scale Microscopy of 'Glazed' Layers Formed during High Temperature Sliding Wear at 750°C***

The spectrum from EDX analysis of the surface generated under sliding wear at  $0.314 \text{ m.s}^{-1}$  and  $750^\circ\text{C}$  for 4,522 m, Fig. 40b, reveals the dominant presence of Co, Ni, Cr and O on the 'glaze' surface [19,24]. Quantification of the results on average gives 34.2% Co, 36.2% Cr, 16.7% Ni, 3.8% Si and 1.3% Fe (all at%). However, analysis by TEM-EDS showed some location-to-location variation. The dominant phases identified by XRD included  $\text{CoCr}_2\text{O}_4$  and  $\text{Ni}_{2.9}\text{Cr}_{0.7}\text{Fe}_{0.36}$ .

Fig. 41a is a cross-sectional composite TEM micrograph of the surface formed during wear [19,24]. It reveals the surface layer (glazed surface), the deformed substrate and the 'glazed' layer/substrate interface. The wear-affected region (total thickness  $\sim 3 \mu\text{m}$ ) consists of three layers; the top most layer (the 'glaze' layer) has a uniform grain structure of size 5 to 15 nm, some of the grains displaying contrast, while the dislocation density in this area is low. The interfacial layer consists of grains of 10-20 nm and has a higher dislocation density. The layer just beneath the interfacial layer shows subsurface deformation and elongated grains. The SAD pattern from the 'glaze' layer (Fig. 42) consists of spots arranged in concentric circles, indicating the presence of small grains with high angle boundaries, multiple boundaries and large misorientations (formation of misorientated lattice-fragmentation). The poorly-defined irregular boundaries indicate non-equilibrium high-energy configuration. The indexed SAD pattern also revealed the presence of oxides of Ni, Cr and Co (indexing not shown here).

Sub-surface deformation is illustrated in Fig. 41b [19,24]. Dislocations, present as networks inside the deformed (elongated) grains, have been observed in the deformed substrate. Shearing deformation took place in the substrate as a response to the sliding process.

The present results clearly indicate the formation of a nano-structured 'glaze' oxide layer during high temperature sliding wear under the specified conditions. The creation of nano-structures is confirmed by the STM topography, indicating grains of between 5 and 10 nm (Fig. 43) [3,19,20,24]. These results again demonstrate that

such a nano-structured surface is extremely effective in conferring high resistance to wear.

It has been indicated by various authors [3,19,20,110] that, in many systems, surfaces with ultra-fine structure are generated during high temperature sliding wear. Mechanical mixing involving repeated welding, fracture and re-welding of the debris generated from both contacting surfaces is responsible for the generation of the ultra-fine structured surfaces. Moreover, the detailed TEM studies presented here has enabled understanding of the formation mechanisms of wear resistant nano-structured surfaces.

It is clear that the initial processes responsible for generating the ‘glazed’ layer at both 20 and 750°C are ‘deformation of the surface’, ‘intermixing of the debris generated from the wear and the counterface surfaces’, ‘oxidation’, ‘further mixing’ and ‘repeated welding and fracture’. These processes are aided by high temperature oxidation and diffusion. The positron annihilation studies confirmed the presence of vacancy clusters consisting of five vacancies [110].

The next stage in the process involves deformation of oxides and generation of dislocations, leading to the formation of sub-grains. These sub-grains are then further refined, with increasing misorientation resulting in nano-structured grains with high angle boundaries (a process called “fragmentation”), a non-equilibrium state indicated by poorly defined and irregular grain boundaries. High internal stress is created inside the grains; the dislocation density and arrangement depend on the grain size, with smaller grains containing fewer dislocations. The process leads to the formation of high energy grain boundaries with a high defect density [116-122].

#### ***4.4.4 Other Systems***

Such nano-structured ‘glaze’ layers are not unique to Nimonic 80A when slid against Stellite 6 (0.314 m.s<sup>-1</sup>, 7N load, 4,522 m sliding distance). For example, using AFM, Incoloy MA956 has also been shown to form nano-structured ‘glaze’ layers when slid against Stellite 6 [22] and Incoloy 800HT at 750°C (Fig. 44) [123]. In the case of the Incoloy MA956 / Stellite 6 system, this nano-structured ‘glaze’ formed has been found to originate from both Co-Cr-dominated oxide debris at 0.314 m.s<sup>-1</sup> and Fe-Cr-dominated debris at 0.905 m.s<sup>-1</sup>; the sliding speed and composition having no noticeable affect on ‘glaze’ structure with this latter system.



## **5.0 Wear Maps: A Useful Design Aid for Selecting Wear Resistant Materials and Surfaces**

### **5.1 Introduction**

Lancaster [25], Welsh [26,27], So [28,29], Rose [2], Inman [3, 20-23] and others [41,85] have shown that various combinations of load, temperature and sliding speed can significantly affect wear behaviour, regardless of whether or not a protective 'glaze' can form.

Several authors have also constructed wear maps in an attempt to present wear data in a more easily understood format, allowing prediction of likely wear mode under specified sliding conditions. Lim [124,125] (Fig. 45), Childs [126] (Fig. 46a) and, more recently, Riahi and Alpas [127], Chen and Alpas [128], Yang *et al.* [129], Grimanelis and Eyre [130,131] and Elleuch *et al.* [132] have constructed wear maps for various sliding systems based on load / pressure and sliding speed. Other wear related parameters have also been used and Kato and Hokkirigawa [133] developed an abrasive wear map using 'degree of penetration (of asperities)' and 'shear strength at the contact interface' as key parameters (Fig. 46b). Adachi *et al.* [134] used 'severity of contact' and 'thermal severity of contact' for ceramic wear.

The following section discusses recent developments in high temperature wear maps made by the present authors, following a brief review of earlier work by Lim.

### **5.2 Work by Lim**

Lim [124] attempted to collate the available data for mild steels into a single comprehensive wear map (Fig. 45) using dimensionless parameters of Normalised Velocity versus Normalised Load. This showed that the selection of sliding conditions and configuration can greatly affect the wear behaviour and transitions observed, with load, sliding speed and temperature potentially having a large influence on the boundaries between the different modes of wear.

For example, it can be seen that, if a relatively high fixed load is used, with increasing sliding speed, a transition from severe-to-mild wear is observed (Welsh [26]). More complex forms result at lower loads when sliding speeds are at much higher values (Archard and Hirst [31], and Welsh [26]). Similarly, if speed is fixed at an arbitrarily

low value, increasing load may see a switch from mild to severe wear (Ward [124]) whilst a higher speed can result in a more complex curve (Welsh [26]). To summarise, when two surfaces are worn against each other, the outcome can be a variety of apparently contradictory results. Thus, mapping is necessary to understand the relative behaviours in different tests and the potential outcome under a given set of sliding conditions.

### 5.3 Dissimilar Interfaces

As discussed previously, Inman, Rose and Datta [3,21,22] studied the effects of temperature and sliding speed on several Superalloys using dissimilar interfaces. This section refers specifically to Nimonic 80A [21] and Incoloy MA 956 [22] worn against Stellite 6. For both systems, the data have been used to create simple ‘temperature versus sliding speed’ wear maps [21,22] (Figs. 47 and 48). The weight change data are presented in Figs. 30 and 49.

For both systems [22], mild wear with low weight loss dominates at  $0.314 \text{ m.s}^{-1}$  regardless of temperature (Figs. 47 and 48). Up to  $450^\circ\text{C}$ , a low temperature mild wear regime occurs, with the wear surfaces separated by a layer of Co-Cr oxide particles (i.e. loose debris – Figs. 24a and 13a – potentially underlain by a more compacted layer – Section 4.3.2), primarily sourced from the Stellite 6. Increased agglomeration and sintering of the debris has been observed at  $390^\circ\text{C}$ , with isolated patches of ‘glaze’ at  $450^\circ\text{C}$  (although most of the oxide remained as loose debris). Mild wear persists between  $510^\circ\text{C}$  (Figs. 24b and 13b) and  $750^\circ\text{C}$  (Figs. 24c and 13c), with the still Stellite 6-sourced oxide sintering to form comprehensive ‘glaze’ layers with nanostructured surfaces [3,19,20,22,24] (discussed in Section 4.4); with extremely low weight change with some very slight weight gains due to oxide development (Figs. 47 and 48). At all temperatures, there was virtually no initial severe wear period, with sufficient Co-Cr oxide debris forming extremely rapidly.

The Nimonic 80A versus Stellite 6 system [21] is characterised by three distinct wear regimes at  $0.654 \text{ m.s}^{-1}$  (Fig. 47); up to  $390^\circ\text{C}$ , a low temperature ‘low weight loss’ mild wear regime (Fig. 30) was observed, with a layer of Stellite 6-sourced Co-Cr oxide particles separating the wear surfaces (Fig. 41a). A metallic severe wear (especially of the Nimonic 80A) regime dominated between  $450^\circ\text{C}$  and  $630^\circ\text{C}$  (Fig. 25b) with no visible oxide between  $450^\circ\text{C}$  and  $570^\circ\text{C}$ . This severe wear regime

was also observed at 630°C, now accompanied by a small amount of NiO and Cr<sub>2</sub>O<sub>3</sub> generated by thermal and frictional heating; however, this oxide was insufficient to impede metal-to-metal contact. and may instead have assisted wear by abrasion.

A mild oxidational wear regime was evident at 690°C and 750°C, although Nimonic 80A weight losses (Fig. 30) remained high due to abrasion. This abrasion was caused by large amounts of Nimonic 80A-sourced NiO and Cr<sub>2</sub>O<sub>3</sub>, which (unlike Co-Cr oxides generated at 0.314 m.s<sup>-1</sup>) showed little tendency to sinter and form 'glaze'.

The sliding behaviour at 0.905 m.s<sup>-1</sup> exhibited the same three sliding regimes observed at 0.654 m.s<sup>-1</sup> [21]. However, greater frictional heating resulted in a downward shift in the low-temperature-mild-wear-to-severe-wear transition from 390-450°C to 270-390°C. Increased amounts of loose NiO and Cr<sub>2</sub>O<sub>3</sub> debris occurred at 570°C upwards, but not sufficient to lower the severe-wear-to-abrasive-mild-wear transition from 690°C.

The behaviour for the Incoloy MA956 versus Stellite 6 system follows the same general pattern at 0.654 and 0.905 m.s<sup>-1</sup> as that of Nimonic 80A versus Stellite 6 [22]. (Fig. 48). However, in this case, the high temperature mild wear regime confers protection, with the mixed Fe-Cr and Co-Cr oxides at 0.654 m.s<sup>-1</sup> or the largely Fe-Cr oxides at 0.905 m.s<sup>-1</sup> readily sintering to form 'glaze' layers. Such 'glaze' is observed from 510°C upwards, (450°C after extended sliding at 0.905 m.s<sup>-1</sup>) after a period of early severe wear (Fig. 14b) that decreases in length with increasing temperature. At and above 630°C, rapid 'glaze' formation (Fig. 14c) almost completely eliminates early severe wear (Fig. 49).

A later study by Inman and Datta [23] looked to improve Nimonic 80A versus Stellite 6 wear map resolution between 630 and 750°C by adding extra test sliding speeds. Rudimentary wear maps were also developed separately for Nimonic 80A and Incoloy MA956 as sample materials versus an Incoloy 800HT counterface [3].

Such sliding studies indicate the potential for complex behaviour during sliding of dissimilar materials. In such cases, the necessity for mapping wear behaviour to assist prediction of mild or severe wear is important, if potentially catastrophic material failure is to be avoided.

### **5.3.1 Oxide Chemistry**

These studies also indicate that the readiness for a wear-generated oxide to form 'glaze' layers depends not just upon the sliding conditions, but also on the chemical composition of the oxide. For example, Co-Cr-based oxides readily form wear protective 'glaze' layers at high temperature [1, 19-24], while Fe-Cr-based oxides [1,22] can also form fairly robust wear protective layers under adverse sliding conditions. NiO and Cr<sub>2</sub>O<sub>3</sub> oxides produced from Nimonic 80A do not too readily sinter together to develop into 'glaze' and can actually enhance wear by abrasion [1,4,5]; however, NiO (produced from Nickel 200<sup>TM</sup>) [1] has been shown to easily form a 'glaze' in the absence of Cr<sub>2</sub>O<sub>3</sub>.

## **6.0 Summary**

In writing this chapter strong emphasis has been placed on scientific principles underpinning the phenomenon of high temperature wear. At the outset a review of some of the well-known and relevant wear theories and models, supported by experimental findings on conventional and advanced materials, has been presented. This background information has provided a framework to discuss new areas of high temperature wear. In this context the high temperature wear behaviour of those materials which have provided new information has been considered. Particular attention has been focussed on high temperature wear behaviour of Oxide Dispersion Strengthened and Nimonic alloys, and intermetallic materials involving like-on-like and unlike-on-unlike combinations. The most significant part of this chapter includes the exposition of the phenomena of glaze formation at fundamental levels. Here the novel aspect is the inclusion of nano-scale elaboration of the processes of glaze formation underpinned by fundamental information gathered from TEM and STM/STS investigations. In this area significant reliance has been placed on the authors' own research.

## Glossary

<b>abrasion</b>	The removal of material from a solid surface by the mechanical action of another solid. The second solid may be in the form of a second body (the opposing sliding surface) or third body (wear debris).
<b>abrasive wear</b>	The removal of surface material from an object by the action of another agent or medium. This may be the surface of another object or by hard particles trapped between the two interacting surfaces – referred to as ‘two body’ and ‘three body’ abrasion respectively. The hard particles or surface must be 1.3 times harder than the soft material from which material is removed.
<b>adhesion / cohesion</b>	<p>The action of intermolecular forces at surfaces or interfaces in close contact, holding those surfaces together. Such forces may include chemical bonding (chemical adhesion), inter-solubility (diffusive adhesion), Van-der-Waals forces (dispersive adhesion) and electrostatic forces (electrostatic adhesion). Surface interlocking may also occur (mechanical adhesion) via material filling surface voids or pores. Adhesion is of greater influence during contact of clean metallic surfaces (and thus during severe wear), as there are no contaminants to prevent this contact. Adhesion is also more effective in a vacuum, where there is no surrounding atmosphere to affect it.</p> <p>Adhesion is normally used to describe attraction between dissimilar molecules and cohesion between like molecules.</p>
<b>asperity</b>	A protruding, raised area of (sliding) surface.
<b>block-on-cylinder</b>	A test configuration used to study unidirectional sliding wear, with the ‘block’ (either stationary or in reciprocating motion) as the sample material and the ‘cylinder’ (normally rotating) as the counterface.
<b>coefficient of friction</b>	Dimensionless value describing the resistance experienced by two surfaces in movement against each other. The higher the value, the greater the ability to resist movement. The ‘frictional force’ is that which needs to be applied to overcome this resistance to movement.
<b>compacted oxide layer</b>	Often wear-protective layers of oxide are formed as a ‘tribocorrosion’ product, when two metals (or a metal and ceramic) are slid against each other at high temperature in an oxygen-containing atmosphere.

<b>compacted particles</b>	Debris forming a compacted oxide layer.
<b>counterface (countersurface)</b>	The material or surface sliding against the sample.
<b>critical oxide thickness ('ξ')</b>	According to Quinn's oxidational wear model [63], this is the maximum thickness of compacted oxide layer or 'glaze' that can develop and remain mechanically stable. Beyond this, the oxide becomes unstable, generating a wear particle.
<b>critical transition temperature</b>	The minimum temperature according to Jiang [17] at which sintering can occur within a compacted oxide layer, allowing a solid wear-protective layer (or 'glaze') to form on top of it before it is broken down.
<b>cross-slip</b>	Transfer of (screw) dislocation glide from one slip plane to another during deformation.
<b>cutting</b>	The physical deformation due to a harder asperity or third body being pushed through a softer material where adhesion is high. The movement of the harder material over the softer material results in the creation of a deeper groove upon the sample surface than seen with 'wedge-forming' or ploughing, with long strips of debris forming at the point of contact.
<b>delamination</b>	Fatigue-related material loss by repeated loading and unloading of surface layers, as asperities of the opposite surface pass over it. This assists the propagation of sub-surface cracks, which link together and allow surface material to break away. Such a process leads to the generation of the large, flat, angular debris seen during severe wear.
<b>dissimilar interface system</b>	A configuration where the sample and counterface are of different materials.
<b>ejection</b>	The removal of wear debris from the sliding wear interfaces such that it can no longer play an 'active' part in the wear process.
<b>fretting</b>	Damage due to repeated relative motion of sliding surfaces against each other, for example, due to vibration or oscillation.
<b>'glaze'</b>	Compacted oxide layer, usually referring to a more wear protective, sintered form generated (normally) at elevated temperatures.

<b>High Angle Annular Dark Field in STEM</b>	Images formed by gathering scattered electrons with an annular dark field detector. An ‘Annular Dark Field’ (ADF) image generated only by very high angle, incoherently scattered electrons, is highly sensitive to variations in atomic number of the elements in the sample (Z- contrast images) and is hence known as ‘High Angle Annular Dark Field’ or HAADF.
<b>HIPped (hot isostatically pressed)</b>	A method of alloy or material production by powder metallurgy methods, using a combination of temperature and (isostatic) pressure to produce the final item.
<b>intermetallic</b>	Materials composed of defined proportions of two or more metallic elements and possibly one or more non-metallic elements. Such materials typically have a highly ordered crystal lattice structure composed of the constituent parts, but not necessarily the same as any of the constituent parts.
<b>ion-implantation</b>	The implantation of ions of one material into the crystal lattice of another solid, thereby bringing about a desired change in the physical properties of that solid (i.e. doping).
<b>material transfer</b>	Transfer of material at the wear interface from one wear surface to the other.
<b>mechanical alloying</b>	The mixing of two or more solid phase materials to produce material of different composition and possibly phase to either of the original materials. During sliding wear (i.e. severe wear), this may happen where the two parent sliding surfaces are of different composition, due to material transfer between and mixing at the sliding interface. This mechanically alloyed material may then potentially re-adhere to either parent sliding surface.
<b>mild wear</b>	Wear in which direct contact between the sliding surfaces are separated by corrosion debris (generally oxide), often less than 1 $\mu\text{m}$ diameter. This debris may take the form of compacted oxide or ‘glaze’ layers. Where the two sliding surfaces are metallic, the debris being generally non-metallic prevents adhesion and (metallic) transfer. Coefficient of friction values are thus usually much lower. Wear values are generally, but not always, lower than severe wear, however, such debris can act abrasively and instead enhance wear.
<b>‘Orowan’ stress</b>	The stress required to bow a dislocation between particles or impurities, acting as obstacles within a crystal lattice.

<b>oxide dispersion strengthened (ODS) alloy</b>	An alloy in which a fine dispersion of oxides have been introduced, to strengthen the material by interfering with the operation of slip systems during material deformation.
<b>phase transition</b>	Thermally or mechanically induced change in crystallographic structure, for example, from ‘face-centred cubic’ to ‘body-centred cubic’ in iron or mild steel, or ‘face-centred cubic’ to ‘hexagonal close-packed’ in cobalt-rich alloys.
<b>pin-on-disk</b>	A test configuration used to study sliding wear, with the ‘pin’ (or in some cases ‘button’ or ‘coupon’) as the sample material and the ‘disk’ as the counterface. The ‘pin’ may be held stationary against a rotating ‘disk’ to study unidirectional sliding wear, or moved backwards and forward against a stationary ‘disk’ to study reciprocating or fretting wear.
<b>ploughing</b>	<p>A general term, covering the three related terms of ‘ploughing’, ‘wedge-forming’ and ‘cutting’, being defined as the physical deformation due to a harder material ploughing through a softer material or rather the work required to carry this out.</p> <p>Ploughing is also referred to more specifically as the physical deformation due to a harder material being pushed through a softer material where adhesion forces are weak. The grooves created are shallower than with ‘cutting’ or ‘wedge-forming’, with lower penetration of the harder asperity or third body into the softer material. Formation of wear debris particles cannot be clearly seen at the point of contact.</p>
<b>Positron Annihilation (PA)</b>	A major technique in Materials Science, originally applied in condensed-matter physics, now widely used in metals and alloys to provide information on defect structures.
<b>precipitate</b>	A metallurgical term for a solid particle or volume of material forming within an alloy, with a composition and possibly crystal structure different from that of the surrounding alloy.
<b>retention</b>	The continued residency of wear debris at the wear interface, such that it may continue to play an active part in the wear process.
<b>‘run-in’ wear</b>	A normally brief period of severe wear due to initial metal-to-metal contact almost always observed before mild wear is established.



<b>sample</b>	The material or surface undergoing wear testing.
<b>Scanning Electron Microscopy (SEM)</b>	A type of microscope in which the surface of a sample is scanned with a high energy beam of electrons. An image of the sample surface is created from secondary electrons that are ejected from it.
<b>Scanning Transmission Electron Microscopy (STEM)</b>	A variation of TEM in which the electrons pass through the specimen and the electron optics focus the beam in to a narrow spot over the sample in a raster. The rastering of the beam across the sample is used to perform various analyses such as annular dark field (ADF) imaging, energy dispersive X-ray (EDX) analysis and electron loss spectroscopy (EELS) simultaneously, allowing direct correlation of image and quantitative data.
<b>Scanning Tunneling Microscopy (STM)</b>	An imaging technique based on the concept of quantum tunneling. In STM a conducting surface is brought very near to the surface (metallic/semiconductor) when a bias between the two allows electrons to tunnel through the vacuum between them. At low voltage the tunneling current is a function of local density of states (LODS) at the Fermi level of the sample. The changes in current accompanying the tip movement over the surface are translated in to an image.
<b>Scanning Tunneling Spectroscopy (STS)</b>	A technique employed within an STM, to probe the local density of electronic states, and band gap of surfaces and materials on surfaces at the atomic scale. The technique allows observation of changes in constant current topographies with tip-sample bias, local measurements of IV curves and tunneling conductance $dI/dV$ . This allows investigations of small areas (5 angstrom diameter, the area in which the tunneling current flows).
<b>scuffing</b>	Roughening of surfaces by plastic flow, whether or not there is material loss or transfer.
<b>Selected Area Diffraction Pattern (SAD)</b>	This technique is generally performed inside a TEM, in which electrons pass through a thinned sample (see 'TEM'). As the wave length (a fraction of a nano-metre) and the spacing between atoms are comparable, the atoms act as diffraction gratings to the electrons. Some of the electrons are scattered to particular angles determined by the material crystal structures (allowing identification and analysis) and form a spot pattern image on the TEM screen.

<b>severe wear</b>	The wear encountered typically where two metallic surfaces are in direct sliding contact, without an intervening compacted oxide or 'glaze' layer, or other protective coating. Such wear is characterised by high coefficient of friction values, high levels of adhesion, plastic deformation and to varying degrees, (mainly metallic) material transfer between the surfaces. Also typical of severe wear is the generation of large, flat, angular, generally metallic wear debris with sizes of up to 0.1 mm (or greater) due to 'delamination'.
<b>sliding wear</b>	The removal of material from wear surfaces due to relative motion of sliding surfaces against each other.
<b>slip direction</b>	The direction on the slip plane with the highest linear density.
<b>slip plane</b>	The crystallographic close packed plane in which dislocation movement can occur.
<b>slip system</b>	A combination of slip planes and directions defined by crystallographic arrangement (i.e. body-centred cubic, face-centred cubic, hexagonal close-packed).
<b>'third body' / 'three body' wear</b>	The interaction of two wear surfaces during sliding, in combination with a third agent (i.e. debris). This third agent may be termed 'active' (it is retained between the wear surfaces and modifies the wear process) or 'passive' (it is ejected and has no effect).
<b>torque transducer</b>	A device for measuring torque in a rotating system. In tribology, changes in torque due to sliding surface contact can be used to determine the coefficient of friction.
<b>Transmission Electron Microscopy (TEM)</b>	A widely used technique in Materials Science where an electron beam is transmitted through a thinned sample placed in vacuum with a typical energy of 100-400 KeV. The electron beam is then focussed by a series of magnetic field lenses into a typical spot of diameter 1-10nm. A TEM image is created from those electrons that pass through the sample.
<b>tribocorrosion, tribo-oxidation</b>	The enhanced generation of corrosion product (normally oxide) during sliding wear. The conjoint action of tribology and corrosion / oxidation.
<b>tribology</b>	The study of the science and technology of interacting surfaces in relative motion, and including the related subjects of lubrication, friction and wear. Derived from the Greek verb τριβο ("tribo"), meaning 'to rub'.

<b>‘two body’ wear</b>	The interaction of two wear surfaces during sliding, in the absence of a third agent (i.e. wear debris) between the wear surfaces.
<b>unidirectional sliding</b>	Where the sample and counterface move in only one direction relative to each other.
<b>Van-der-Waals’ forces</b>	Attractive forces between unbonded atoms and molecules (significant for very small particles of less than 5 $\mu\text{m}$ in diameter).
<b>Vickers Hardness Number (VHN)</b>	A parameter defining the hardness of an engineering material. The Vickers Hardness Number is that obtained by application of a predefined load through a diamond pyramidal (or Vickers) indenter. The size of the indent created is used to obtain a measure of materials hardness.
<b>wear</b>	Loss of material from one or more surfaces by mechanical action.
<b>wear behaviour, wear regime, wear mechanism</b>	The type of wear observed (i.e. mild or severe wear).
<b>wear debris</b>	The material removed from sliding surfaces during wear. This may be metallic (dominant during severe wear) or oxide (dominant during mild wear).
<b>wear map, wear mechanism map</b>	A plot that shows the effect on wear mechanism of two or more sliding variables (i.e. load, temperature, sliding speed), allowing prediction of wear mechanism where the values of these variables are known.
<b>wear rate</b>	The rate of material removal during sliding.
<b>wear volume</b>	The volume of material removed during sliding.
<b>wedge-forming</b>	The physical deformation due to a harder asperity or third body being pushed through a softer material where adhesion is moderate. Material is pushed up ahead of asperities on the counterface, resulting in a grooved wear scar with transverse cracks. The depth of groove created is lower than for the ‘cutting’ model, but higher than for ‘ploughing’.

## List of Symbols Used

$A$	i) True area of contact; ii) Hamaker constant;
$P$	Applied load;
$H$	Material indentation hardness;
$W$	Work Volume;
$L$	Sliding distance;
$K_a$	Probability of a wear particle being generated;
$K_l$	'K factor' ( $K_l=K_a/H$ );
$D$	Depth of wear;
$p$	Mean pressure (load / area);
$v$	Speed;
$t$	i) Time of sliding; ii) Time required to grow oxide layer of critical thickness;
$F$	Force of attraction;
$R$	i) Radius of particle of sphere; ii) Gas constant;
$r$	distance affecting mutual action of Van der Waals' forces;
$\gamma$	Surface energy;
$\gamma_o$	Surface energy at standard temperature and pressure;
$E$	Activation energy for bonding;
$K_p$	Oxidation rate (parabolic rate constant);
$A_p$	Arrhenius constant;
$Q_p$	Activation energy for oxidation;
$T, T_o$	Temperature in Kelvin (absolute temperature);
$P$	Applied load;
$H$	Indentation hardness;
$W$	Work Volume;
$L$	Sliding distance;
$A$	True area of contact;
$\xi$	Critical oxide layer thickness;
$1/K_a$	Number of encounters (contacts between surfaces) required to generate an oxide layer of critical thickness;
$\tau$	Length of time of each encounter (contact between surfaces);
$V$	Sliding speed;
$d$	Distance for which sliding contact is maintained;

$\Delta m$	Growth of oxide per unit area;
$f$	Mass fraction of oxide;
$\rho$	Oxide average density;
$F$	Contact frequency;
$K_{Ic}$	Fracture Toughness

## References

- [1] P.D. Wood, Ph.D. Thesis “The Effect of the Counterface on the Wear Resistance of Certain Alloys at Room Temperature and 750°C”, Northumbria University, UK (1997).
- [2] S.R. Rose, Ph.D. Thesis “Studies of the High Temperature Tribological Behaviour of Some Superalloys”, Northumbria University, UK (2000).
- [3] I.A. Inman, Ph.D. Thesis “Compacted Oxide Layer Formation under Conditions of Limited Debris Retention at the Wear Interface during High Temperature Sliding Wear of Superalloys”, Northumbria University, UK (2003), published by ‘Dissertation.com’ (2006).
- [4] F.H. Stott, D.S. Lin, G.C. Wood “The structure and mechanism of formation of the “glaze” oxide layers produced on Ni-based alloys during wear at high temperatures”, *Corrosion Science* **13** (1973) 449 - 469.
- [5] M. Johnson, P. Moorhouse, J.R. Nicholls, DTI Industry Valve Project, 61-68 (1990).
- [6] J-N. Aoh, J-C. Chen “On the wear characteristics of Co-based hard-facing layer after thermal fatigue and oxidation”, *Wear* **250-251** (2001) 611.
- [7] Singh, J. and Alpas, A.T. “High-temperature Wear and Deformation Processes in Metal Matrix Composites,” *Metallurgical and Materials Transactions A* **27** (1996) 3135-3148.
- [8] F.H. Stott, J. Glascott, G.C. Wood “Factors affecting the progressive development of wear-protective oxides on iron-base alloys during sliding at elevated temperatures”, *Wear* **97** (1984) 93-106.
- [9] M.G. Gee, N.M. Jennett “High resolution characterisation of tribochemical films on alumina”, *Wear* **193** (1995) 133-145.
- [10] P.D. Wood, P.K. Datta, J.S. Burnell-Gray, N. Wood “Investigation into the high temperature wear properties of alloys contacting against different counterfaces”, *Materials Science Forum* **251-254** (1997) 467-474.
- [11] Wisbey, C.M. Ward-Close, “Wear resistant surfaces on high temperature titanium alloy and titanium aluminide by diffusion bonding”, *Materials Science and Technology* **13** (1997) 349-355.
- [12] J. Jiang, F.H. Stott, M.M. Stack, ”The effect of partial pressure of oxygen on the tribological behaviour of a Ni-based alloy, N80A, at elevated temperatures”, *Wear* **203-204** (1997) 615-625.
- [13] X.Y. Li, K.N. Tandon “Microstructural characterization of mechanically mixed layer and wear debris in sliding wear of an Al alloy and an Al based composite”, *Wear* **245** (2000) 148-161.
- [14] J. Jiang, F. H. Stott, M. M. Stack “A generic model for dry sliding wear of metals at elevated temperatures” *Wear* **256** (2004) 973-985.
- [15] J. Jiang, F. H. Stott, M. M. Stack “The role of triboparticulates in dry sliding wear” *Trib. Int.* **31-5** (1998) 245-256.
- [16] J. Jiang, F. H. Stott, M. M. Stack “Characterization of wear scar surfaces using combined three-dimensional topographic analysis and contact resistance measurements” *Trib. Int.* **30-7** (1997) 517-526.

- [17] J. Jiang, F. H. Stott, M. M. Stack “A mathematical model for sliding wear of metals at elevated temperatures” *Wear* **181-183** (1995) 20-31.
- [18] J. Jiang, F. H. Stott, M. M. Stack “Some frictional features associated with the sliding wear of the Ni-base alloy N80A at temperatures to 250°C” *Wear* **176** (1994) 185-194.
- [19] S. Datta, I. Inman, H.L. Du, Q. Luo “Microscopy of ‘glazed’ layers formed during high temperature wear, Invited Talk at the Institute of Materials”, Tribology Meeting, London, November 2001.
- [20] I.A. Inman, S. Datta, H.L. Du, J.S. Burnell-Gray, S. Pierzgalski and Q. Luo “Studies of High Temperature Sliding Wear of Metallic Dissimilar Interfaces”, *Tribology International* **38** (2005) 812–823.
- [21] I.A. Inman, S.R. Rose, P.K. Datta “Development of a Simple ‘Temperature versus Sliding Speed’ Wear Map for the Sliding Wear Behaviour of Dissimilar Metallic Interfaces”, *Wear* **260** (2006) 919–932.
- [22] I.A. Inman, S.R. Rose, P.K. Datta “Studies of High Temperature Sliding Wear of Metallic Dissimilar Interfaces II: Incoloy MA956 versus Stellite 6”, *Tribology International* **39** (2006) 1361–1375.
- [23] I.A. Inman, P.S. Datta “Development of a Simple ‘Temperature versus Sliding Speed’ Wear Map for the Sliding Wear Behaviour of Dissimilar Metallic Interfaces II” *Wear* **265** (2008) 1592–1605.
- [24] I.A. Inman, S. Datta, H.L. Du, J.S. Burnell-Gray, S. Pierzgalski, Q. Luo “Microscopy of ‘glazed’ layers formed during high temperature sliding wear at 750°C”, *Wear* **254** (2003) 461-467.
- [25] J.K. Lancaster “The Formation of Surface Films at the Transition Between Mild and Severe Metallic Wear”, *Proc. Royal Society London, A* **273** (1962) 466-483.
- [26] N.C. Welsh “The Dry Wear of Steels 1, the General Pattern of Behaviour” *Phil. Trans.*, **257A** (1965) 31-50.
- [27] N.C. Welsh “The Dry Wear of Steels 2, Interpretation and Special Features” *Phil. Trans.*, **257A** (1965) 51-70.
- [28] H. So “Characteristics of Wear Results Tested by Pin-on-Disc at Moderate to High Speeds”, *Tribo. Int.*, **25-5** (1996) 415-423.
- [29] H. So “Wear Behaviours of Laser-Clad Stellite Alloy 6”, *Wear* **192** (1996) 78-84.
- [30] J.F. Archard and W. Hirst “The Wear of Metals under Unlubricated Conditions”, *Proc Royal Society London, A* **236** (1956) 397-410.
- [31] J.F. Archard and W. Hirst “An Examination of a Mild Wear Process” *Proc. Royal Society London, A* **238** (1957) 515-528.
- [32] T.F.J. Quinn “Review of Oxidational Wear. Part 1: The Origins of Oxidational Wear” *Tribo. Int.*, **16** (1983) 257-270.
- [33] H-K. Oh, K-H. Yeon, H.Y. Kim “The Influence of Atmospheric Humidity on the Friction and Wear of Carbon Steels” *Journal of Materials Processing Technology*, **95** (1999) 10-16.
- [34] F.H. Stott and G.C. Wood “The Influence of Oxides on the Friction and Wear of Alloys”, *Tribo. Int.*, **11** (1978) 211-218.

- [35] F.P. Bowden and D. Tabor “Friction, an Introduction to Tribology” Publ. Heinemann, London (1973).
- [36] T.S. Eyre and D. Maynard “Surface Aspects of Unlubricated Metal-to-Metal Wear” *Wear* **18**, (1971) 301-310.
- [37] J.T. Burwell and C.D. Strang “On the Empirical Law of Adhesive Wear”, *J. Applied Physics* **23** (1952) 18-28.
- [38] K. Ludema “Scuffing, Run-in and the Function of Surface Films, Particularly Oxides” *Review Paper for Interdisciplinary Collaboration in Tribology Project, NASA-Lewis* (1981).
- [39] D. Tabor “Wear – A Critical Synoptic View” *Proc. Int. Conference on Wear of Materials, St. Louis, Missouri in April 1977, ASME* (1978) 1-10.
- [40] E.C. Rabinowicz “Friction and Wear of Materials” Publ. New York Wiley (1965).
- [41] P.J. Blau “Mechanisms for Traditional Friction and Wear Behaviour of Sliding Metals” *Wear* **72** (1981) 55-66.
- [42] A. Iwabuchi “The Role of Oxide Particles in the Fretting Wear of Mild Steel” *Wear* **151** (1990) 301-311.
- [43] A. Iwabuchi, H. Kubosawa and K. Hori “The Effect of Oxide Particles Supplied at the Interface before Sliding on the Severe – Mild Wear Transition”, *Wear* **128** (1988) 123-137.
- [44] A. Iwabuchi, H. Kubosawa and K. Hori “The Dependence of the Transition of Severe to Mild Wear on Load and Surface Roughness When the Oxide Particles Are Supplied before Sliding” *Wear* **139** (1990) 319-333.
- [45] E.R. Leheup and R.E. Pendlebury “Unlubricated Reciprocating Wear of Stainless Steel with an Interfacial Air Flow”, *Wear* **142** (1991) 351 – 372.
- [46] C. Colombie, Y. Berthier, A. Floquet and L. Vincent “Fretting: Load Carrying Capacity of Wear Debris” *Trans. ASME* **106F** (1984) 194-201.
- [47] K. Hiratsukam, T. Sasada and S. Norose “The Magnetic Effect on the Wear of Metals” *Wear* **110** (1986) 251-261.
- [48] D.A. Rigney “Transfer, Mixing and Associated Chemical and Mechanical Processes during the Sliding of Ductile Materials” *Wear* **245** (2000) 1 – 9.
- [49] F.H. Stott, J.Glascott and G.C. Wood “Models for the Generation of Oxides during Sliding Wear”, *Proc Royal Society London A* **402** (1985) 167-186.
- [50] J.L. Sullivan and N.W. Granville “Reciprocating Sliding Wear of 9% Cr Steel in Carbon Dioxide at Elevated Temperatures”, *Tribo. Int.*, **17** (1984) 63-71.
- [51] F.H. Stott and D.R.G. Mitchell “The Influence of Coating on Wear at Elevated Temperatures” *Surface Engineering, Volume 1 Fundamentals of Coatings*, Ed. P.K. Datta and J.S. Gray, Royal Society of Chemistry (1993) 141-150.
- [52] J.S. Halliday and W. Hirst “The Fretting Corrosion of Mild Steel” *Proc. Royal Society London, A* **236** (1956) 411-425.
- [53] F.H. Stott “High-Temperature Sliding Wear of Metals”, *Trib. Int.*, **35** (2002) 489-495.



- [54] D.S. Lin, F.H. Stott, G.C. Wood, K.W. Wright and J.H. Allen “The Friction and Wear Behaviour of Nickel-Based Alloys during High Temperature Wear”, *Wear* **24** (1973) 261-278.
- [55] D.S. Lin, F.H. Stott, G.C. Wood “The Effects of Friction and Wear Behaviour of Some Commercial Nickel Base Alloys”, *Trans ASLE* **17, 4** (1973) 251-262.
- [56] F.H. Stott, D.S. Lin, G.C. Wood “The Wear and Friction of Nickel-Base Alloys under Oxidising Conditions”, Proc. 5<sup>th</sup> Eur. Congr. on Corrosion (1973) 452-455.
- [57] F.H. Stott, D.S. Lin, G.C. Wood “‘Glazes’ Produced on Nickel-Based Alloys during High Temperature Wear”, *Nature Physical Science*, **242** (April 2 1973) 75-77.
- [58] F.H. Stott, D.S. Lin, G.C. Wood and C.W. Stevenson “The Tribological Behaviour of Nickel and Nickel-Chromium Alloys at Temperature from 20 to 800°C”, *Wear* **36** (1976) 147-174.
- [59] F.H. Stott, J. Glascott and G.C. Wood “The Transition from Severe to Mild Sliding Wear for Fe-12%Cr-Base Alloys at Low Temperature”, *Wear* **97** (1984) 155-178.
- [60] F.H. Stott “The Role of Oxidation in the Wear of Alloys”, *Tribology International*, **31** (1998) 61-71.
- [61] T.F.J. Quinn “Oxidational Wear”, *Wear* **18** (1971) 413-419.
- [62] T.F.J. Quinn “Computational Methods Applied to Oxidational Wear”, *Wear* **199** (1996) 169-180.
- [63] T.F.J. Quinn “Oxidational Wear Modelling: Part 1”, *Wear* **153** (1992) 179-200.
- [64] T.F.J. Quinn “Oxidational Wear Modelling: Part 2 – The General Theory of Oxidational Wear”, *Wear* **175** (1994) 199-208.
- [65] A. Iwabuchi, K. Hori, and H. Kudo “The Effect of Temperature, Preoxidation and Presliding on the Transition from Severe Wear to Mild Wear for S45C Carbon Steel and SUS 304 Stainless Steel” Proc. Int. Conf. Wear of Materials, New York (1987) 211-220.
- [66] K. Langgath, A. Kluge and H. Ryssel “Wear of Steels After Implantation of Oxygen Ions Or Oxidation at 670K”, *Wear* **155** (1992) 343-351.
- [67] J. Mølgaard “A Discussion of Oxidation, Oxide Thickness and Oxide Transfer in Wear”, *Wear* **40** (1976) 277-291.
- [68] V. Kuzucu, M. Ceylan, H. Çelik and I. Aksoy “Microstructure and Phase Analysis of Stellite 6 Plus 6 Wt.% Mo Alloy” *J. Mat. Proc. Tech.*, **69** (1997) 257-263.
- [69] P. Crook and C.C. Li “The Elevated Temperature Metal-to-Metal Wear Behaviour of Selected Hard Facing Alloys” *Wear of Materials*, ASME Publication 110254, (1983) 272-279.
- [70] M. Bartsch, A. Wasilkowska, A. Czyrska-Filemonowicz and U. Messerschmidt “Dislocation Dynamics in the Oxide Dispersion Strengthened Alloy Incoloy MA956”, *Mat. Sci. Eng.*, **A272** (1999) 152-162.

- [71] A. Fujita, M. Shinohara, M. Kamada and H. Yokota "Improvement of Creep Rupture Ductility in Ni-Base Superalloy Nimonic 80A and Its Material Properties", *Isij International*, **38** (1998) 291-299.
- [72] N. Soda and T. Sasada "Mechanisms of Lubrication by Surrounding Gas Molecules in Adhesive Wear" *ASME Trans., J. Lubr. Technol.*, **100,4** (1978) 492-499.
- [73] W-Z Wu, J-D. Xing and J-Y. Su "An Investigation on Three Body Abrasive Wear Test at Elevated Temperature" *Wear* **210** (1997) 299-303.
- [74] Nam. P. Suh and H.C. Sin "The Genesis of Friction" *Wear* **69**, (1981) 91-114.
- [75] S.L. Rice, F.A. Moslehy and J. Zhang "The Role of Wear Particles in Modifying Coefficients of Friction – Wear Particles: From the Cradle to the Grave", Proceedings of the 18<sup>th</sup> Leeds-Lyon Symposium on Tribology, 3-6<sup>th</sup> September 1991, Lyon, France, Ed. D. Dowson, Publ. Elsevier, 463-467.
- [76] H. Hesmat "The Rheology and Hydrodynamics of Dry Powder Lubrication" *Tribology Trans.* **34, 3** (1991) 433-439.
- [77] K.C. Ludema "Third Bodies in Wear Models – Wear Particles: From the Cradle to the Grave", *Proceedings of the 18<sup>th</sup> Leeds-Lyon Symposium on Tribology*, 3-6<sup>th</sup> September 1991, Lyon, France, Ed. D. Dowson, Publ. Elsevier, 155-160.
- [78] D.J. Shaw "Colloid and Surface Chemistry" Fourth Edition, Publ. Butterworth Heinemann (1992).
- [79] Y.H. Zhou, M. Harmelin, J. Bigot "Sintering Behaviour of Ultra-Fine Fe, Ni and Fe-25 Wt. % Ni Powders", *Scripta Metallurgica*, **23** (1989) 1391-1396.
- [80] P.K. Datta, H.L. Du, E. Kuzmann, I.A. Inman "Near Surface Structural Changes of 'glaze' Layers Formed during High Temperature Sliding Wear", to be published in *Wear*.
- [81] K.J. Bhansali "Adhesive Wear of Nickel- and Cobalt-Base Alloys", *Wear* **160** (1980) 95-110.
- [82] K. Razavizadeh and T.S. Eyre "Oxidative Wear of Aluminium Alloys", *Wear* **79** (1982) 325-333.
- [83] I. Garcia, A. Ramil and J.P. Celis "A Mild Oxidation Model Valid for Discontinuous Contacts in Sliding Wear Tests: Role of Contact Frequency", *Wear* **254** (2003) 429-440.
- [84] J. Mølgaard and V.K. Srivastava "The Activation Energy of Oxidation in Wear", *Tribo. Int.*, **16** (1983) 305-314.
- [85] C. Subramaniam "Wear of Al-12.3 Wt% Si Alloy Slid Against Various Counterface Materials" *Scripta Metallurgica* **25** (1991) 1369-1374.
- [86] H. So "Characteristics of Wear Results Tested by Pin-on-Disc at Moderate to High Speeds", *Tribo. Int.*, **Vol. 25, No. 5** (1996) 415-423.
- [87] D.H. Buckley "Adhesion, Friction and Wear of Cobalt and Cobalt-Base Alloys" *Cobalt* **38** (1968) 20-28.
- [88] D.H.E. Persson "Laser processed low friction surfaces", Licentiate of Philosophy Dissertation, Uppsala University (2003).

- [89] D.H.E. Persson "On the Mechanisms behind the Tribological Performance of Stellites", Ph.D. Thesis, Uppsala University (2003).
- [90] F.H. Stott, C.W. Stevenson and G.C. Wood "Friction and Wear Properties of Stellite 31 at Temperatures from 293 to 1074K" *Metals Tech.*, **4** (1977) 66-74.
- [91] K.C. Antony "Wear-resistant cobalt-base alloys" *Journal of Metals*. **35-2** (1983) 52-60.
- [92] E.A. Brandes and G.B. Brook "Smithells Metals Reference Book: Seventh Edition", *Butterworth Heinemann* (1992).
- [93] I.A. Inman "High Temperature 'Like-on-like' Sliding of Nimonic 80A under Conditions of Limited Debris Retention", *Unpublished Work*, Northumbria University (2003).
- [94] M. Vardavoulias "The Role of Hard Second Phases in the Mild Oxidational Wear Mechanism of High-Speed Steel Based Materials", *Wear* **173** (1994) 105-114.
- [95] P.D. Wood, *Unpublished Work*.
- [96] "Incoloy Alloy MA956" Special Metals Corporation, Publ. No. SMC-008.
- [97] I.A. Inman "The effects of pre-oxidation on the high temperature wear of  $\gamma$ -TiAl", *Internal Report*, Northumbria University / University of Birmingham (2005).
- [98] C.X. Li, J. Xia and H. Dong "Sliding wear of TiAl intermetallics against steel and ceramics of Al<sub>2</sub>O<sub>3</sub>, Si<sub>3</sub>N<sub>4</sub> and WC/Co", *Wear* **261** (2006) 693-701.
- [99] J. Takadoum, H. Houmid-Bennani and D. Mairey "The wear characteristics of silicon nitride", *J. Eur. Ceram. Soc.* **18** (1998) 553-556.
- [100] D.J. Barnes, J.E. Wilson, F.H. Stott and G.C. Wood "The Influence of Oxide Films on the Friction and Wear of Fe-5%Cr Alloy in Controlled Environments", *Wear* **45** (1977) 634-640.
- [101] D.H. Buckley "Influence of Chemisorbed Films on Adhesion and Friction of Clean Iron", *NASA Center for Aerospace Information*, **NASA-TN-D-4775** (1968).
- [102] D.J. Barnes, F.H. Stott and G.C. Wood "The Frictional Behaviour of Iron and Iron-Chromium Alloys at Elevated Temperatures", *Wear* **45** (1977) 199-209.
- [103] D.J. Barnes, J.E. Wilson, F.H. Stott and G.C. Wood "The Influence of Specimen Geometry and Sliding Mode on the Friction and Wear of Iron-Chromium Alloys in Controlled Environments", *Wear* **45** (1977) 97-111.
- [104] Feng, I-Ming and Uhlig "Fretting Corrosion of Mild Steel in Air and in Nitrogen", *Journal of Applied Mechanics*, **Vol 21, No.4** (1954) 395-400.
- [105] K.H.R. Wright "An Investigation of Fretting Corrosion", *Proceedings of the Institution of Mechanical Engineers*, **Vol. 1B, No. 11** (1952-53) 556-574.
- [106] R.B. Waterhouse "Fretting Corrosion", *Pergamon Press*, New York (1972).
- [107] R.C. Bill "Fretting Wear of Iron, Nickel and Titanium under Varied Environmental Conditions", *Wear of Materials*, ASME, New York (1979) 356-370.
- [108] I.M. Hutchings "Tribology: Friction and Wear of Engineering Materials", *Edward Arnold* (1992).

- [109] A.F. Smith “The Unlubricated Reciprocating Sliding Wear of 316 Stainless Steel in Co<sub>2</sub> at 20 – 600°C”, *Tribo. Int.*, **19** (1986) 65-71.
- [110] H.L. Du, P.K. Datta, I.A. Inman, E. Kuzmann, K. Suvegh, T. Marek, A. Vértes “Investigations of microstructures and defect structures in wear affected region created on Nimonic 80A during high temperature wear” *Tribology Letters*, **18-3** (2005) 393-402.
- [111] B Chattopadhyay and G.C. Wood “The Transient Oxidation of Alloys”, *Oxidat. Metals*, **2** (1970) 373-399.
- [112] F.H. Stott “High-Temperature Sliding Wear of Metals”, *Trib. Int.*, **35** (2002) 489-495.
- [113] H.L. Du, P.K. Datta, I. Inman, R. Geurts, C. Kübel “Microscopy of wear affected surface produced during sliding of Nimonic 80A against Stellite 6 at 20°C” *Materials Science and Engineering* **A357** (2003) 412-422.
- [114] H.L. Du, A. Aljarany, P.K. Datta, J.S. Burnell-Gray, “Oxidation behaviour of Ti-46.7Al-1.9W-0.5Si in air and Ar-20%O<sub>2</sub> between 750 and 950°C”, *Corrosion Science* **47** (2005) 1706–1723.
- [115] A.A. Aljarany, Ph.D. Thesis “Studies of the Degradation Behaviour of  $\gamma$ -TiAl and Fe<sub>3</sub>Al Intermetallics”, University of Northumbria, UK, 2002.
- [116] H. Gleiter, “Nanocrystalline Materials”, *Progress in Materials Science* **33** (1989) 223-315.
- [117] R.Z. Valiev R.K. Islamgaliev, I.V. Alexandrov, “Bulk nanostructured materials from severe plastic deformation”, *Progress in Materials Science* **45** (2000) 103-189.
- [118] T.C. Lowe, R.Z. Valiev, “Producing nanoscale microstructures through severe plastic deformation”, *JOM* **52** (2000) 27-28.
- [119] A.K. Ghosh, W. Huang, “Severe deformation nased progress for grain subdivision and resulting microstructures, in: T.C. Lowe and R.Z. Valiev (Ed.), Investigations and applications of severe plastic deformation”, Kluwer Academic Publications, pp. 29-36, 2000.
- [120] R.S. Mishra, S.X. McFadden, A.K. Mukherjee, “Analysis of tensile superplasticity in nanomaterials”, *Materials Science Forum* **304-306** (1999) 31-38.
- [121] R.S. Mishra, A.K. Mukherjee, “Superplasticity in nanomaterials, in A.K. Ghosh and T.R. Bieler (Ed.), Superplasticity and Superplastic Forming”, TMS Warrendale (1998) 109-116.
- [122] R.S. Mishra, S.X. McFadden, A.K. Mukherjee, “Tensile superplasticity in nanocrystalline materials produced by severe plastic deformation, in: T.C. Lowe and R.Z. Valiev (Ed.), Investigations and applications of severe plastic deformation”, Kluwer Academic Publications (1994) 231-240.
- [123] I.A. Inman, “Nano-scale studies of ‘glaze’ layers formed on Incoloy MA956 when slid against Incoloy 800HT at 750°C”, *Unpublished Work*, Northumbria University (2003).
- [124] S.C. Lim “Recent Development in Wear Maps”, *Tribo. Int.* **31**, Nos. 1-3 (1998) 87-97.

- [125] S.C. Lim “The relevance of wear-mechanism maps to mild-oxidational wear”, *Tribo. Int.* **35**, No. 11 (2002) 717-723.
- [126] T.H.C. Childs “The Sliding Wear Mechanisms of Metals, Mainly Steels”, *Tribo. Int.* **13** (1980) 285-293.
- [127] A. R. Riahi and A. T. Alpas "Wear map for grey cast iron" *Wear* **255** (2003) 401-409.
- [128] H. Chen and A. T. Alpas “Sliding wear map for the magnesium alloy Mg-9Al-0.9 Zn (AZ91)" *Wear* **246** (2000) 106-116.
- [129] S.H. Yang, H.Kong, E-S. Yoon and D.E. Kim "A wear map of bearing steel lubricated by silver films" *Wear* **255** (2003) 883-892.
- [130] D. Grimanelis and T.S. Eyre “Wear characteristics of a diffusion bonded sintered steel with short term surface treatments” *Wear* **262** (2007) 93-103.
- [131] D. Grimanelis and T.S. Eyre "Sliding wear mapping of an ion nitrocarburized low alloy sintered steel" *Surf. & Coat. Tech.* **201-6** (2006) 3260-3268.
- [132] K. Elleuch, R. Elleuch, R. Mnif, V. Fridrici and P. Kapsa "Sliding wear transition for the CW614 brass alloy", *Tribo. Int.* **39-4** (2006) 290-296.
- [133] K. Kato and K. Hokkirigawa “Abrasive Wear Diagram”, *Proc. Eurotrib '85*, Vol. 4, Section 5.3, Elsevier, Amsterdam (1985) 1-5.
- [134] K. Adachi, K. Kato and N. Chen "Wear map of ceramics" *Wear* **203-204** (1997) 291-301.

### **Withdrawn References**

- [135] E.O. Ezugwu, Z.M. Wang and A.R. Machado – “The Machinability of Nickel Based Alloys: A Review”, *J. Mat. Proc. Tech.*, **86** (1999) 1-16.
- [136] "Nimonic Alloy 80A" *Special Metals Corporation*.
- [137] Anon., Unpublished Work – *Special Metals (Wiggins) Ltd*.
- [138] “Tribaloy Technical Data”, *Deloro Stellite*.
- [139] R. Liu, M.X. Yao, P.C. Patnaik and X. Wu – “Effects of Heat Treatment on Mechanical and Tribological Properties of Cobalt-Base Tribaloy Alloys”, *J. Mat. Eng. & Perf.* **45** (1977) 161-176.
- [140] W.O. Soboye and T.S. Srivatsan “Advanced Structural Materials: Properties, Design Optimization, and Applications”, *CRC Press* (2007).

# Tables

Burwell and Strang [25]	Tabor	Ludema	Quinn [14 ]
{ Adhesive wear Corrosive wear }	Adhesive wear	Scuffing "Run-in"	Severe wear Mild wear
{ Surface fatigue (pitting) Abrasion Fretting }	Non-adhesive wear	Mechanisms of scuffing and "run-in"	Mechanisms of mild and severe wear
{ Cavitation Erosion }	Mixtures of adhesive and non-adhesive wear	Not covered in Ludema's review	

**Table 1: Quinn's comparison of the various classifications of wear [32]**

Alloy	Description	Hv500g	Av. grain size (µm)
<b>Ma956</b>	ODS alloy strengthened through a yttria dispersion in Fe-Cr-Al matrix	303	3000
<b>PM2000</b>	ODS alloy strengthened through a yttria dispersion in Fe-Cr-Al matrix	311	500
<b>PM2000SD</b>	ODS alloy strengthened through a yttria dispersion in Fe-Cr-Al matrix. Rolled at higher temperature than PM2000 imparting greater ductility	363	80

**Table 2: Description and properties of the ODS alloys investigated [1]**

	Wear rate ( $10^{-16} \text{ m}^3 \cdot \text{m}^{-1}$ )			
	Steel ball		Tungsten carbide ball	
	30% RH	80% RH	30% RH	80% RH
<b>AISI 52100</b>				
<i>Untreated</i>	1,000	100	17.5	17.5
<i>Implanted</i>	1	3.4	1.8	0.3
<b>AISI 440B</b>				
<i>Untreated</i>	19	25	34	85
<i>Implanted</i>	1.4	2.5	2.8	1.8
<b>AISI M2</b>				
<i>Untreated</i>	11.5	2.9	11.2	20
<i>Implanted</i>	3.3	1.9	1.6	3.3

**Table 3: Wear rates of case-hardened steels before and after implantation of oxygen ions, 400 m sliding distance [34] (ion implantation conditions  $5 \times 10^{17} \text{ cm}^{-2}$ , 50 keV; test conditions in air at 30% or 80% relative humidity RH,  $28 \times 10^{-3} \text{ m} \cdot \text{s}^{-1}$ )**

	Wear rate ( $10^{-16} \text{ m}^3 \cdot \text{m}^{-1}$ )			
	Steel ball		Tungsten carbide ball	
	30% RH	80% RH	30% RH	80% RH
<b>AISI 52100</b>				
<i>Untreated</i>	611	7.7	38	1.5
<i>Implanted</i>	68	11.2	38	2.2
<i>Oxidised</i>	1.1	0	0.8	0.8
<b>AISI 321</b>				
<i>Untreated</i>	1,400	72	4,000	32
<i>Implanted</i>	215	72	2,000	16
<i>Oxidised</i>	140	72	0	32
<b>AISI 440B</b>				
<i>Untreated</i>	98	9.1	42	42
<i>Implanted</i>	33	0.2	84	42

**Table 4: Wear rates of case-hardened steels before and after implantation of oxygen ions, 100 m sliding distance [34] (ion implantation conditions  $5 \times 10^{17} \text{ cm}^{-2}$ , 50 keV – 100 keV in case of AISI 52100; test conditions in air at 30% or 80% relative humidity RH,  $28 \times 10^{-3} \text{ m} \cdot \text{s}^{-1}$ )**

Element	Area 1 (Nimonic 80A substrate)		Area 3 (Glaze layer)	
	wt.%	at.%	wt.%	at.%
<b>Al</b>	0.7	1.4	0.4	0.9
<b>Si</b>	0.7	1.3	1.1	2.3
<b>Ti</b>	1.8	2.1	0.4	0.5
<b>Cr</b>	18.7	20.2	25.0	27.4
<b>Fe</b>	0.7	0.7	1.4	1.4
<b>Co</b>	1.0	0.9	49.8	48.2
<b>Ni</b>	76.6	73.4	19.0	18.4
<b>W</b>	-	-	2.9	0.9

**Table 5: Quantification of the EDX spectra in Fig. 35**



## Figures

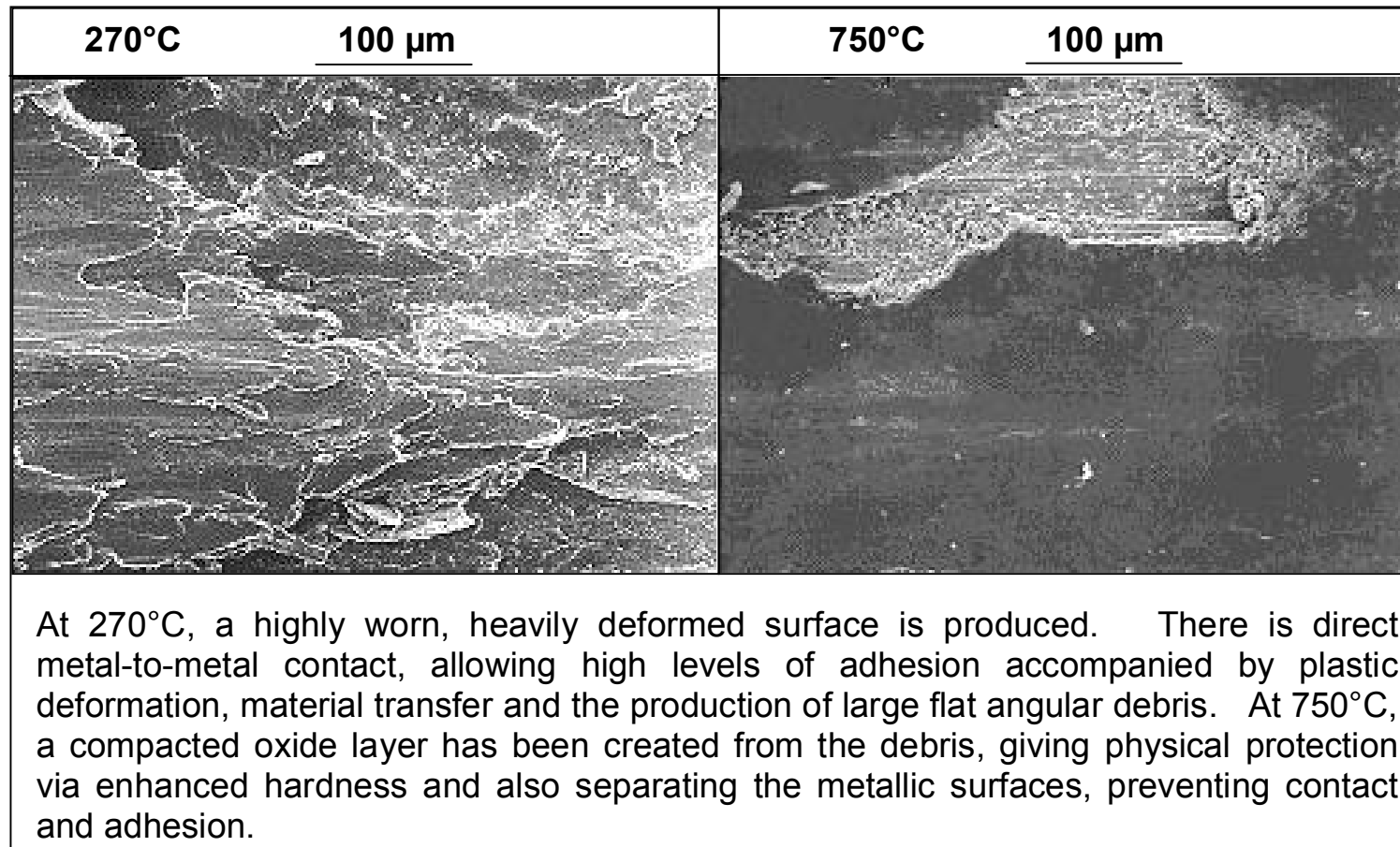


**Fig. 1: Wear surfaces produced during the sliding of Incoloy MA956 against Incoloy 800HT at 270°C and 750°C [2] (load = 7N, sliding speed = 0.654 m.s<sup>-1</sup>, sliding distance = 9,418 m)**

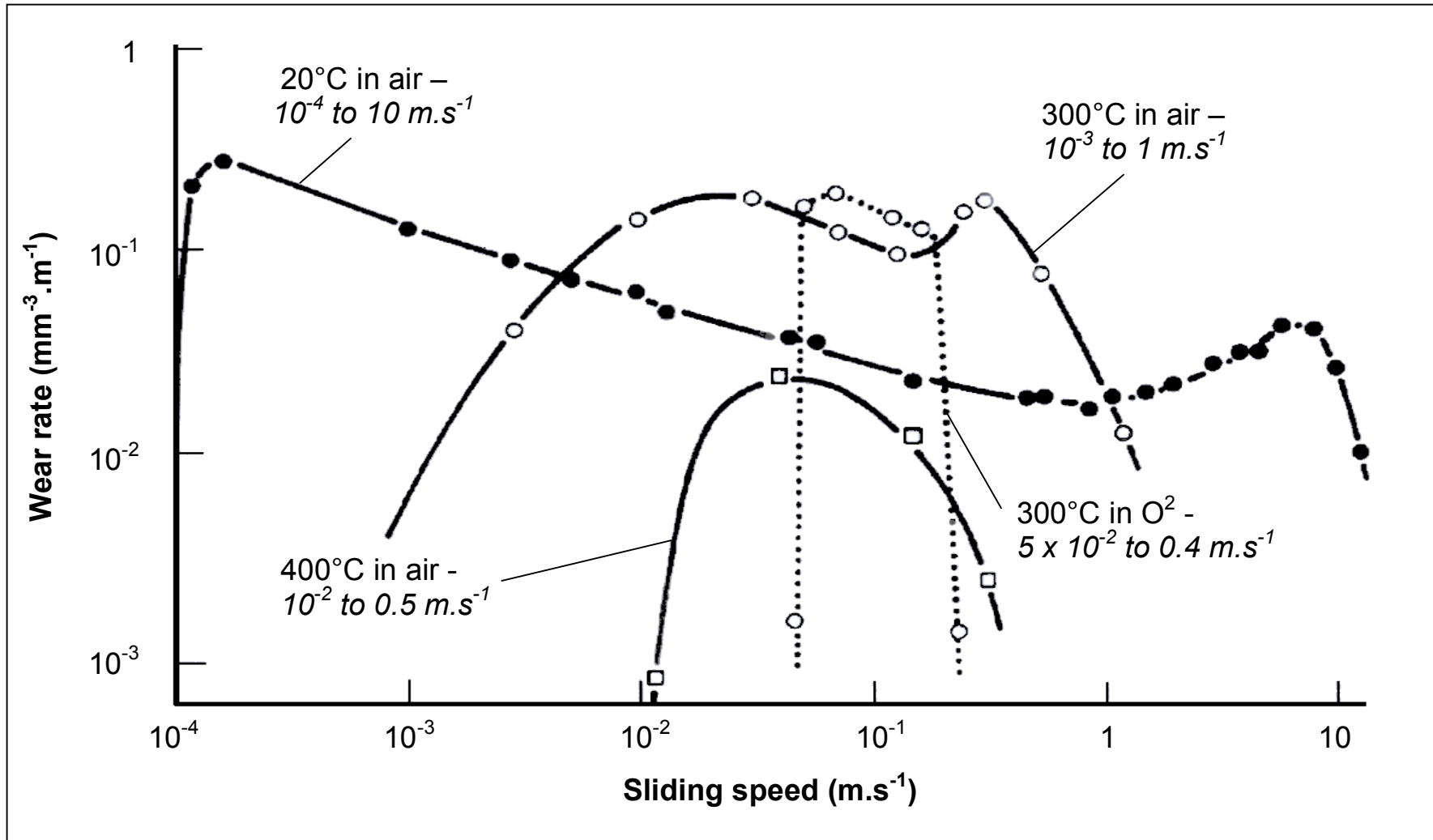


Fig. 2: Variation in wear rate with sliding speed at 20, 300 and 400°C in air and also 300°C in pure oxygen for  $\alpha\beta$  brass sliding against steel [25] (approximate sliding speed ranges for severe wear at each temperature given in italics)

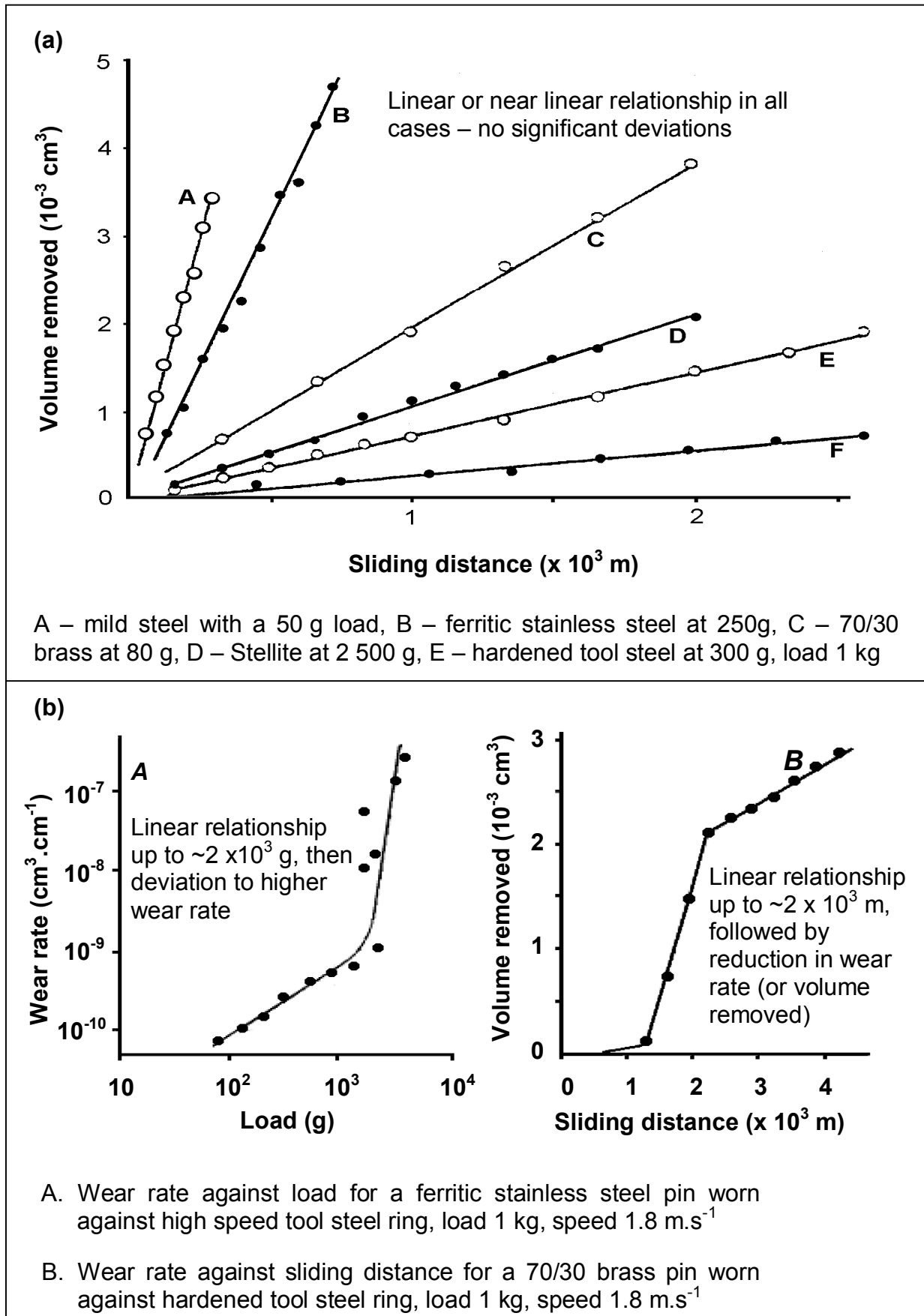


Fig. 3: Experimental Data from Archard and Hirst's Work on Like-on-Like Sliding at  $1.8 \text{ m} \cdot \text{s}^{-1}$  [30]

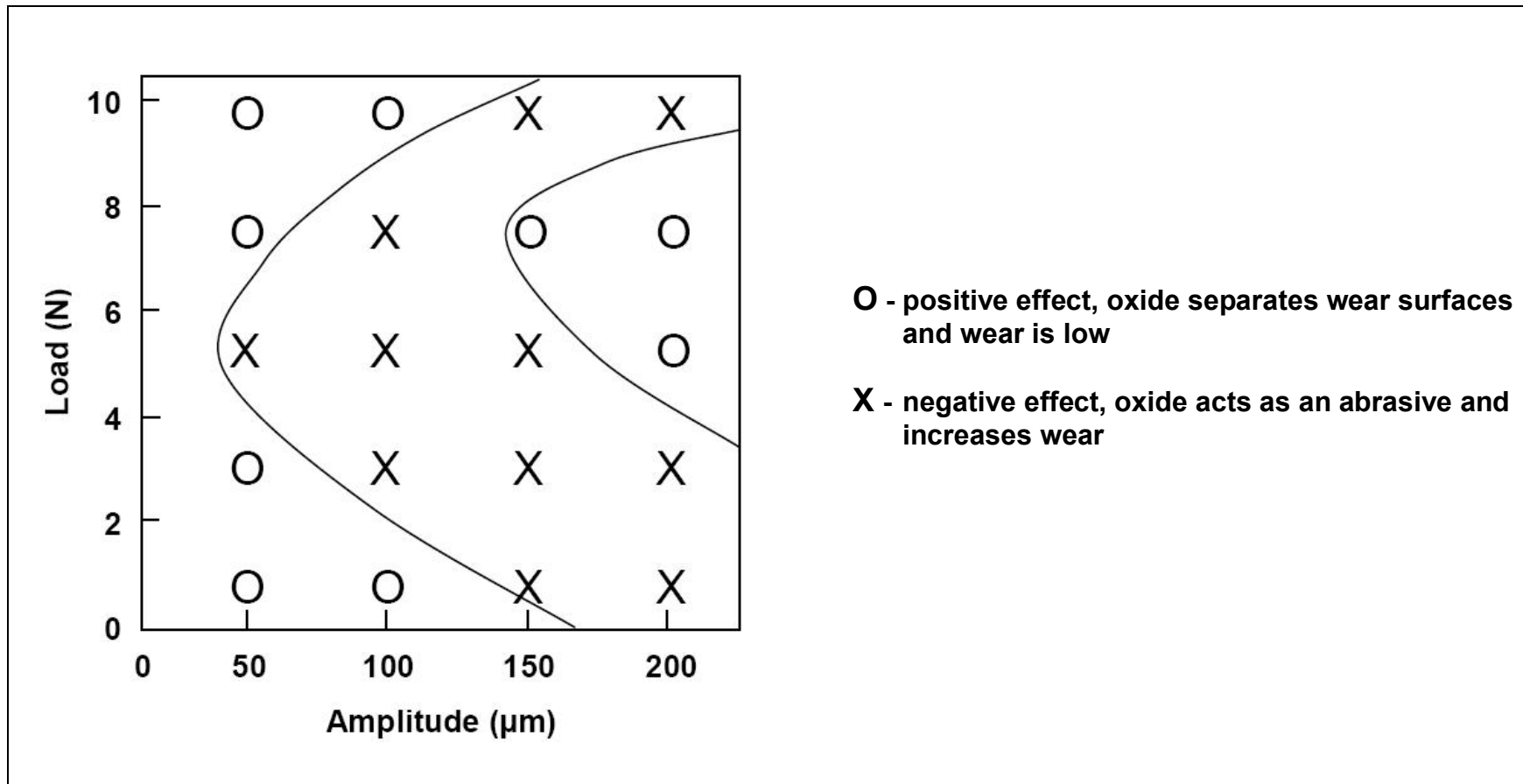


Fig. 4: Effectiveness of wear reduction on S45C plain carbon steel due to the introduction of Fe<sub>2</sub>O<sub>3</sub> particles [41]

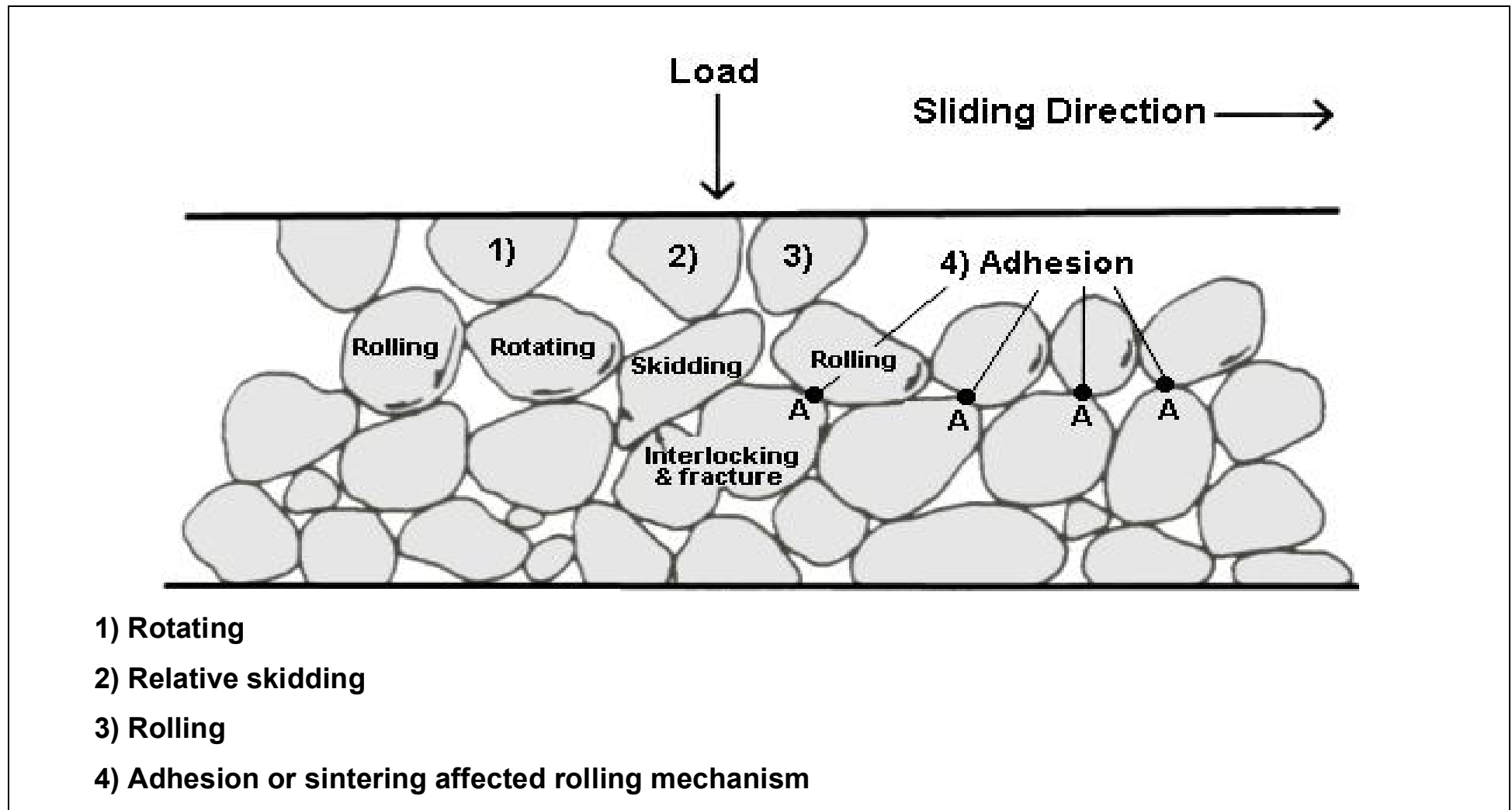
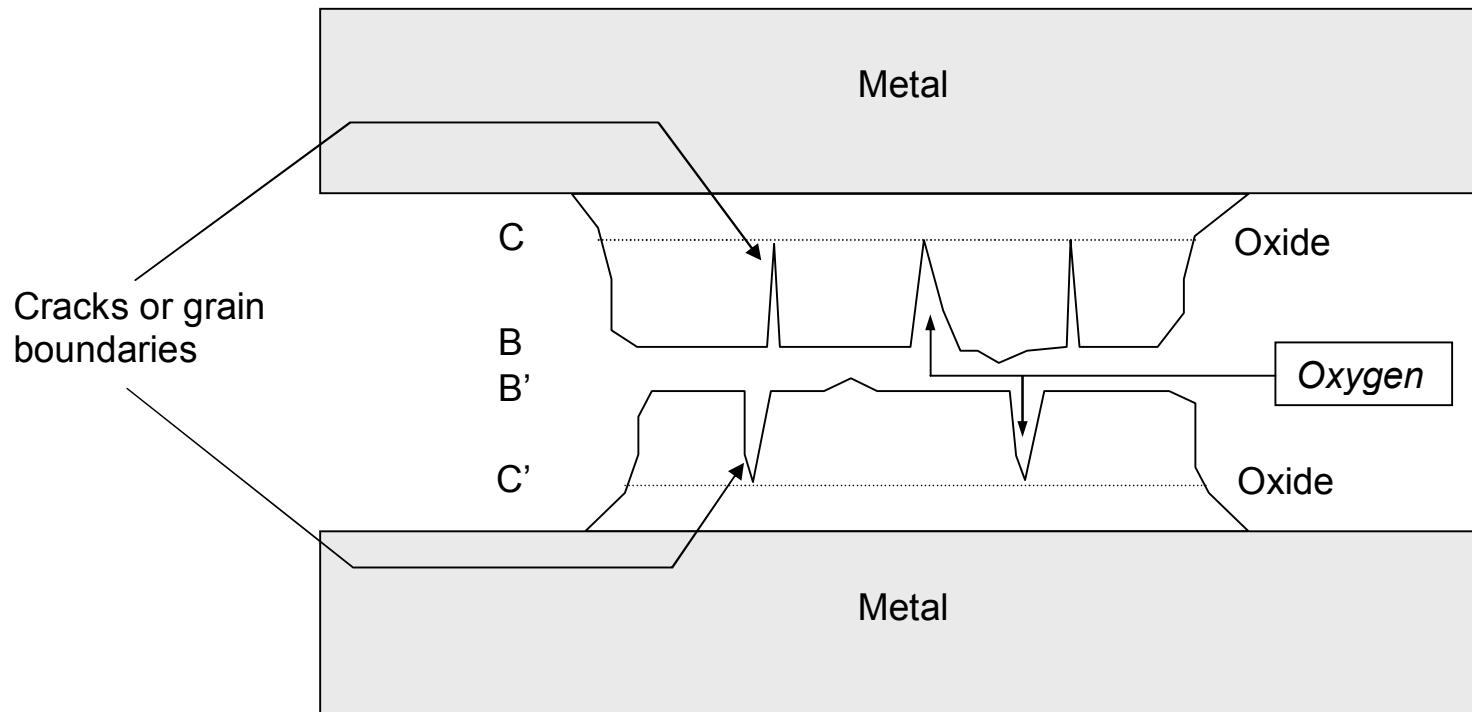


Fig. 5: Mechanisms of possible movement of particles during sliding of particulate materials [18]

Quinn's oxidation model supposes that any oxygen species would have to diffuse right from the surface of the oxide (B or B') to the metal. The presence of cracks and grain boundaries act as points of ingress for oxygen ions and in the case of cracks, molecular oxygen. This means that the distance for diffusion is significantly less where cracks in the outer layers of oxide are prevalent. Diffusion need only take place across the underlying oxide from the crack tips (C and C') to the metal and thus the rate of oxidation is greater.



**Fig. 6: Oxygen transport between oxide plateaux and cracks in the oxides [84]**

- (a)  $1.00 \text{ m.s}^{-1}$  to  $2.66 \text{ m.s}^{-1}$  ( $\bullet$  –  $1.00 \text{ m.s}^{-1}$ ;  $\times$  –  $1.33 \text{ m.s}^{-1}$ ;  $\circ$  –  $2.00 \text{ m.s}^{-1}$ ;  $+$  –  $2.66 \text{ m.s}^{-1}$ )
- (b)  $0.17 \text{ m.s}^{-1}$  to  $1.00 \text{ m.s}^{-1}$  ( $\times$  –  $0.017 \text{ m.s}^{-1}$ ;  $\circ$  –  $0.067 \text{ m.s}^{-1}$ ;  $\Delta$  –  $0.33 \text{ m.s}^{-1}$ ;  $+$  –  $0.66 \text{ m.s}^{-1}$ ;  $\bullet$  –  $1.00 \text{ m.s}^{-1}$ )
- $T_1$  Transition from low speed, low load mild wear to severe wear
- $T_2$  Transition from severe wear to high speed, high load mild wear
- (Arrows show movement of transitions with increasing sliding speed)*

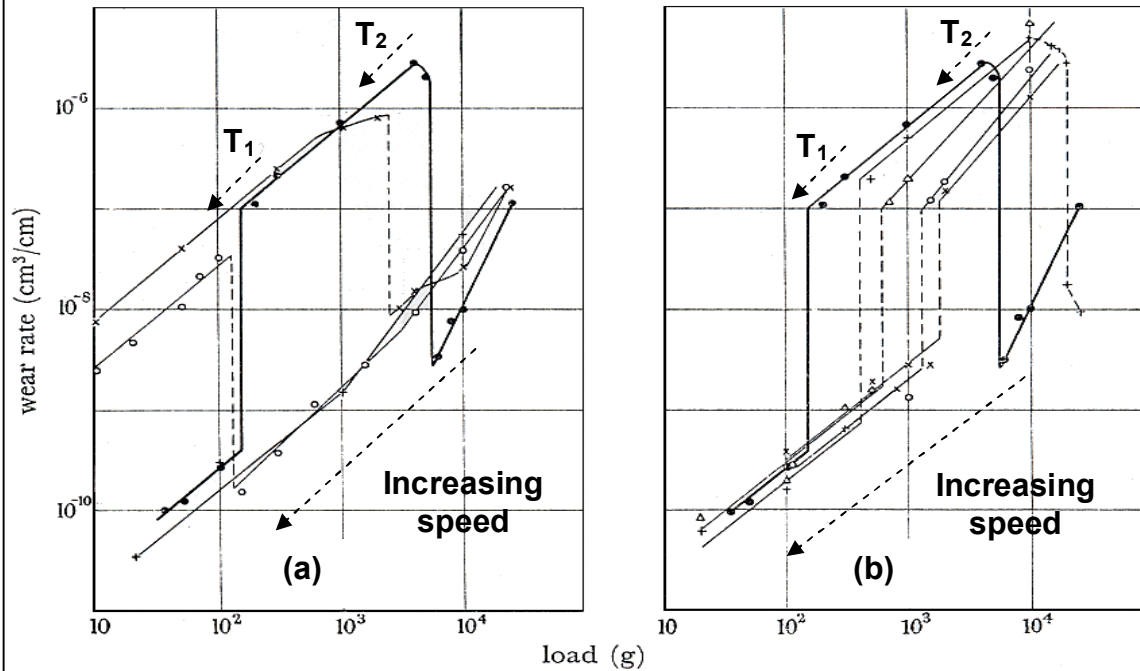


**Fig. 7: Effect of sliding speed on wear rate / load – 0.52% carbon steel [26]**

- (a) Cu, Cu-4.6 wt. % Al and Cu-7.5 wt% Al counterfaces, applied pressure 0.1 MPa
- (b) Mild steel, die steel and partially stabilised zircona counterfaces, applied pressure 0.1 MPa
- (c) Cu, Cu-4.6 wt. % Al and Cu-7.5 wt% Al counterfaces, applied pressure 0.5 MPa
- (d) Mild steel, die steel and partially stabilised zircona counterfaces, applied pressure 0.5 MPa

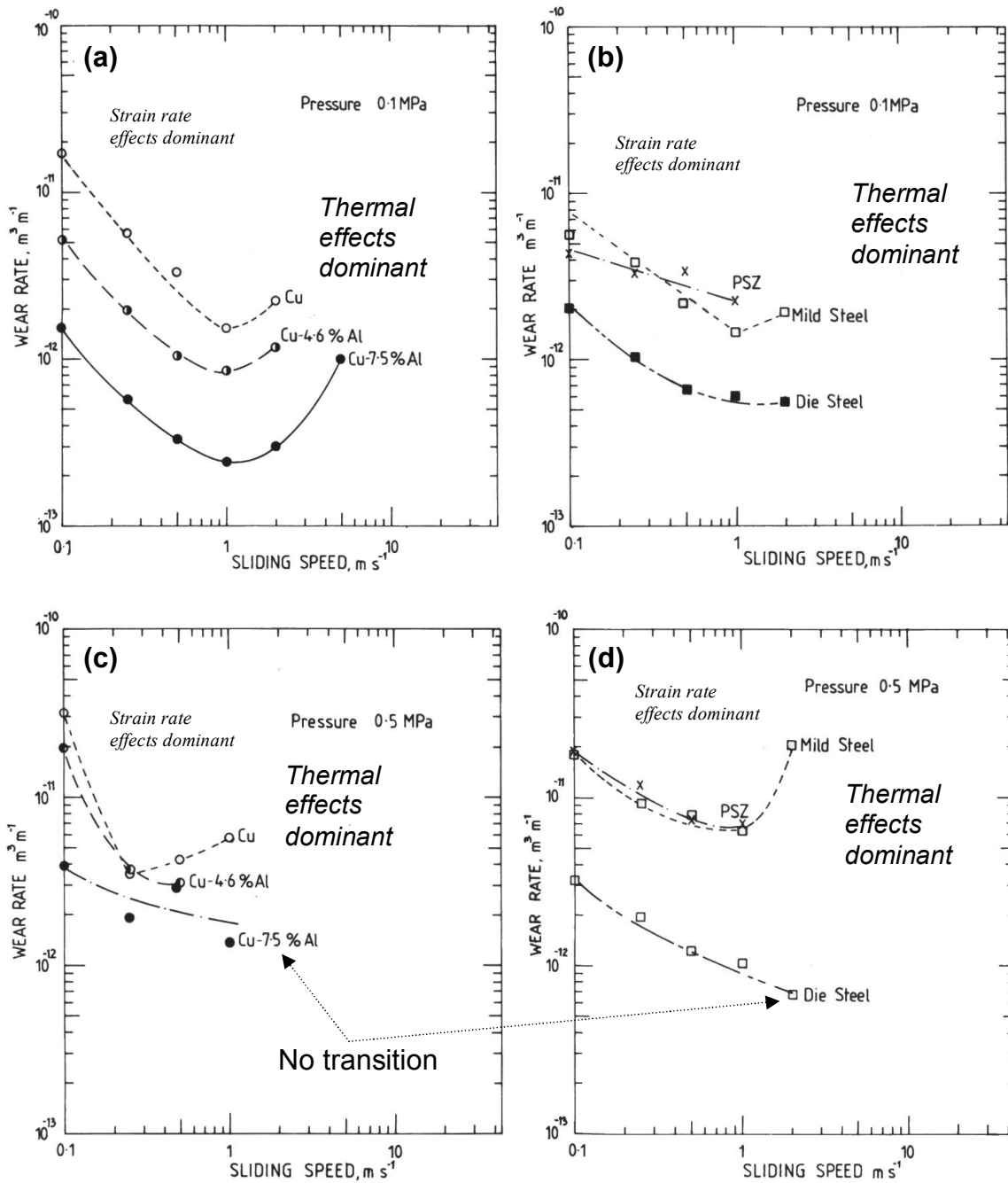


Fig. 8: Effect of sliding speed on wear rate of Al-12.3 wt. % Si versus various counterface materials [85]



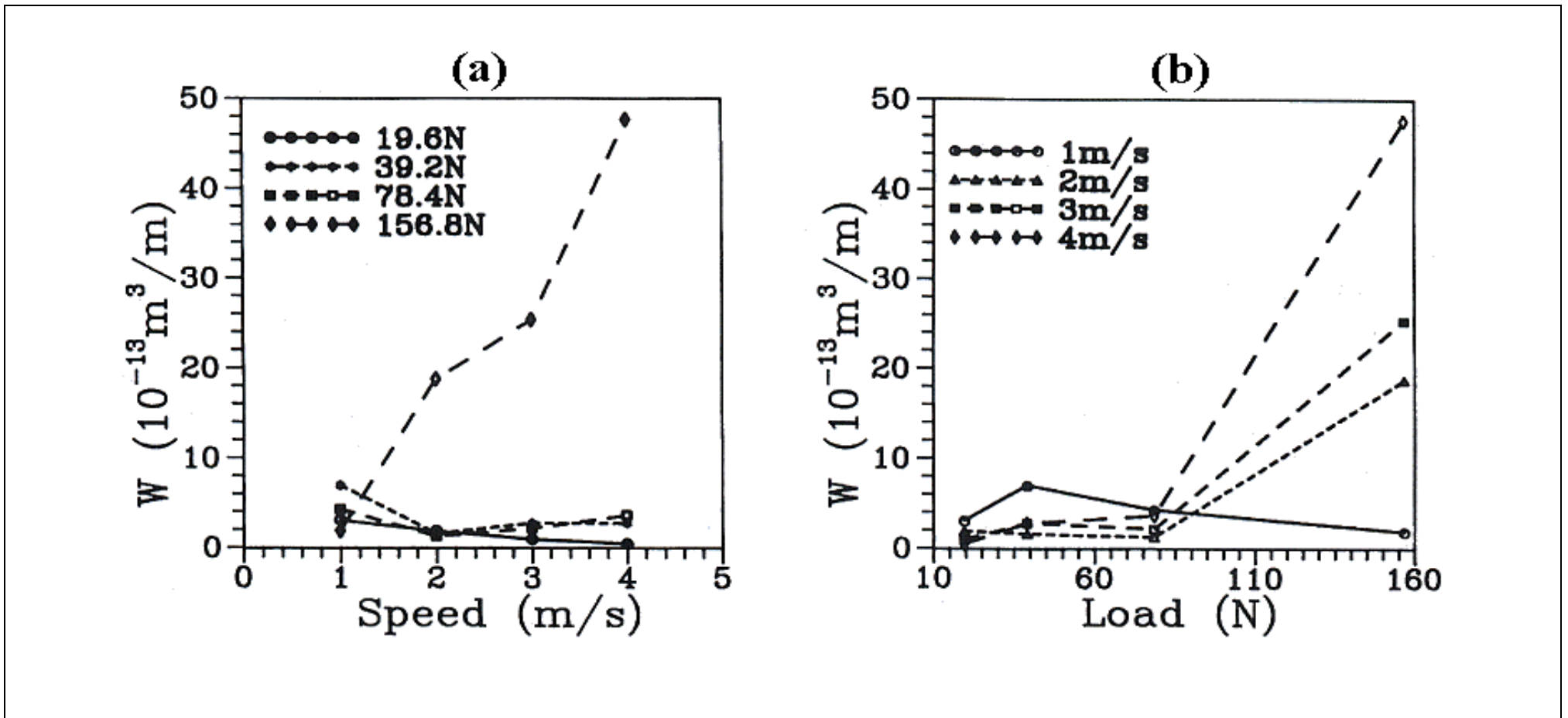
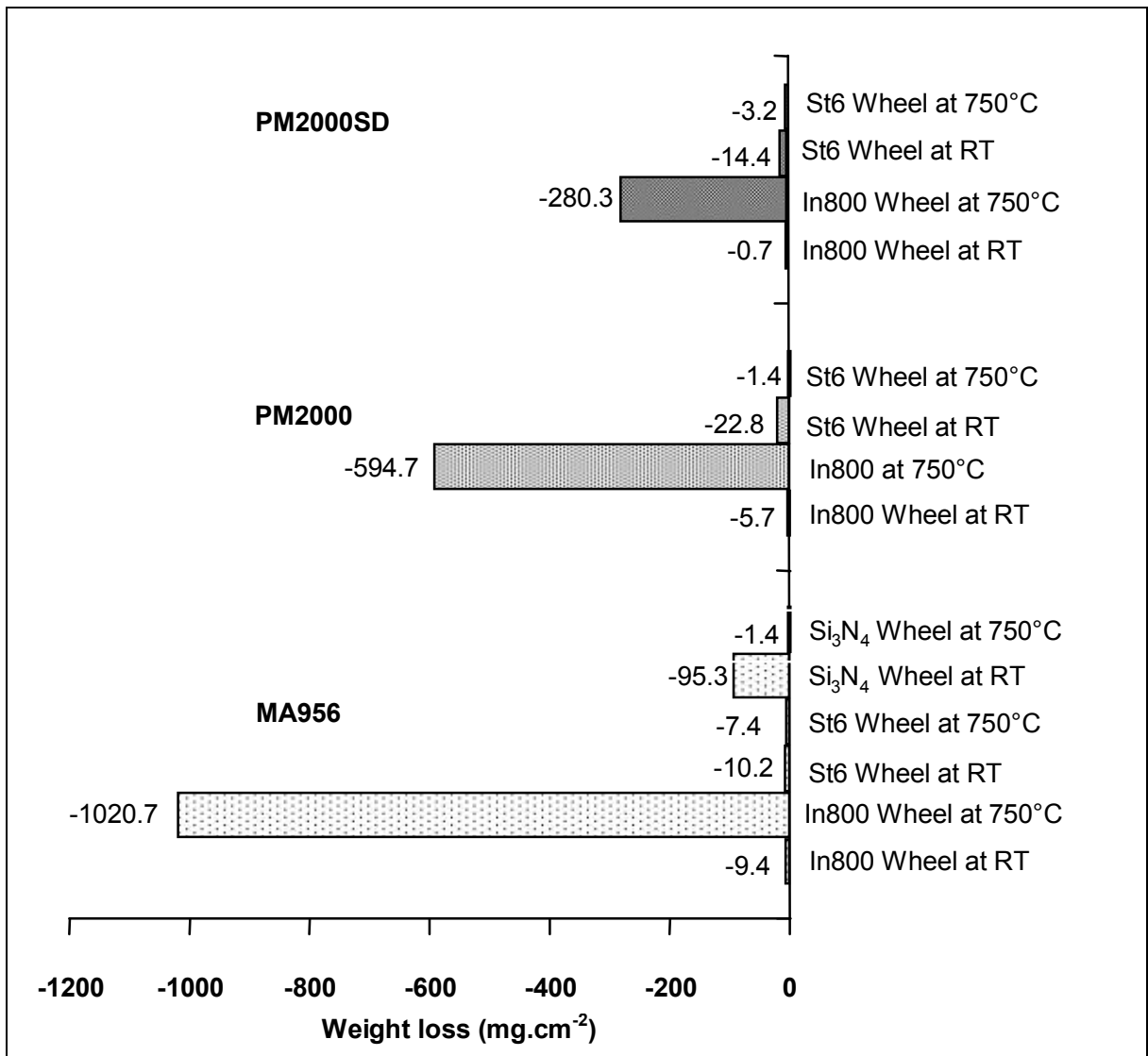
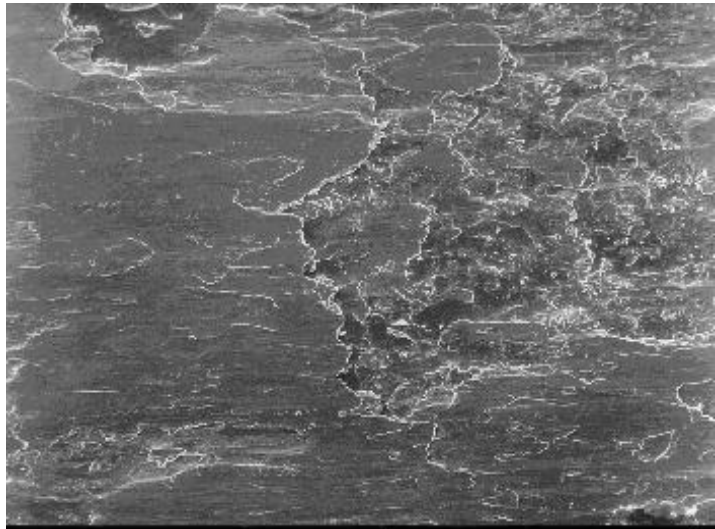
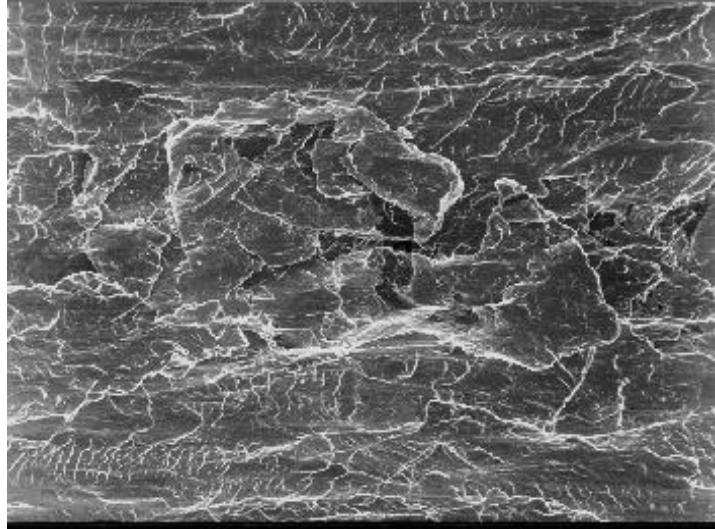
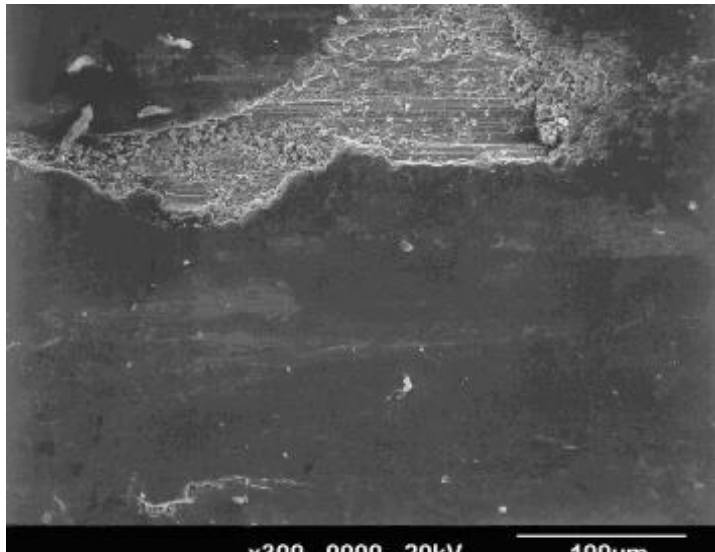


Fig. 9: Variation in wear rate (W) with sliding speed (a) and load (b) for the rubbing of laser-clad Stellite 6 pins with AISI 4340 steel disks [29]

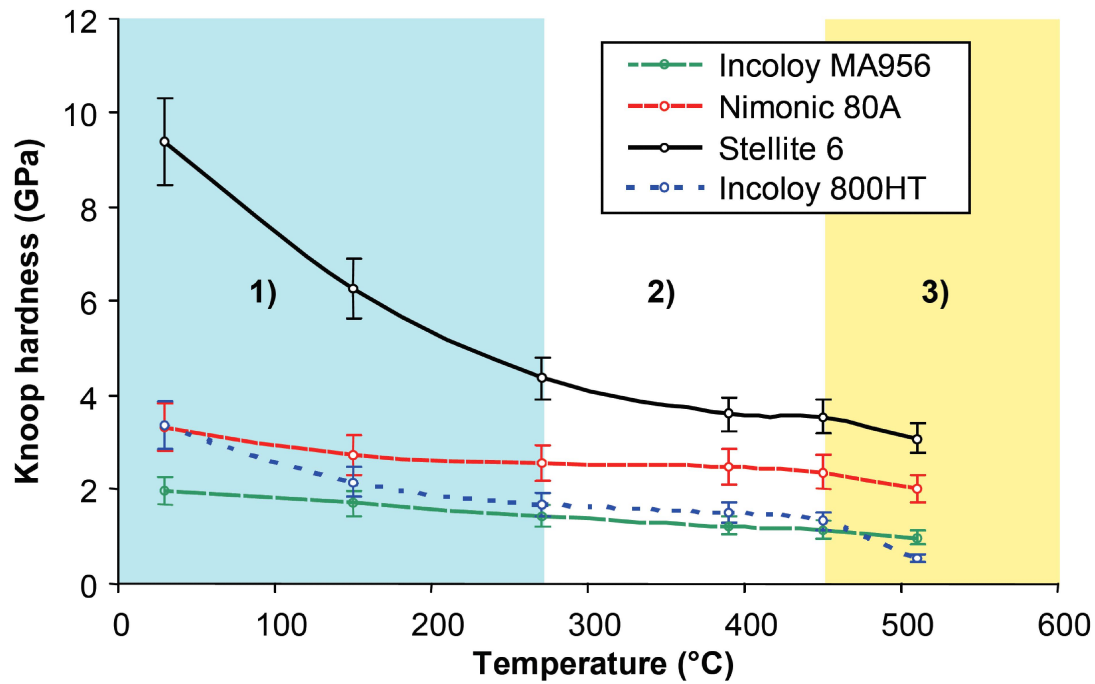


**Fig. 10: Weight change of the ODS alloys worn against various counterfaces at room temperature and 750°C [1] (sliding speed 0.654 m.s<sup>-1</sup>, load 7N)**

 <p data-bbox="432 712 842 745">x100 0000 20kV 500µm</p>	<p data-bbox="951 248 1369 315">A. Room temperature (shown), also typical of 270°C</p> <p data-bbox="999 383 1401 517">Severe wear with high metallic transfer from Incoloy 800HT counterface to Incoloy MA956 sample</p> <p data-bbox="999 584 1409 674">Torn, metallic surface typical of adhesive wear, no traces of oxide</p>
 <p data-bbox="432 1301 842 1335">x300 0000 20kV 100µm</p>	<p data-bbox="951 837 1417 904">B. 510°C (also typical of 390, 450, 570 and 630°C)</p> <p data-bbox="999 972 1401 1106">Severe wear with reduced transfer from Incoloy 800HT counterface to Incoloy MA956 sample</p> <p data-bbox="999 1173 1409 1263">Torn, metallic surface typical of adhesive wear, no clear traces of oxide</p>
 <p data-bbox="432 1890 842 1924">x300 0000 20kV 100µm</p>	<p data-bbox="951 1509 1401 1576">C. 750°C (shown), also typical of 690°C</p> <p data-bbox="999 1644 1417 1778">Smooth 'glaze' layer formation with little debris following period of early severe wear with damage to underlying sample</p>

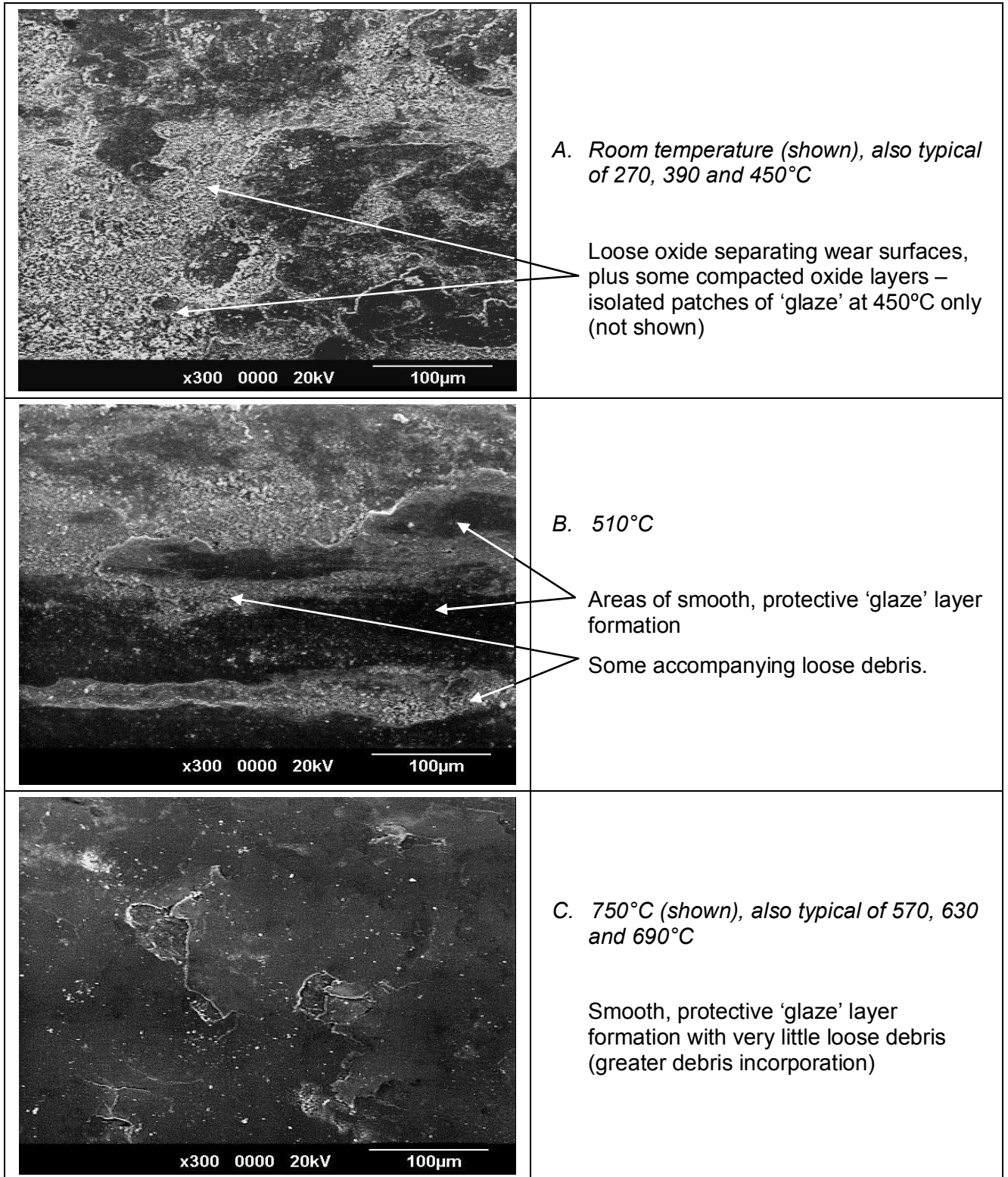
**Fig. 11: SEM micrographs of Incoloy MA956 wear surfaces after sliding at 0.654 m.s<sup>-1</sup> against an Incoloy 800HT counterface at room temperature, 510 and 750°C (sliding distance 9,418 m) [2]**

1. Low temperature oxidational wear, moderate falls (large for Stellite 6) in hardness.
2. Low temperature oxidational wear at 0.314 m.s<sup>-1</sup>, metallic severe wear only at 0.905 m.s<sup>-1</sup>, little change in hardness.
3. 'Glaze' formation for Nimonic 80A vs. Stellite 6 at 0.314 m.s<sup>-1</sup> with high oxidational wear replacing metallic severe wear at 0.905 m.s<sup>-1</sup>. Also, early 'glaze' formation for Incoloy MA956 vs. Stellite 6, with extended early severe wear at 0.905 m.s<sup>-1</sup>.

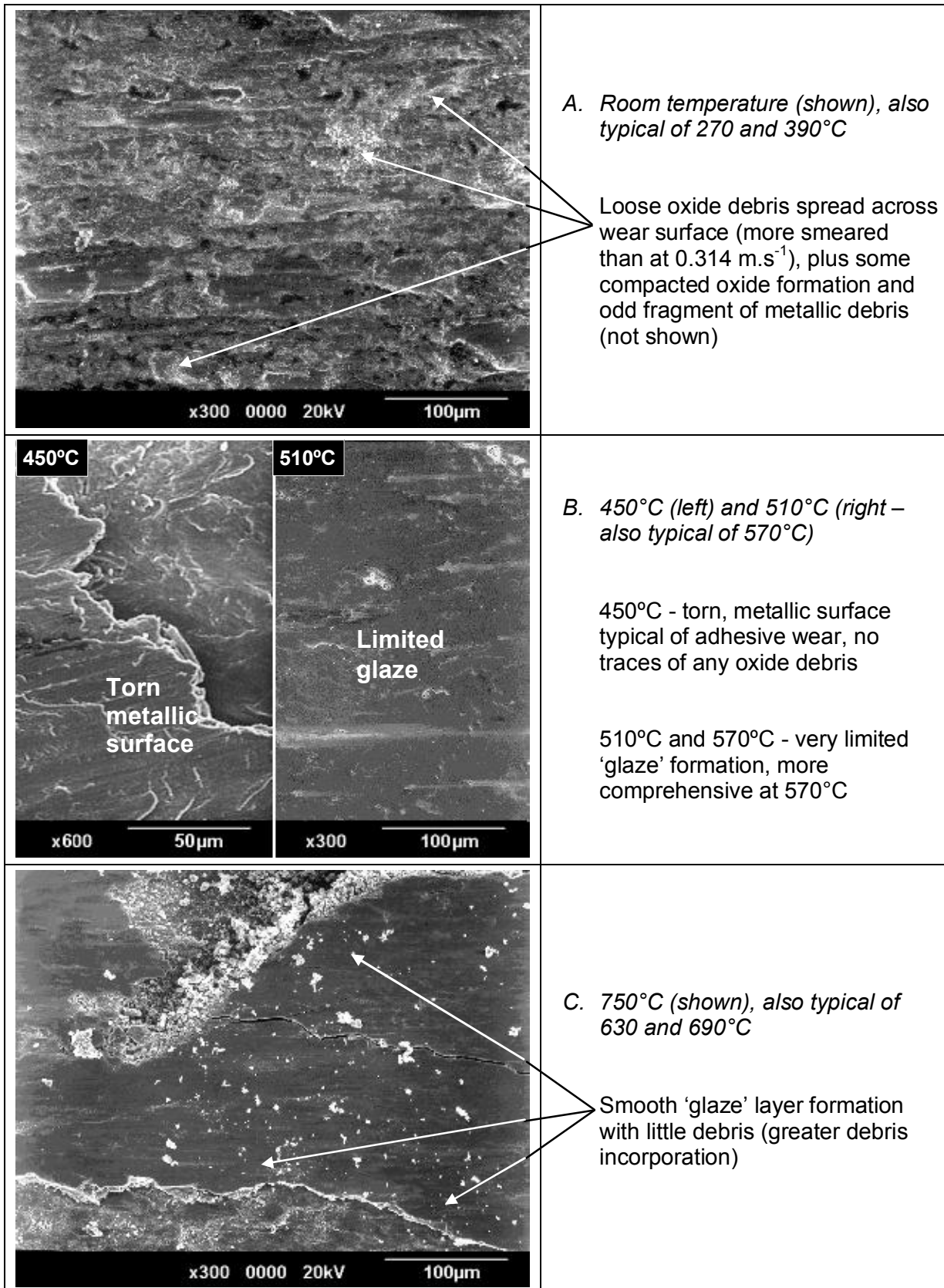


<b>Mean Knoop hardness (GPa)</b>				
<b>Temperature (°C)</b>	<b>Stellite 6</b>	<b>Nimonic 80A</b>	<b>MA956</b>	<b>Incoloy 800</b>
<b>30</b>	9.39	3.33	1.99	3.38
<b>150</b>	6.28	2.75	1.71	2.16
<b>270</b>	4.37	2.58	1.45	1.68
<b>390</b>	3.61	2.50	1.24	1.52
<b>450</b>	3.55	2.37	1.16	1.34
<b>510</b>	3.08	2.01	0.97	0.55

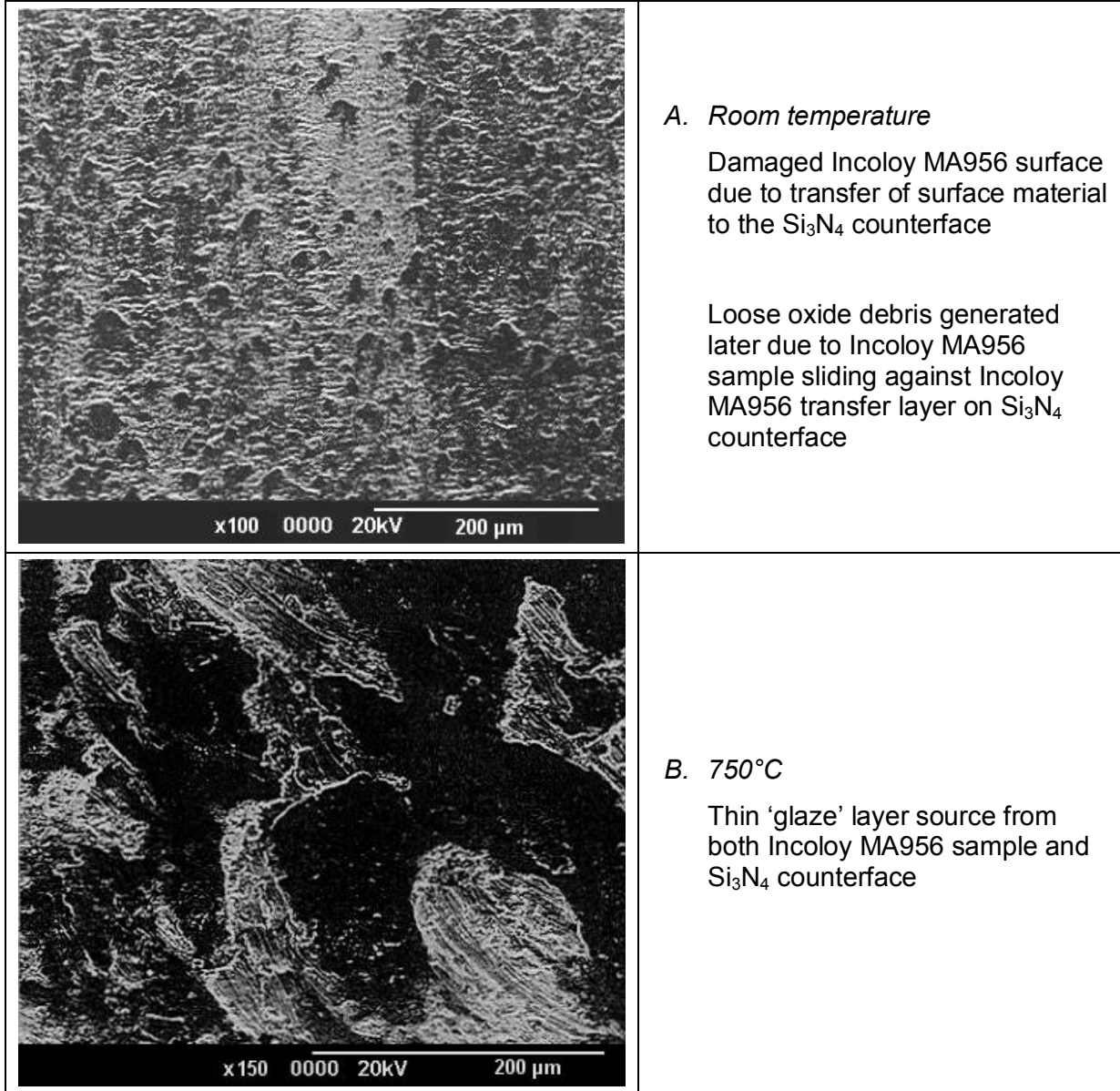
**Fig. 12: Mean Knoop hardness (hot hardness, 50 g load, 12 s dwell time) from room temperature to 510°C [2], with wear regimes with respect to temperature identified for the Nimonic 80A / Stellite 6 and Incoloy MA956 / Stellite 6 systems [2,3]**



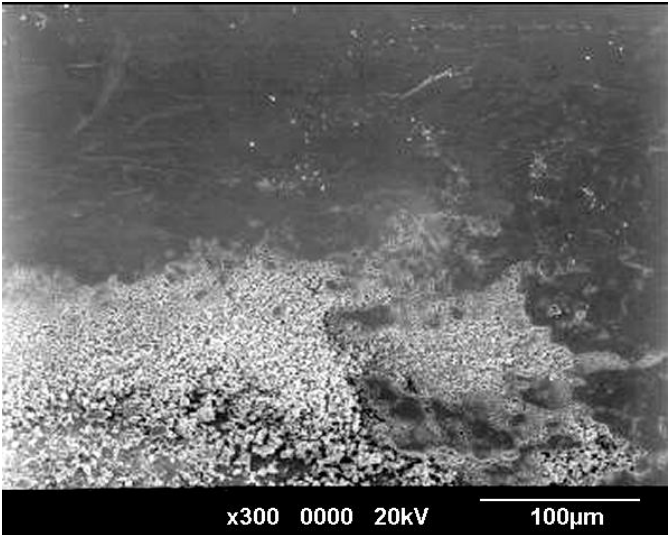
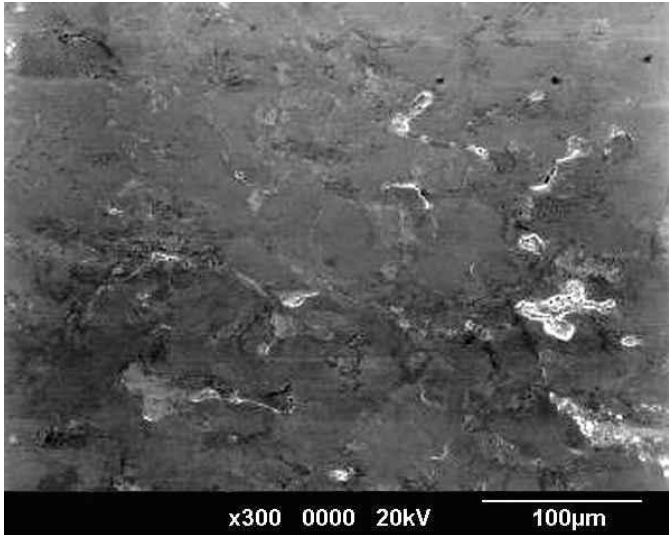
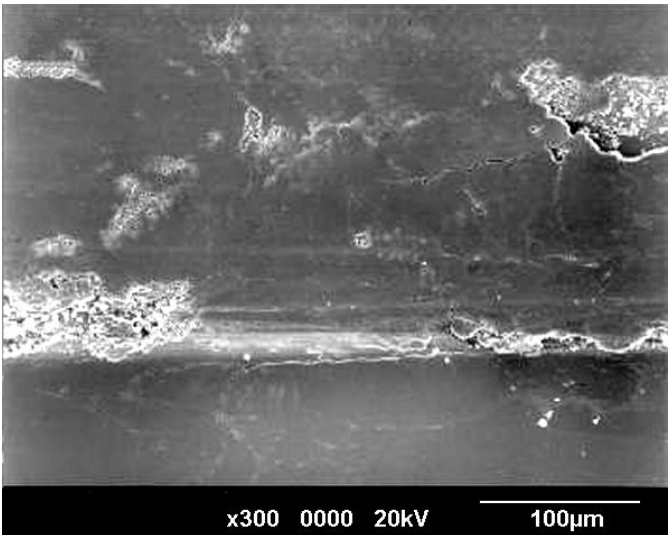
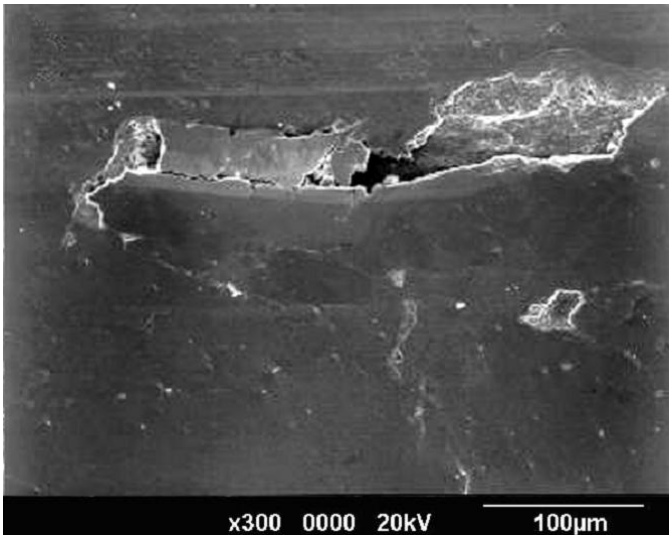
**Fig. 13: SEM micrographs of Incoloy MA956 wear surfaces after sliding at 0.314 m.s<sup>-1</sup> against a Stellite 6 counterface at room temperature, 510 and 750°C [22]**



**Fig. 14: SEM micrographs of Incoloy MA956 wear surfaces after sliding at 0.654 m.s<sup>-1</sup> against a Stellite 6 counterface at room temperature, 450, 510 and 750°C [2] (also representative of 0.905 m.s<sup>-1</sup> [22])**



**Fig. 15: SEM micrographs of Incoloy MA956 wear surfaces after sliding at 0.654 m.s<sup>-1</sup> against a Si<sub>3</sub>N<sub>4</sub> counterface at (a) room temperature and (b) 750°C (load 7N, sliding distance 9,418 m) [1]**

Incoloy 800HT counterface		Stellite 6 counterface	
	<p>(a) 7N</p> <p>Smooth compacted oxide / 'glaze' layers with a little loose debris (underlying sample damaged due to early severe wear)</p>		<p>(c) 7N</p> <p>Smooth compacted oxide / 'glaze' layers</p>
	<p>(b) 25N</p> <p>Smooth compacted oxide / 'glaze' layers and a little loose debris, with some cracking due to high load (underlying sample damaged due to early severe wear)</p>		<p>(d) 25N</p> <p>Smooth compacted oxide / 'glaze' layers, with some cracking due to high load</p>

**Fig. 16: SEM micrographs of Incoloy MA956 worn against an Incoloy 800HT counterface at applied loads of (a) 7N and (b) 25N, and against a Stellite 6 counterface at applied loads of (c) 7N and (d) 25N (750°C, sliding speed 0.654 m.s<sup>-1</sup>, sliding distance 9,418 m) [2]**



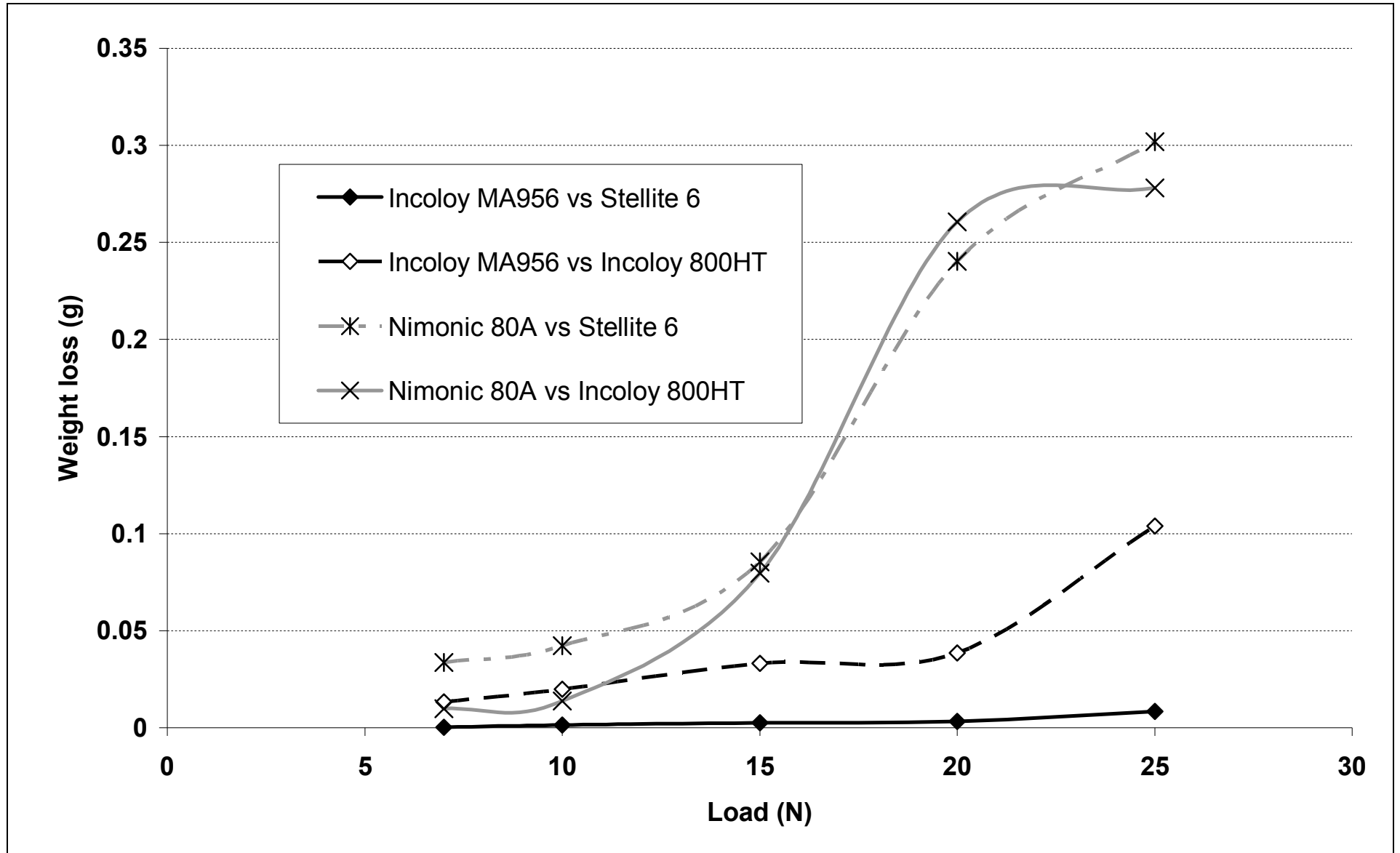
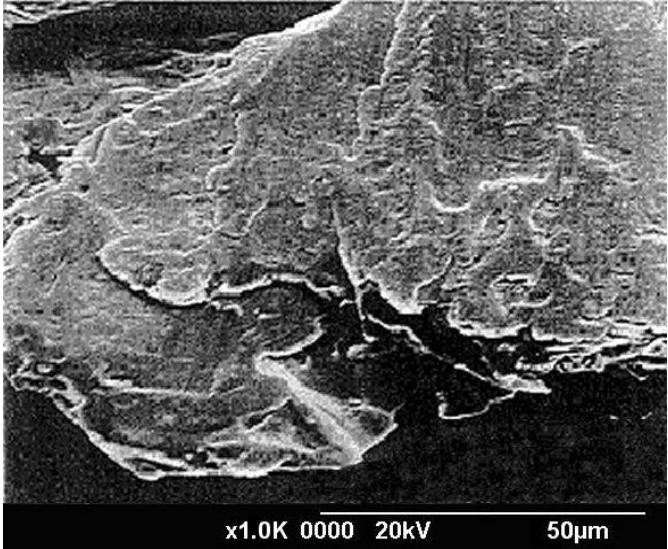
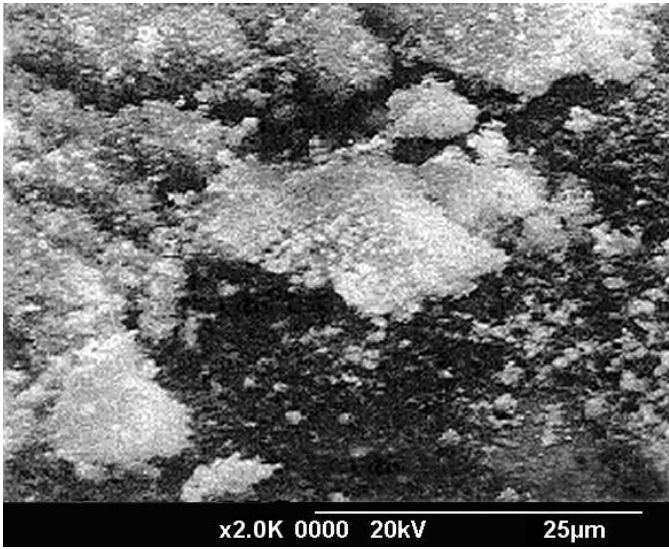
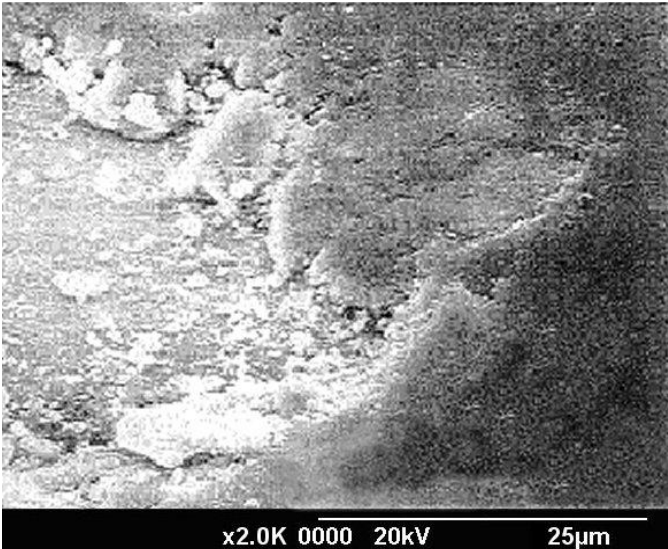
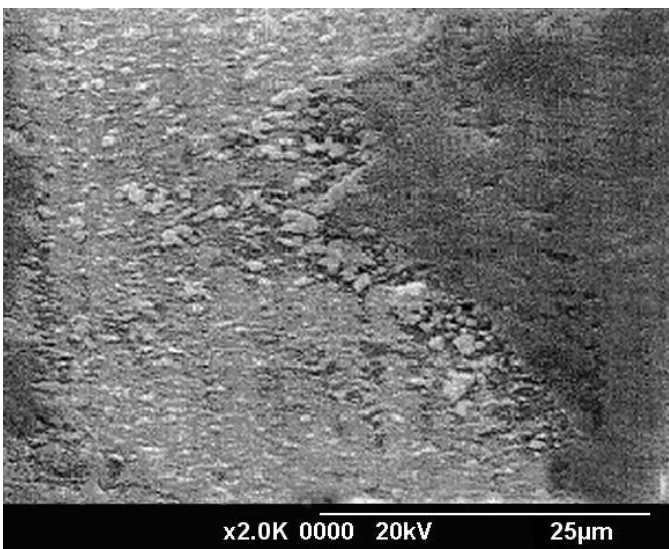
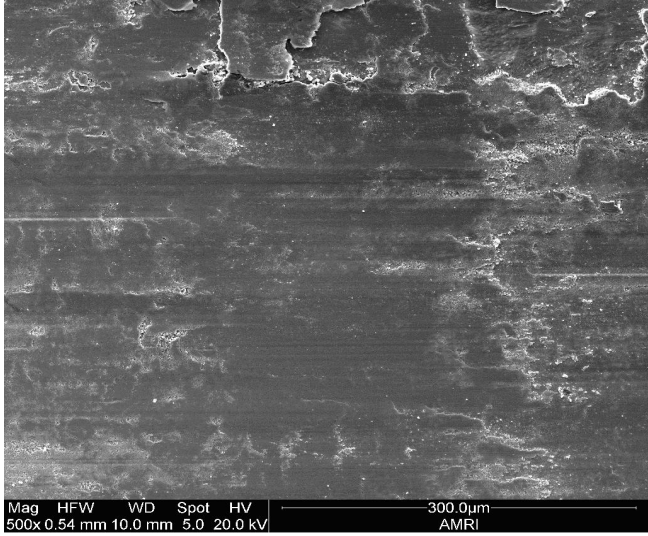
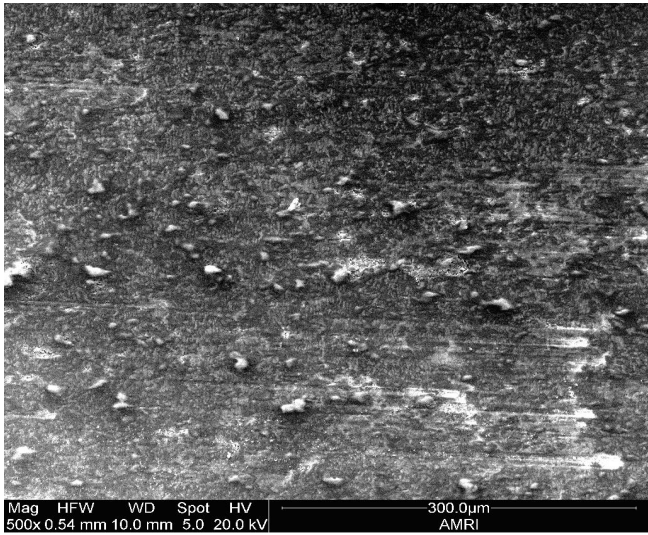
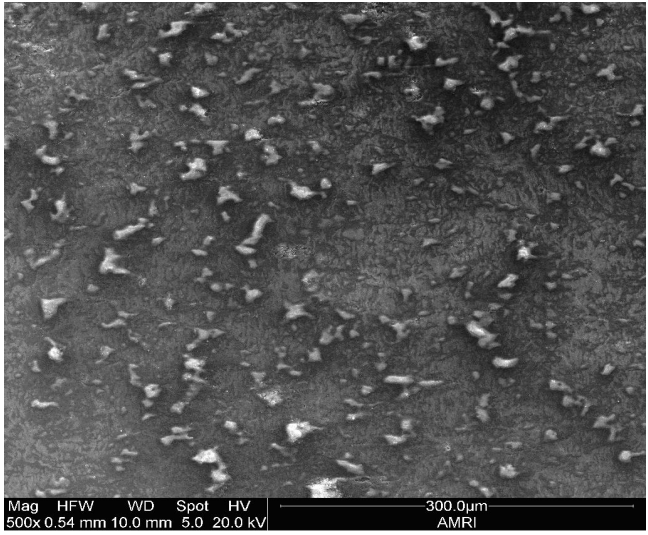


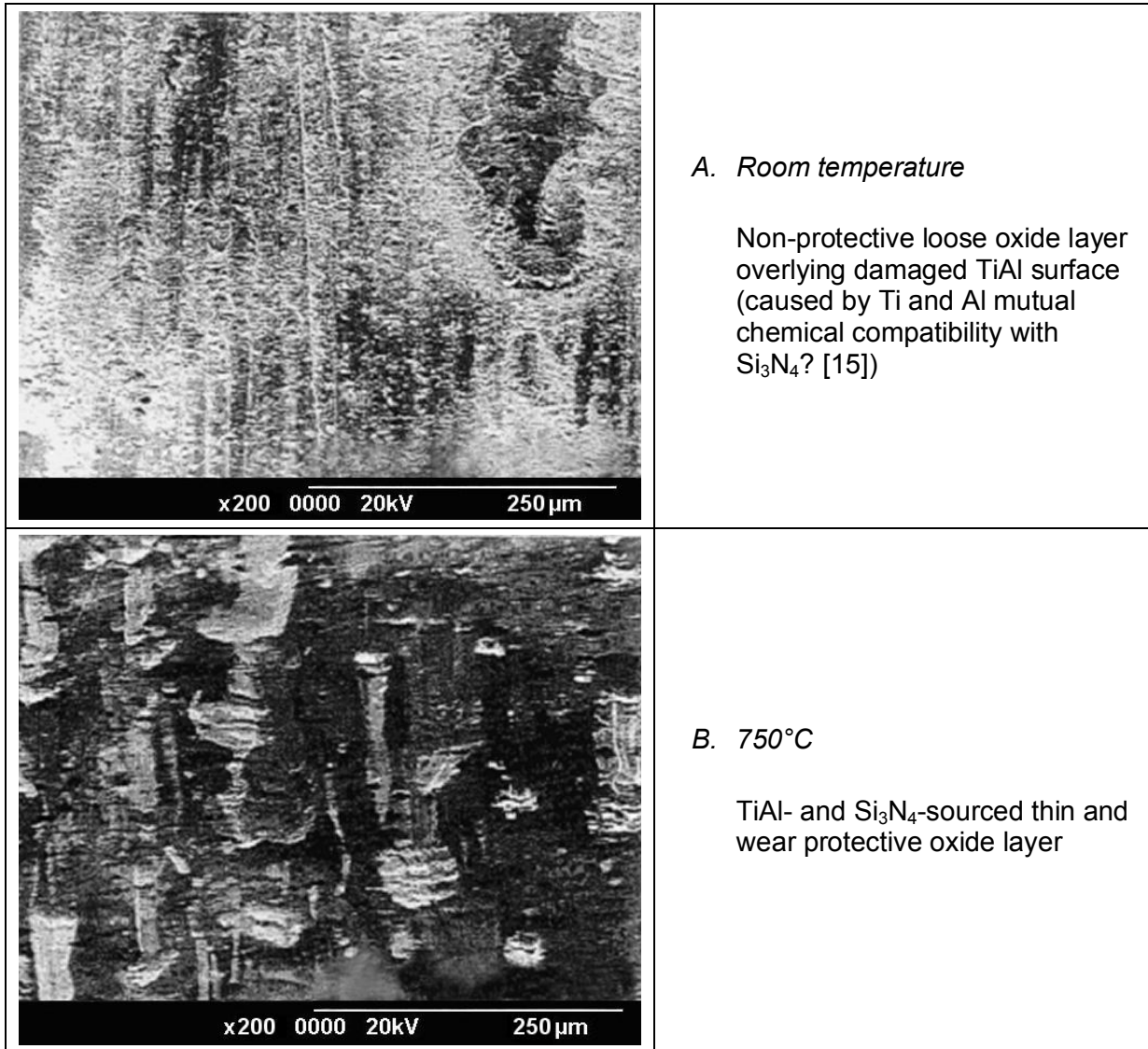
Fig. 17: Weight losses for Incoloy MA956 and Nimonic 80A worn against Incoloy 800HT and Stellite 6 counterface at applied loads of between 7 and 25N (750°C, sliding speed 0.654 m.s<sup>-1</sup>, sliding distance 9,418 m) [2]

Incoloy 800HT counterface		Stellite 6 counterface	
	<p>(a) <i>Room temperature</i></p> <p>Work hardened Incoloy 800HT transfer layer on TiAl surface</p>		<p>(c) <i>Room temperature</i></p> <p>Mixed oxide debris layer of Stellite 6-sourced Co / Cr and TiAl-sourced Ti and Al.</p>
	<p>(b) <i>750°C</i></p> <p>Oxidised layer consisting of Incoloy 800HT-sourced Fe, Ni and Cr, with a little TiAl-sourced Ti and Al</p>		<p>(d) <i>750°C</i></p> <p>Primarily Co-Cr oxide layer on TiAl surface</p>

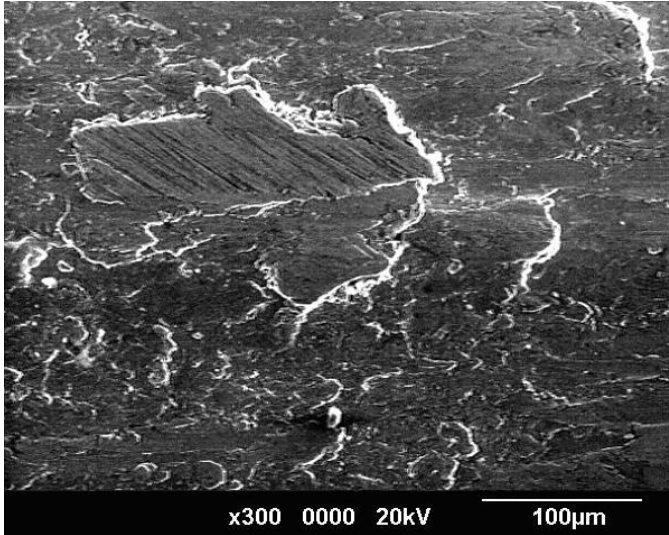
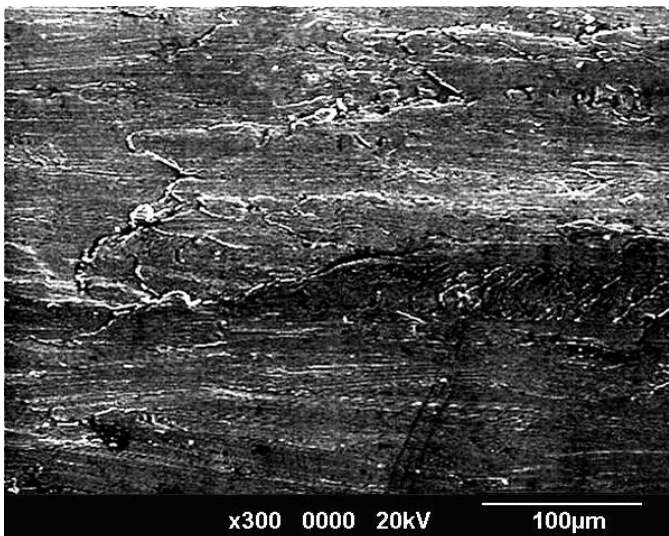
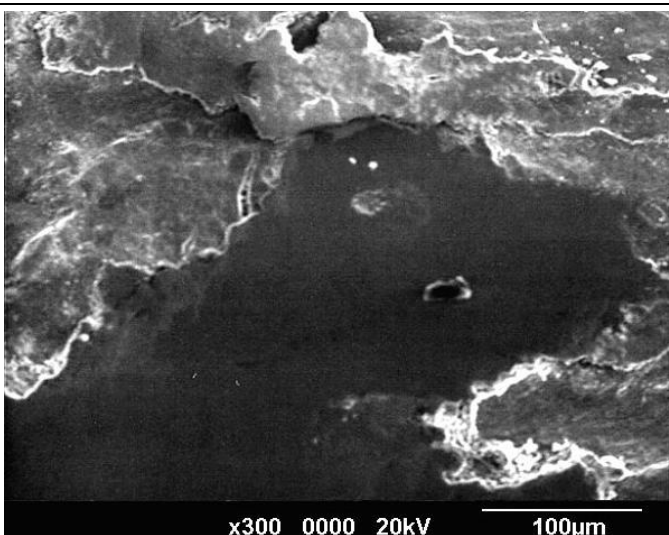
**Fig. 18: SEM micrographs of TiAl worn against an Incoloy 800HT counterface at (a) room temperature and (b) 750°C, and against a Stellite 6 counterface at (c) room temperature and (d) 750°C, sliding speed 0.654 m.s<sup>-1</sup> (load 7N, sliding distance 9,418 m) [1]**

	<p>A. <i>Stellite 6 counterface</i></p> <p>'Glaze' layer up to 3 µm thickness with limited fragmentation and break-away, most evident near top and top right</p> <p>Also some loose debris evident (lighter areas to left and right)</p>
	<p>B. <i>Si<sub>3</sub>N<sub>4</sub> counterface</i></p> <p>'Glaze' layer up to 3 µm thickness overlaid by a few fragments of broken-away 'glaze' of between 1 and 15 µm</p> <p>Also some loose debris and very limited break-away (streaks in bottom right hand corner)</p>
	<p>C. <i>Al<sub>2</sub>O<sub>3</sub> counterface</i></p> <p>Smooth 'glaze' layer up to 3 µm overlaid by fragments of broken-away 'glaze' of between 1 µm and 20 µm in size</p> <p>Little evidence of loose debris</p>

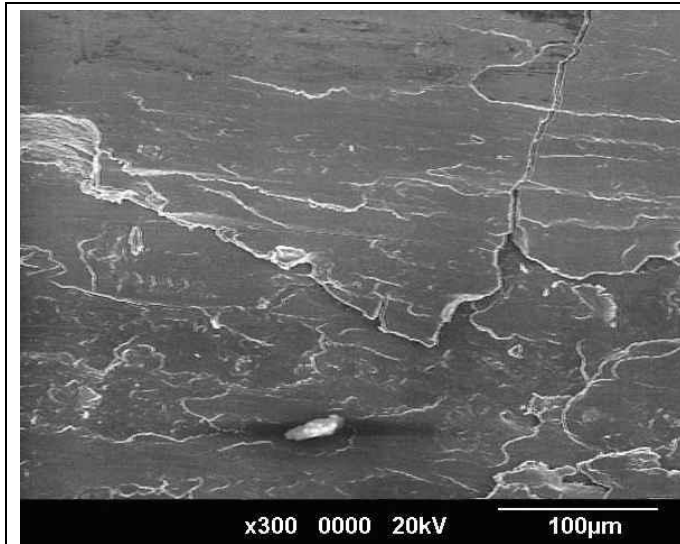
**Fig. 19: SEM micrographs of  $\gamma$ -TiAl wear scar surfaces after wear against Stellite 6, Si<sub>3</sub>N<sub>4</sub> and Al<sub>2</sub>O<sub>3</sub> counterfaces at 750°C, sliding speed 0.314 m.s<sup>-1</sup> (load 7N, sliding distance 4,522 m) [97]**



**Fig. 20: SEM micrographs of TiAl worn against a Si<sub>3</sub>N<sub>4</sub> counterface at (a) room temperature and (b) 750°C, sliding speed 0.654 m.s<sup>-1</sup> (load 7N, sliding distance 9,418 m) [1]**

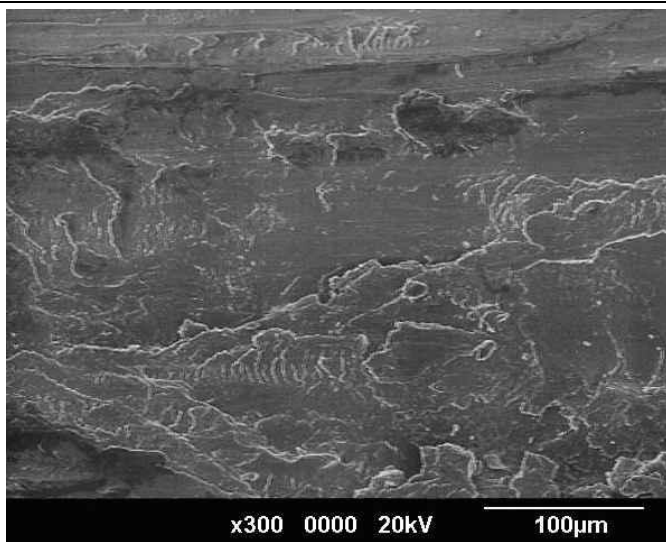
	<p>A. Room temperature (shown), also typical of 270°C</p> <p>Metallic transfer layer with moderate levels of metallic debris generation at room temperature (R.T.) and 270°C</p>
	<p>B. 510°C (shown), also typical of 390, 450, 570 and 630°C</p> <p>Limited patchy metallic transfer at 510°C, surface mostly exposed sample material</p>
	<p>C. 750°C (shown), also typical of 690°C</p> <p>'Glaze' at 750°C, overlying slightly more developed metallic transfer layer than seen at 510°C</p>

**Fig. 21: SEM micrographs of Nimonic 80A wear surfaces after sliding at 0.314 m.s<sup>-1</sup> (load 7N, sliding distance 4,522 m) against an Incoloy 800HT counterface at room temperature, 270, 570 and 750°C [3]**



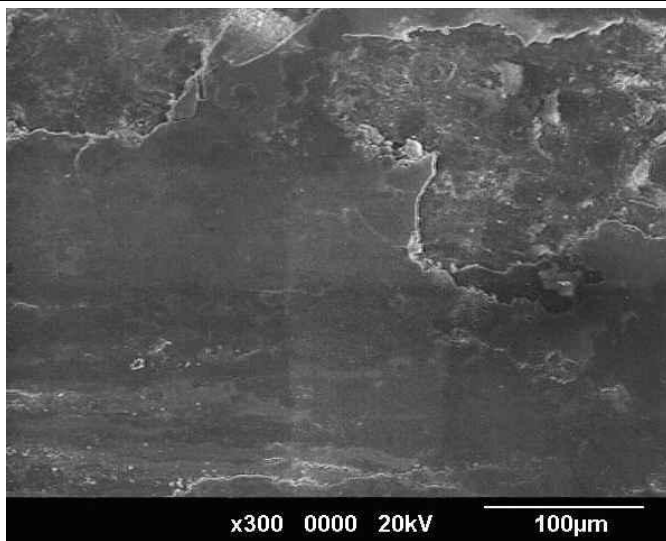
A. Room temperature and 270°C (shown), also typical of 390°C

Metallic transfer layer with moderate levels of metallic debris generation at room temperature (R.T.) and 270°C, greater transfer of metal onto sample surface than at 0.314 m.s<sup>-1</sup> (Fig. A1)



B. 570°C (shown), also typical of 450, 510 and 630°C

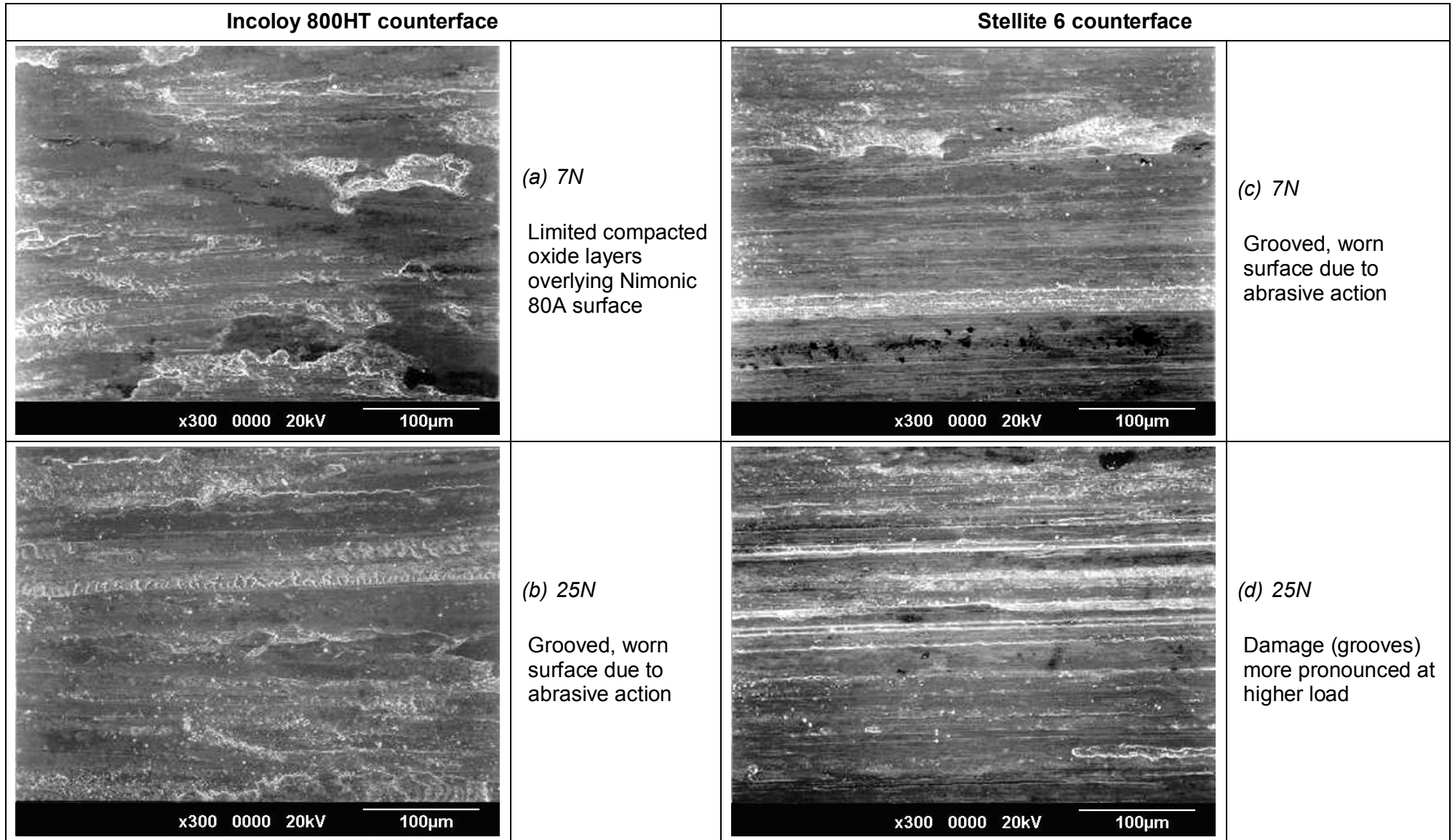
Comprehensive metallic transfer continuing at 510°C (greater than at 0.314 m.s<sup>-1</sup> – Fig. A1) – metallic debris generation from both sample and counterface



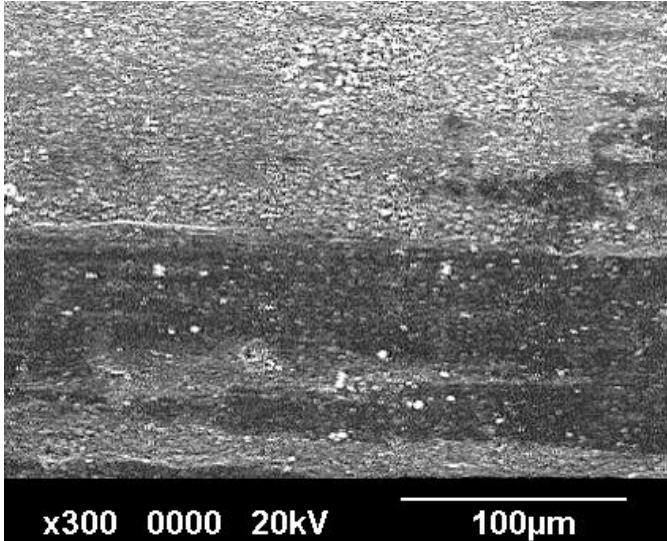
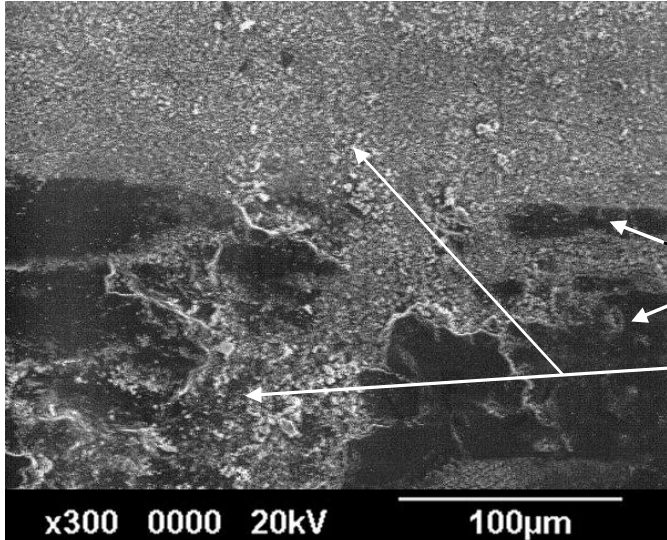
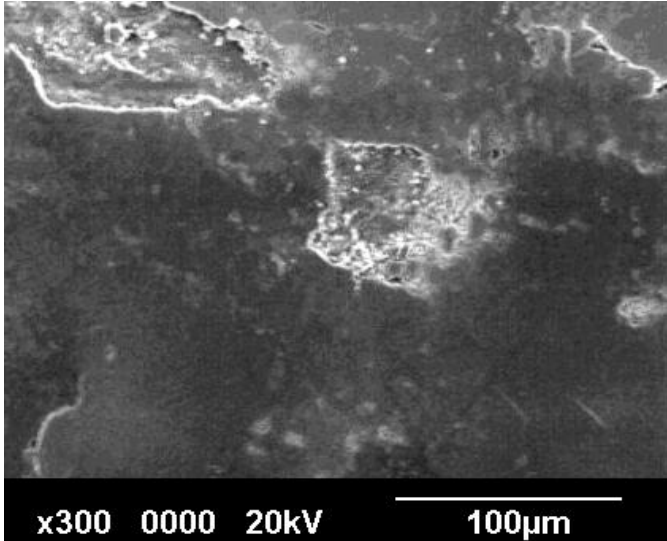
C. 750°C (shown), also typical of 690°C

'Glaze' at 750°C, overlying more limited metallic transfer layer

**Fig. 22: SEM micrographs of Nimonic 80A wear surfaces after sliding at 0.905 m.s<sup>-1</sup> (load 7N, sliding distance 4,522 m) against an Incoloy 800HT counterface at room temperature, 270, 570 and 750°C [3]**



**Fig. 23: SEM micrographs of Nimonic 80A worn against an Incoloy 800HT counterface at applied loads of (a) 7N and (b) 25N, also against a Stellite 6 counterface at applied loads of (a) 7N and (b) 25N (750°C, sliding speed 0.654 m.s<sup>-1</sup>, sliding distance 9,418 m) [2]**

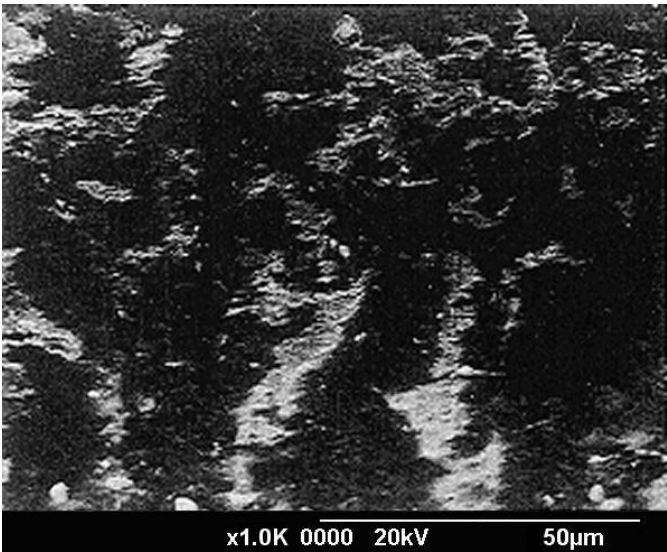
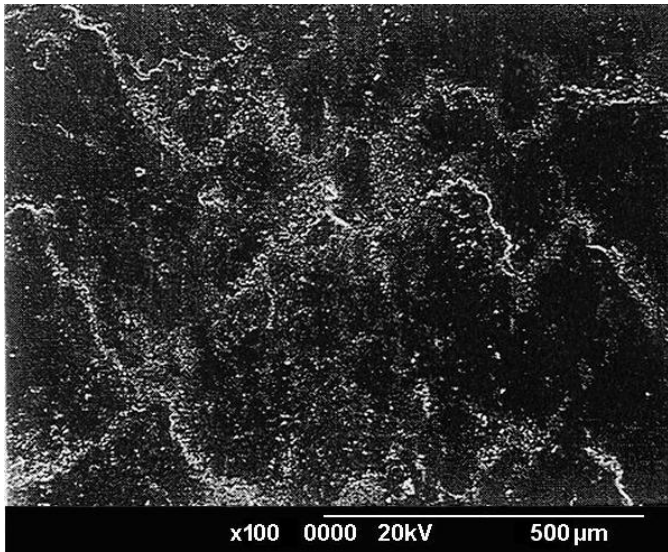
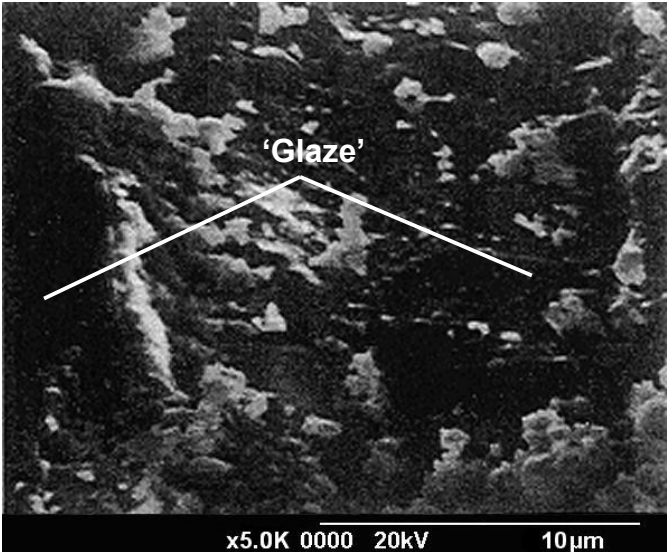
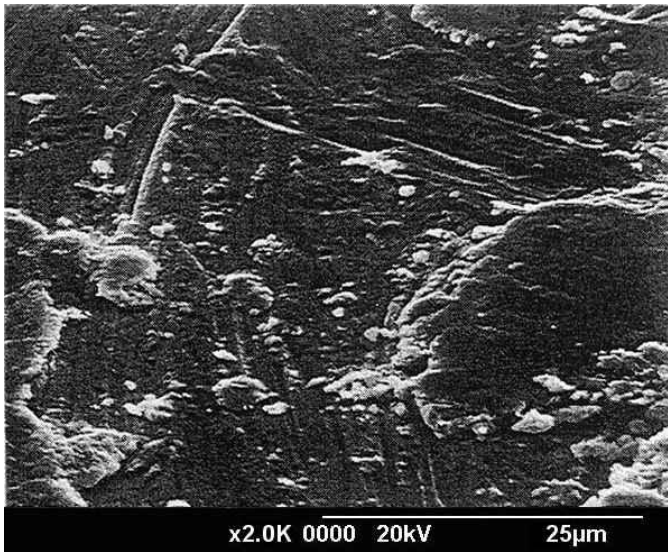
	<p>A. <i>Room temperature (shown), also typical of 270, 390 and 450°C</i></p> <p>Loose oxide separating wear surfaces, plus some compacted oxide layers – isolated patches of ‘glaze’ at 450°C only (not shown)</p>
	<p>B. <i>510°C</i></p> <p>Areas of smooth, protective ‘glaze’ layer formation</p> <p>Some accompanying loose debris.</p>
	<p>C. <i>750°C (shown), also typical of 570, 630 and 690°C</i></p> <p>Smooth, protective ‘glaze’ layer formation with very little loose debris (greater debris incorporation)</p>

**Fig. 24: SEM micrographs of Nimonic 80A wear surfaces after sliding at 0.314 m.s<sup>-1</sup> (load 7N, sliding distance 4,522 m) against a Stellite 6 counterface at room temperature, 510 and 750°C [21]**



	<p>A. Room temperature and 270°C (shown), also typical of 390°C (0.654 m.s<sup>-1</sup> only)</p> <p>Loose oxide separating wear surfaces</p>
	<p>B. 570°C (shown), also typical of 390 (0.905 m.s<sup>-1</sup> only) 450, 510 and 630°C</p> <p>390 (0.905 m.s<sup>-1</sup> only), 450, 510 and 570°C - torn, metallic surface typical of adhesive wear, no traces of any oxide debris</p> <p>630°C – adhesive wear persists, however, some oxide present and assisting wear by abrasion (not shown)</p>
	<p>C. 750°C (shown), also typical of 690°C</p> <p>Parallel grooves due to abrasion (holding some loose oxide debris)</p>

**Fig. 25: SEM micrographs of Nimonic 80A wear surfaces after sliding at 0.654 m.s<sup>-1</sup> (load 7N, sliding distance 4,522 m) against a Stellite 6 counterface at room temperature, 270, 570 and 750°C (also typical of 0.905 m.s<sup>-1</sup>) [21]**

Nimonic 80A sample		Nimonic 90 sample	
	<p>(a) Room temperature</p> <p>Loose oxide (sourced from both Nimonic 80A and Si<sub>3</sub>N<sub>4</sub>) providing only limited protection to Nimonic 80A (cast) surface</p>		<p>(c) Room temperature</p> <p>Loose oxide (sourced from both Nimonic 90 and Si<sub>3</sub>N<sub>4</sub>) providing only limited protection to Nimonic 90 surface</p>
	<p>(b) 750°C</p> <p>Damaged Nimonic 80A (cast) surface with no protective 'glaze' layer</p>		<p>(d) 750°C</p> <p>Areas of 'glaze' formation protecting Nimonic 90 from enhanced wear</p>

**Fig. 26: SEM micrographs of Nimonic 80A (cast) at (a) room temperature and (b) 750°C, also Nimonic 90 at (c) room temperature and (d) 750°C, worn against a Si<sub>3</sub>N<sub>4</sub> counterface, sliding speed 0.654 m.s<sup>-1</sup> (load 7N, sliding distance 9,418 m) [1]**

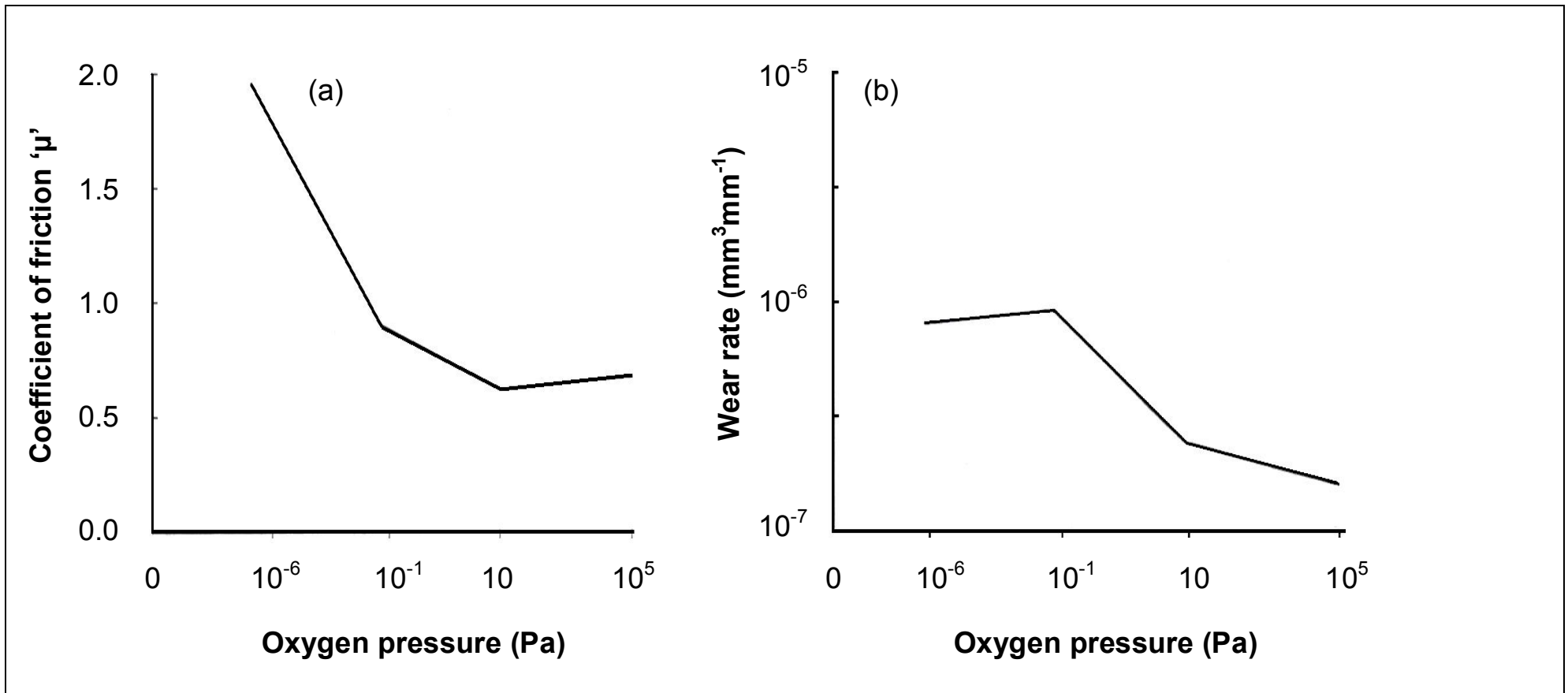


Fig. 27: Variation of coefficient of friction (A) and wear rate (B) of Fe-4.9%Cr with oxygen partial pressure during like-on-like sliding at 20°C [100]

- (a) standard test, no pre-oxidation      (d) pre-oxidation at 300°C for 3 hours  
 (b) pre-oxidation at 300°C for 5 minutes      (e) pre-sliding for 300 m at 300°C  
 (c) pre-oxidation at 300°C for 1 hour      (loose accumulated oxide layer formed)

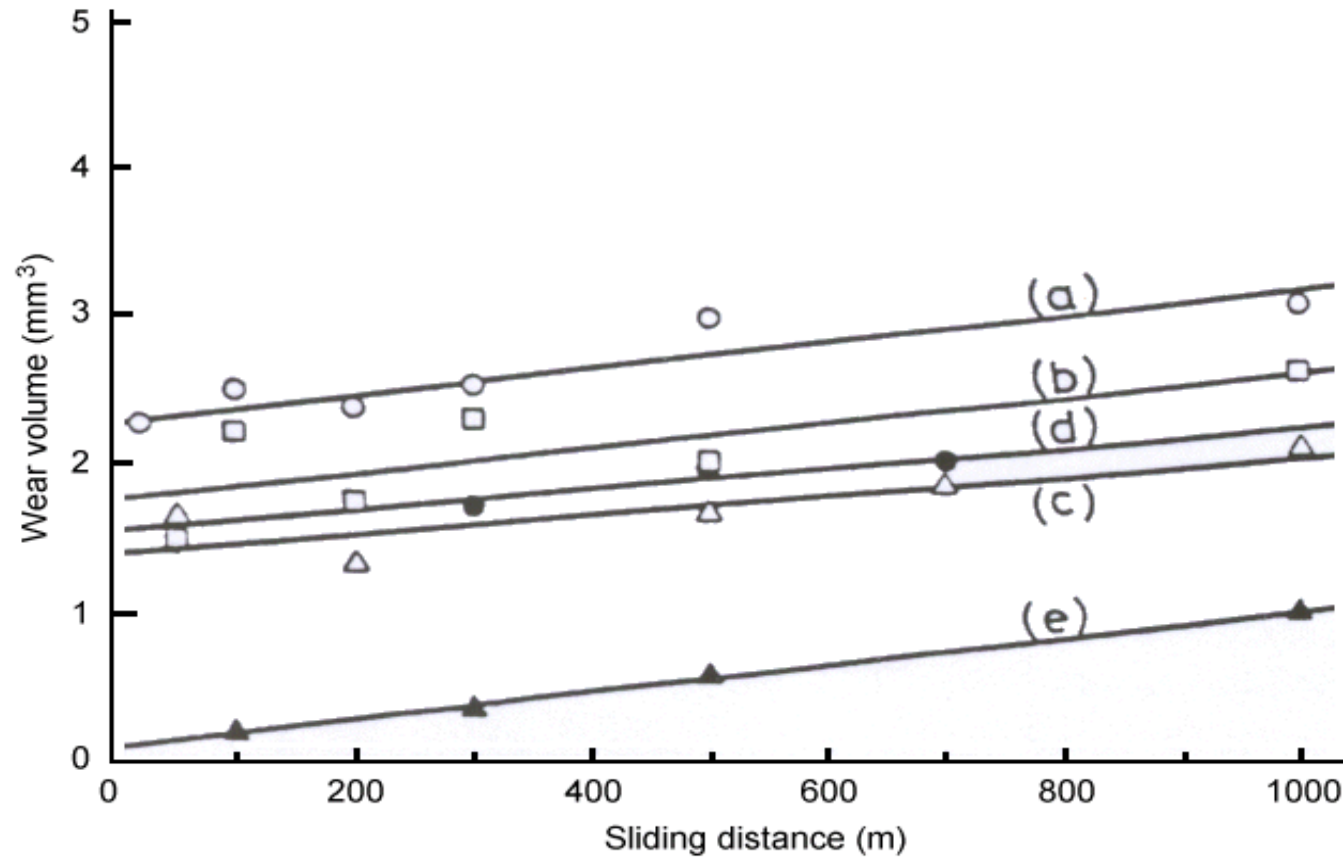
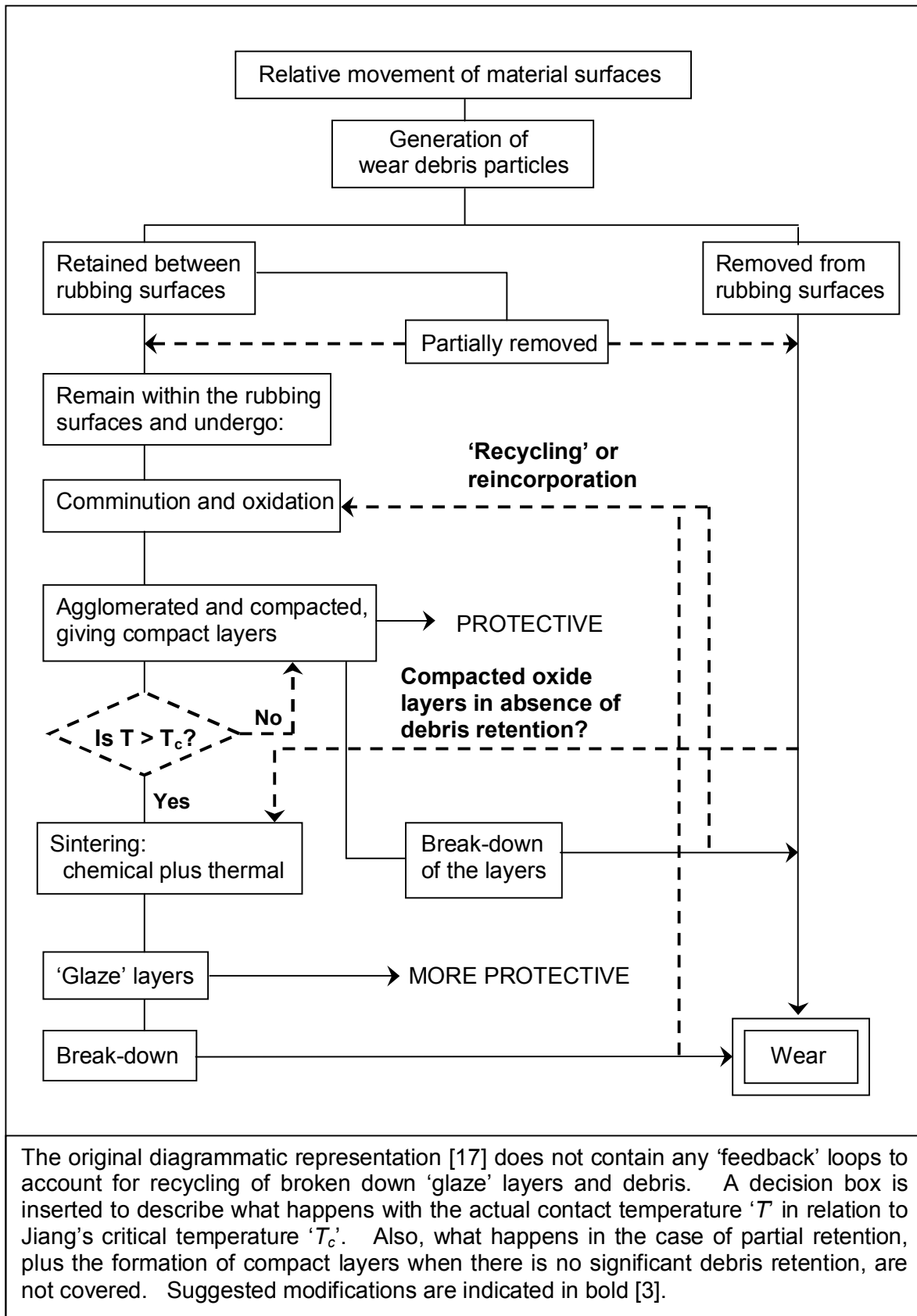
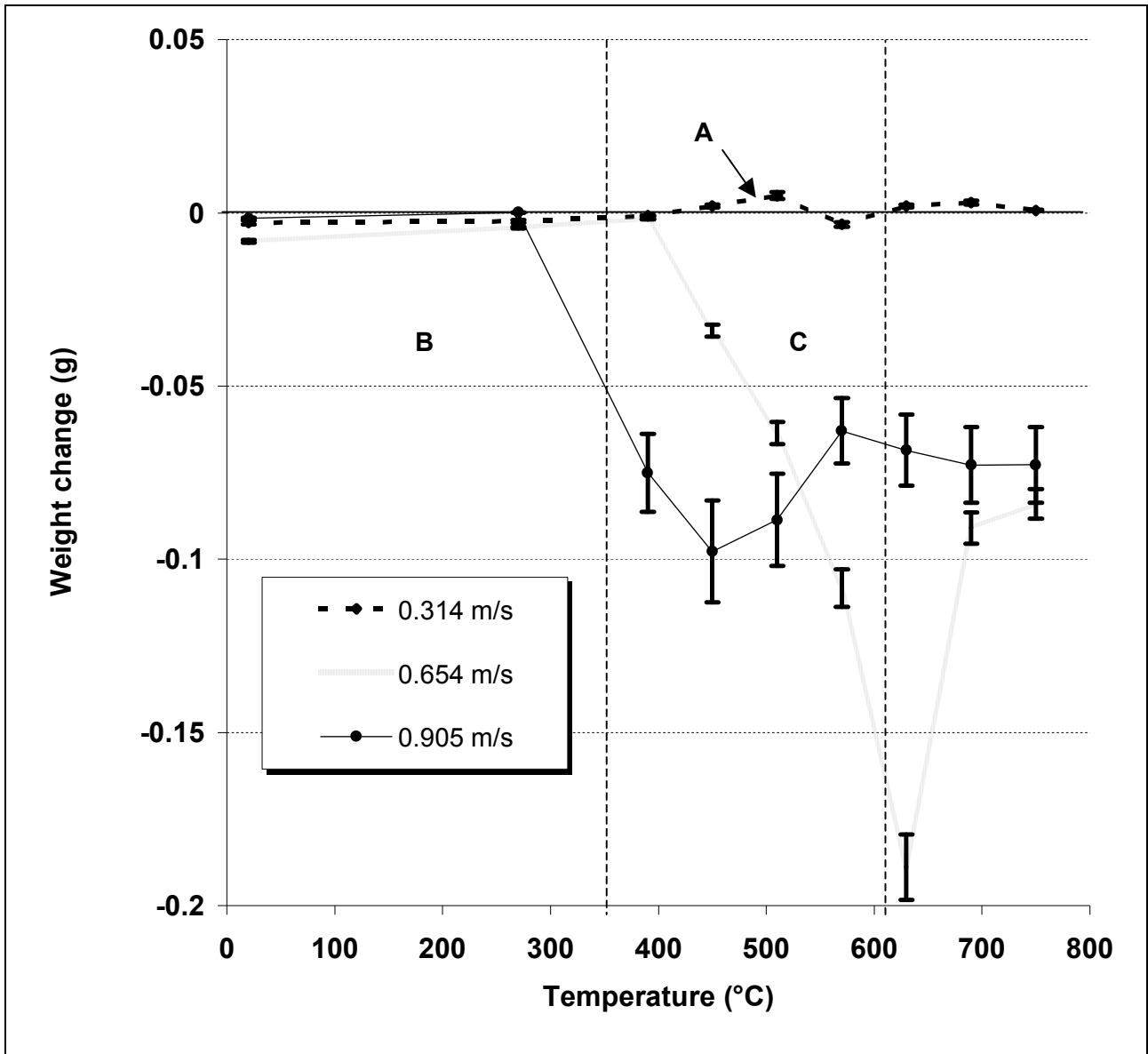


Fig. 28: Effects of pre-oxidation and pre-sliding on wear of S45C at 20°C [33]



**Fig. 29: 'Modified' version of Jiang's diagrammatic representation of sliding wear processes at various temperatures [3,17]**



At 0.314 m.s<sup>-1</sup>:

A. Loose oxide debris spread across wear surface, plus some compacted oxide formation, room temperature to 390°C; smooth 'glaze' layers with only a little loose debris (450°C to 750°C)

At 0.654 and 0.905 m.s<sup>-1</sup>:

B. Loose oxide debris spread across wear surface, plus some compacted oxide formation (room temperature and 270°C at both 0.654 m.s<sup>-1</sup> and 0.905 m.s<sup>-1</sup>, also 390°C at 0.654 m.s<sup>-1</sup>)

C. Torn, metallic surface typical of adhesive wear, no traces of any oxide debris (390°C to 510°C) or only very limited oxide debris formation (at 0.905 m.s<sup>-1</sup> – 570°C; at 0.654 m.s<sup>-1</sup> and 0.905 m.s<sup>-1</sup> – 630°C)

D. Loose oxide but with no compact oxide layers at 0.654 m.s<sup>-1</sup> and only isolated build-ups of oxide at 0.905 m.s<sup>-1</sup>; fine parallel grooves in direction of sliding on Nimonic 80A surface (690°C to 750°C)

**Fig. 30: Weight change versus temperature for Nimonic 80A slid against Stellite 6 at 0.314, 0.654 and 0.905 m.s<sup>-1</sup> (load 7N, sliding distance 4,522 m) [21]**

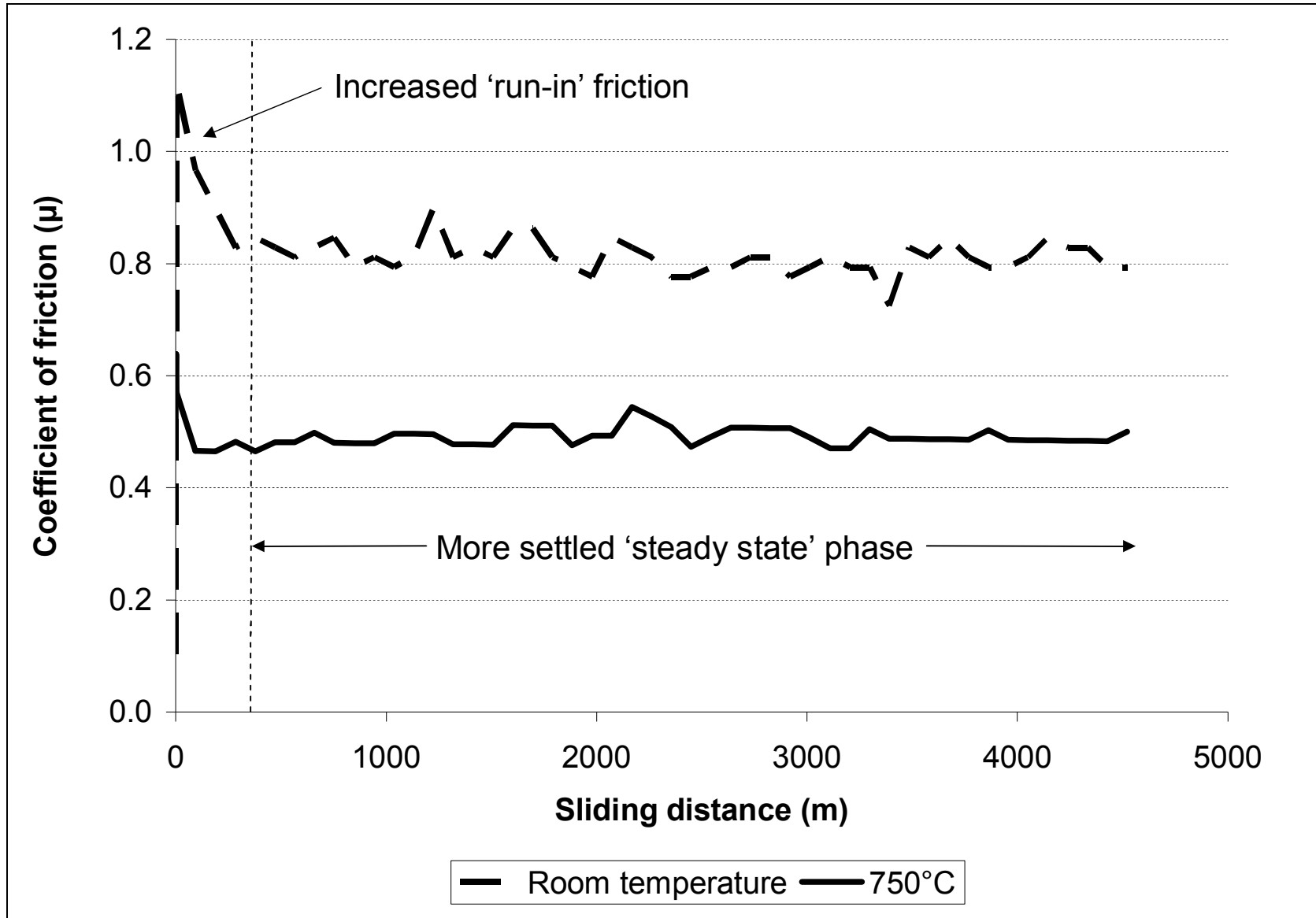
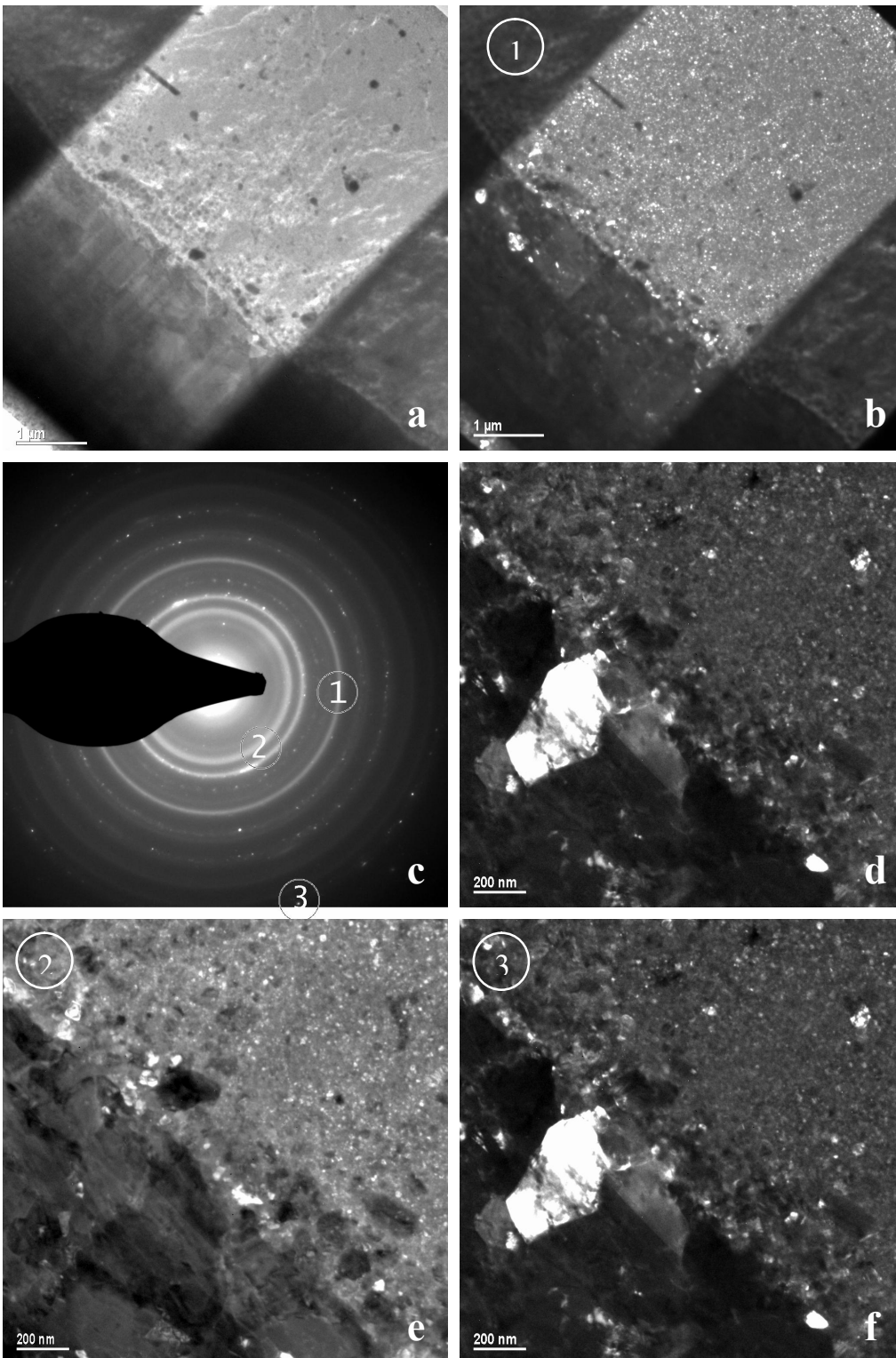
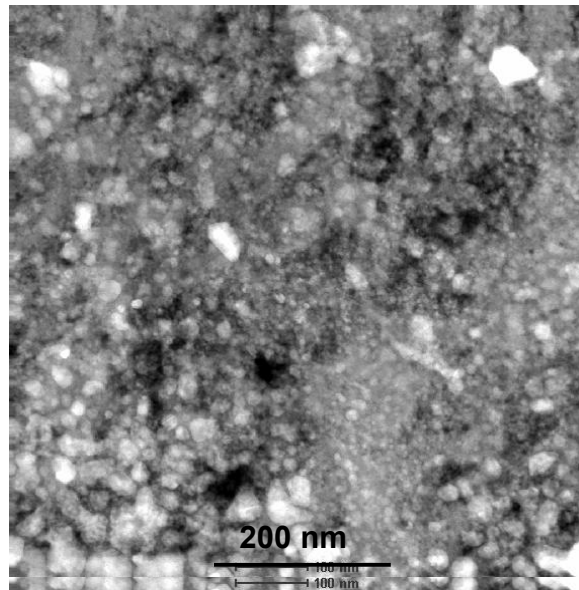
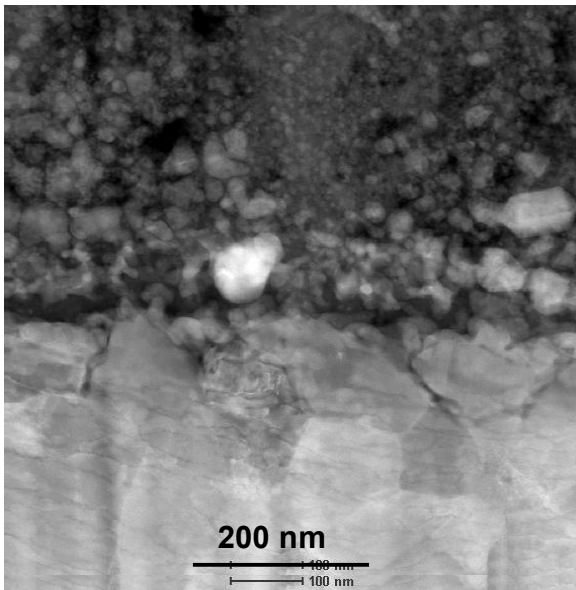
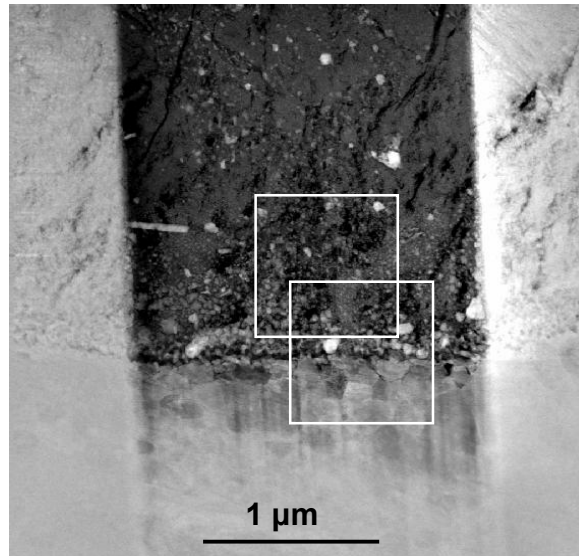


Fig. 31: Coefficient of friction versus time for Nimonic 80A versus Stellite 6 at  $0.314 \text{ m.s}^{-1}$ , room temperature and  $750^\circ\text{C}$  [3, 20, 24]



**Fig. 32: TEM overview of a cross-section of the wear affected surface (Nimonic 80A versus Stellite 6,  $0.314 \text{ m}\cdot\text{s}^{-1}$ ,  $20^\circ\text{C}$ , load 7N, sliding distance 4,522 m): (a) bright-field overview image of the Nimonic 80A and the 'glaze' layer; (b) dark-field image of the nano-crystalline 'glaze' layer (obtained with a 10 micron objective aperture as indicated in the SAD pattern by (1)); (c) selected area diffraction (SAD) pattern of the cross-section; (d) bright-field image of the interface; (e) dark-field image of the nano-crystalline 'glaze' layer close to the interface (as indicated in the SAD pattern by (2)); (f) dark-field image of a larger crystal in the Nimonic 80A close to the interface (as indicated in the SAD pattern by (3)) [113]**





**Fig. 33: HAADF-STEM (200 mm camera length) overview image and close-up of the interface and the nano-crystalline 'glaze' layer (Nimonic 80A versus Stellite 6,  $0.314 \text{ m.s}^{-1}$ ,  $20^\circ\text{C}$ , load 7N, sliding distance 4,522 m) [113]**

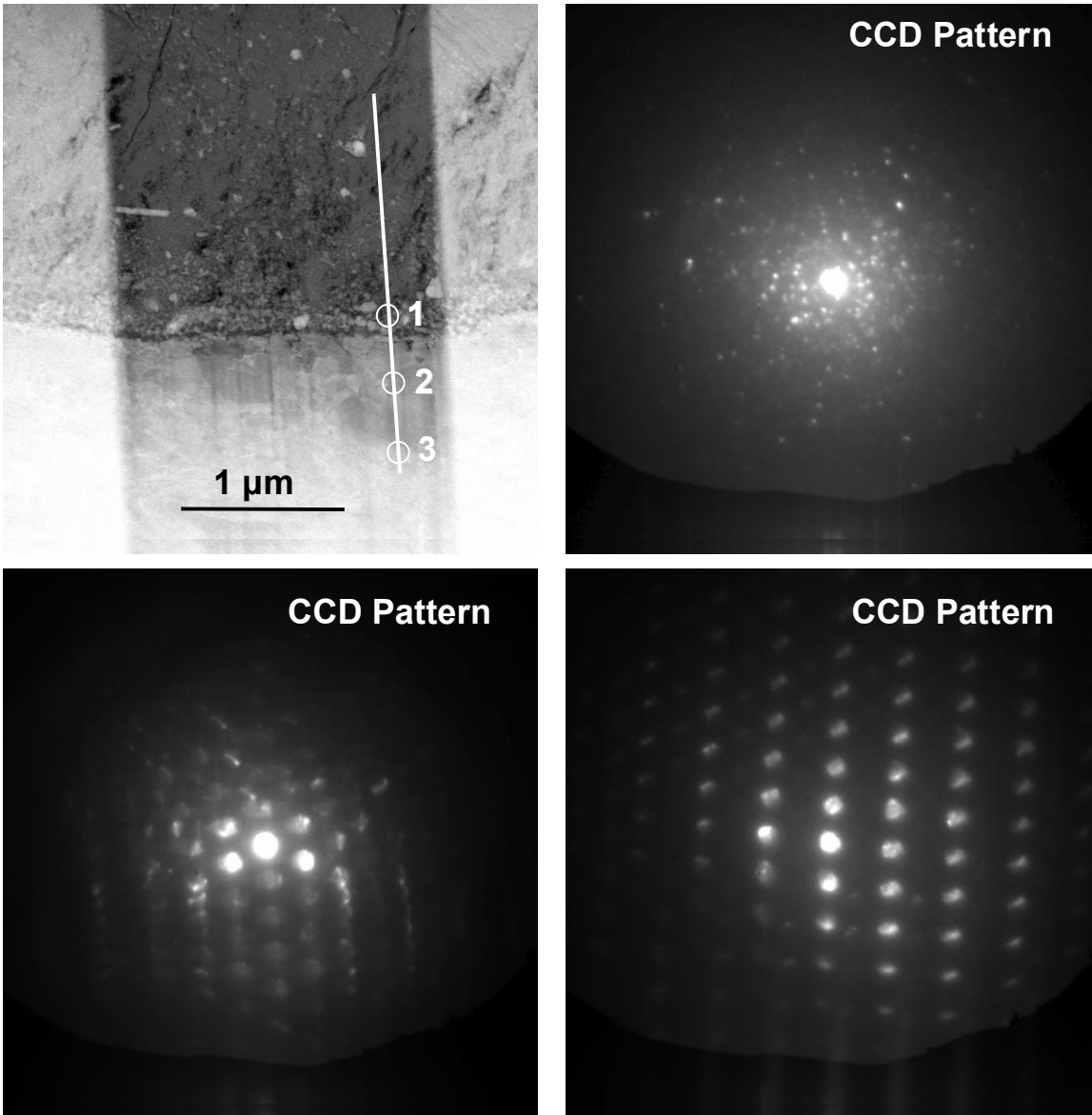


**Fig. 34: HAADF-STEM overview image with examples from a CCD line trace (Nimonic 80A versus Stellite 6,  $0.314 \text{ m}\cdot\text{s}^{-1}$ ,  $20^\circ\text{C}$ , load 7N, sliding distance 4,522 m) [113]**

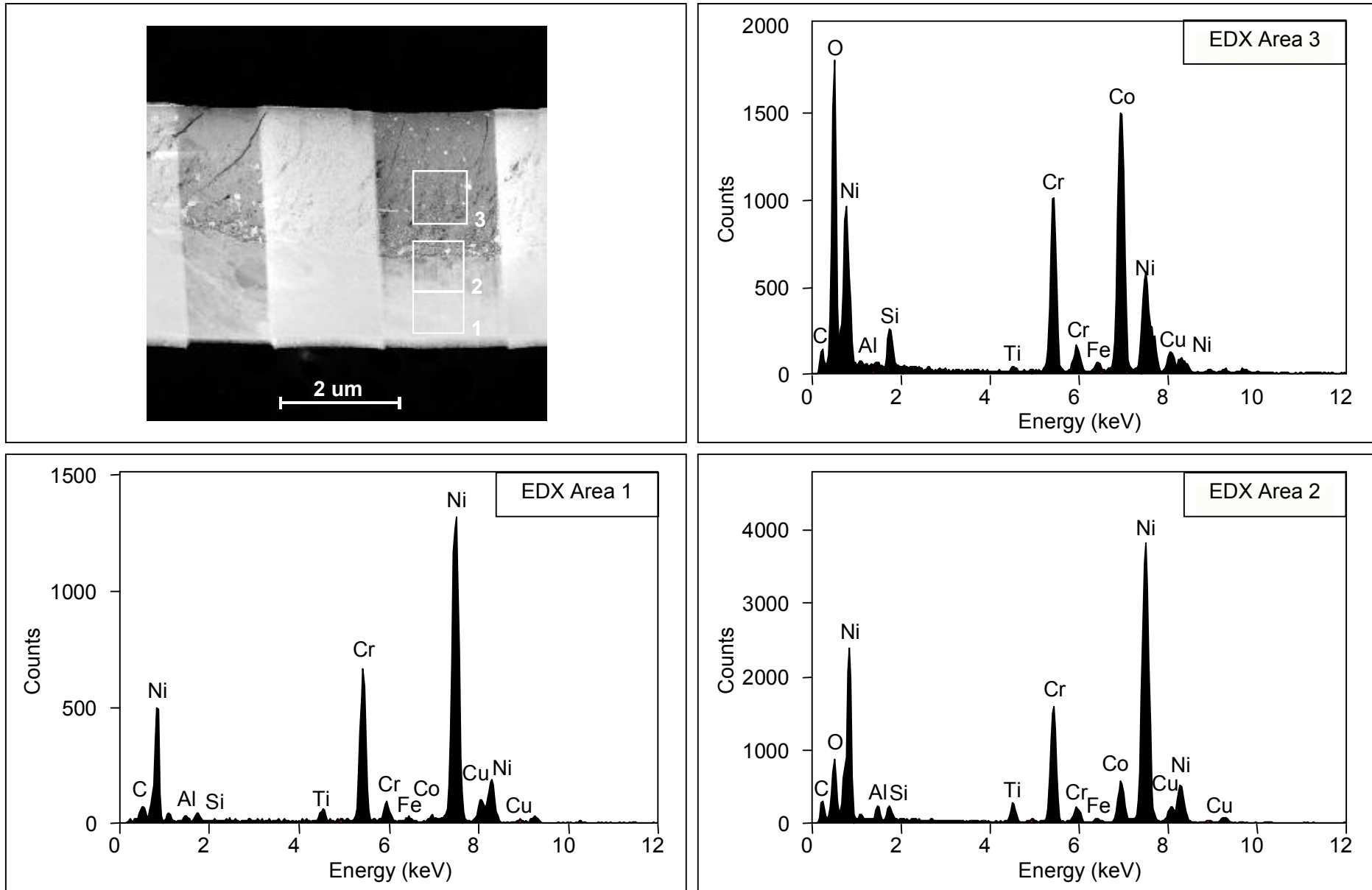


**Fig. 35: HAADF-STEM (200 mm camera length) overview image and local EDX analysis (Nimonic 80A versus Stellite 6, 0.314 m.s<sup>-1</sup>, 20°C, load 7N, sliding distance 4,522 m) [113]**

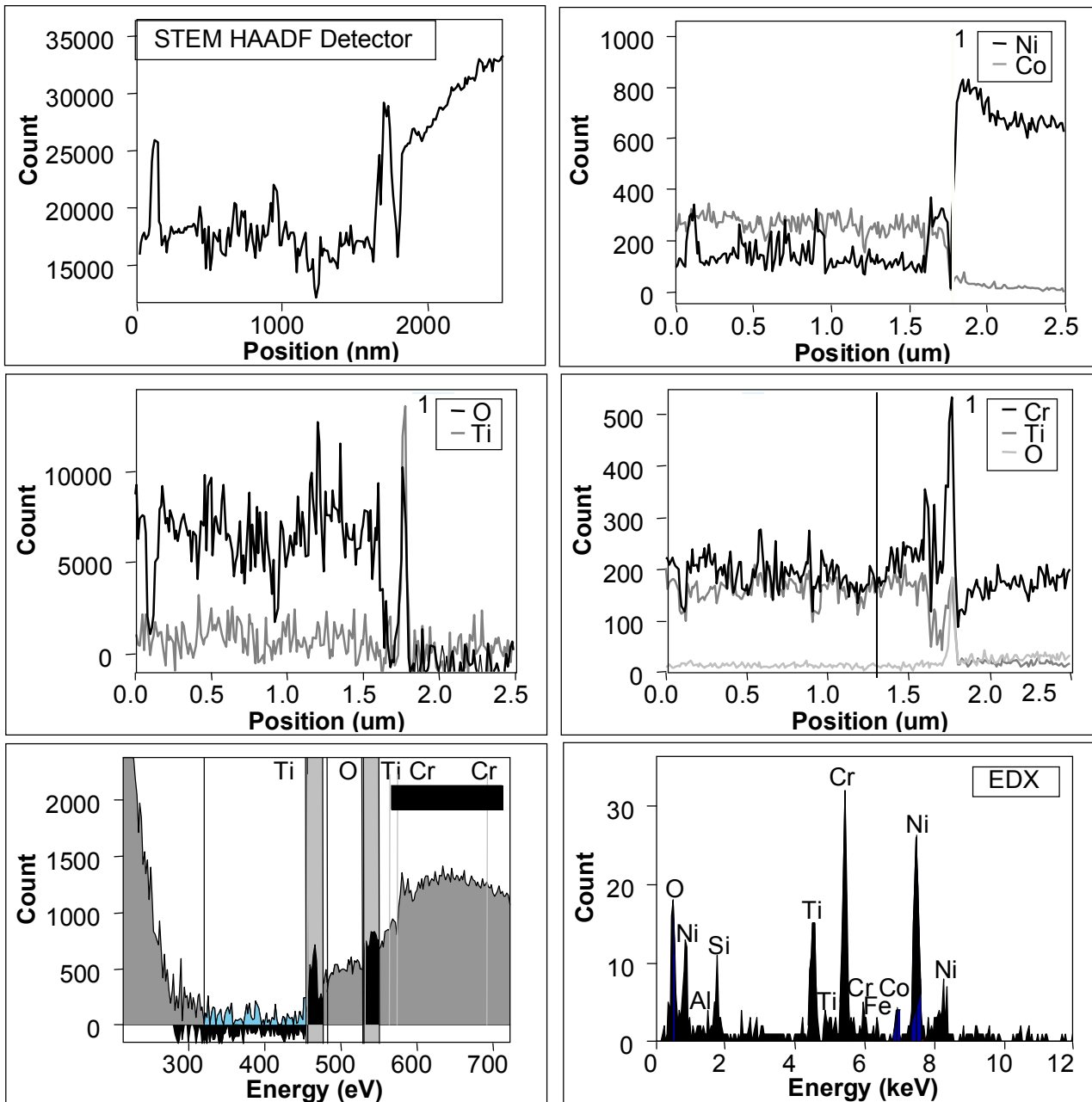
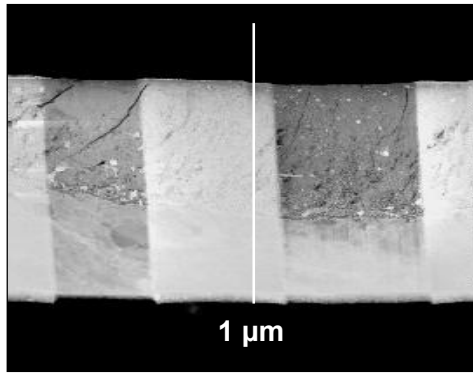


**Fig. 36: HAADF-STEM EELS/EDX line trace revealing the compositional variations of the wear affected surface (Nimonic 80A versus Stellite 6,  $0.314 \text{ m}\cdot\text{s}^{-1}$ ,  $20^\circ\text{C}$ , load  $7\text{N}$ , sliding distance  $4,522 \text{ m}$ ); line trace performed with  $1 \text{ nm}$  probe size and spectra collected every  $10 \text{ nm}$  [113]**

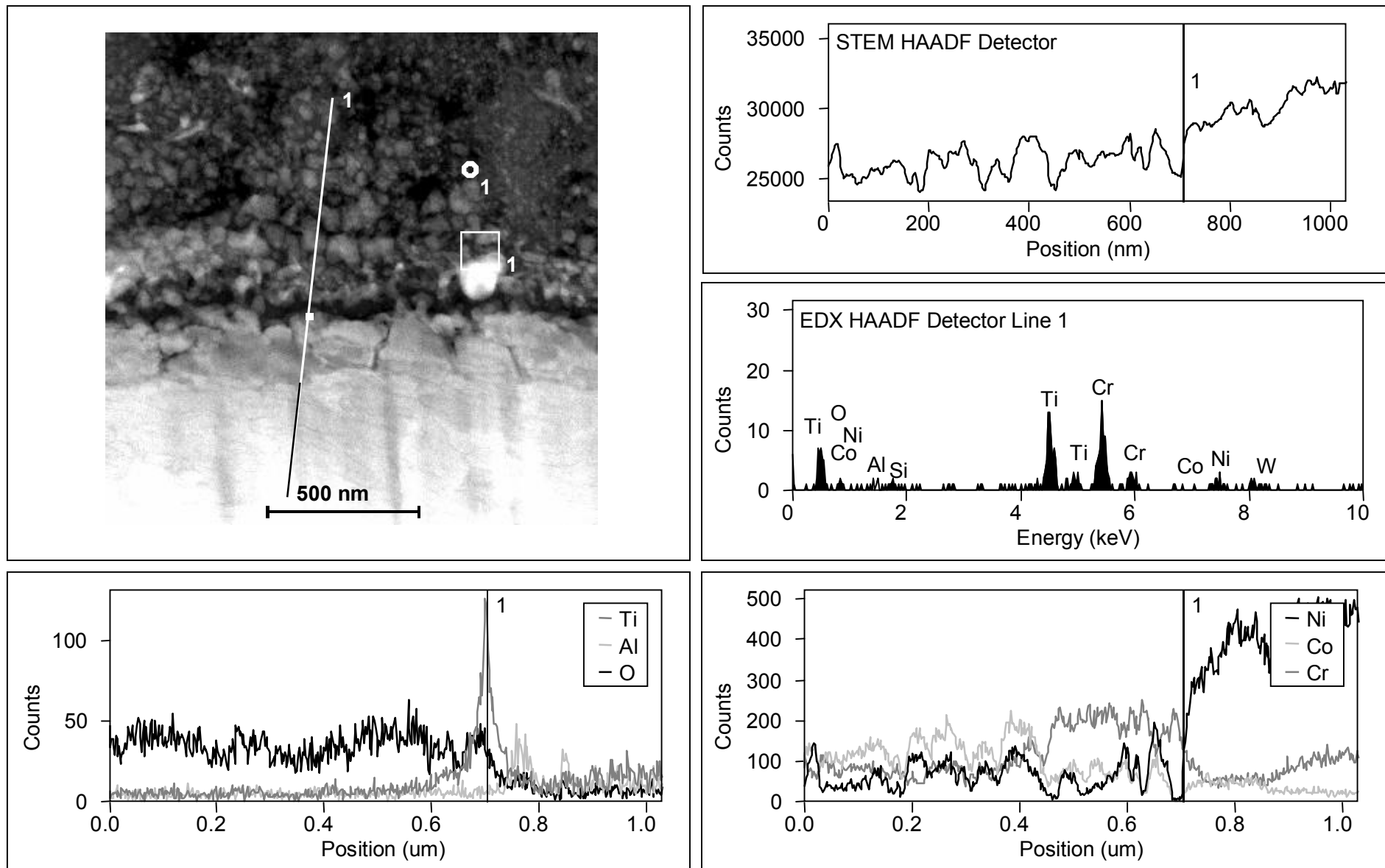


**Fig. 37: HAADF-STEM (200 mm camera length) overview and EDX line trace revealing the compositional variations of the wear interface structure (Nimonic 80A versus Stellite 6,  $0.314 \text{ m}\cdot\text{s}^{-1}$ ,  $20^\circ\text{C}$ , load 7N, sliding distance 4,522 m); the line trace was performed with a 1 nm probe size and spectra collected every 2 nm [113]**

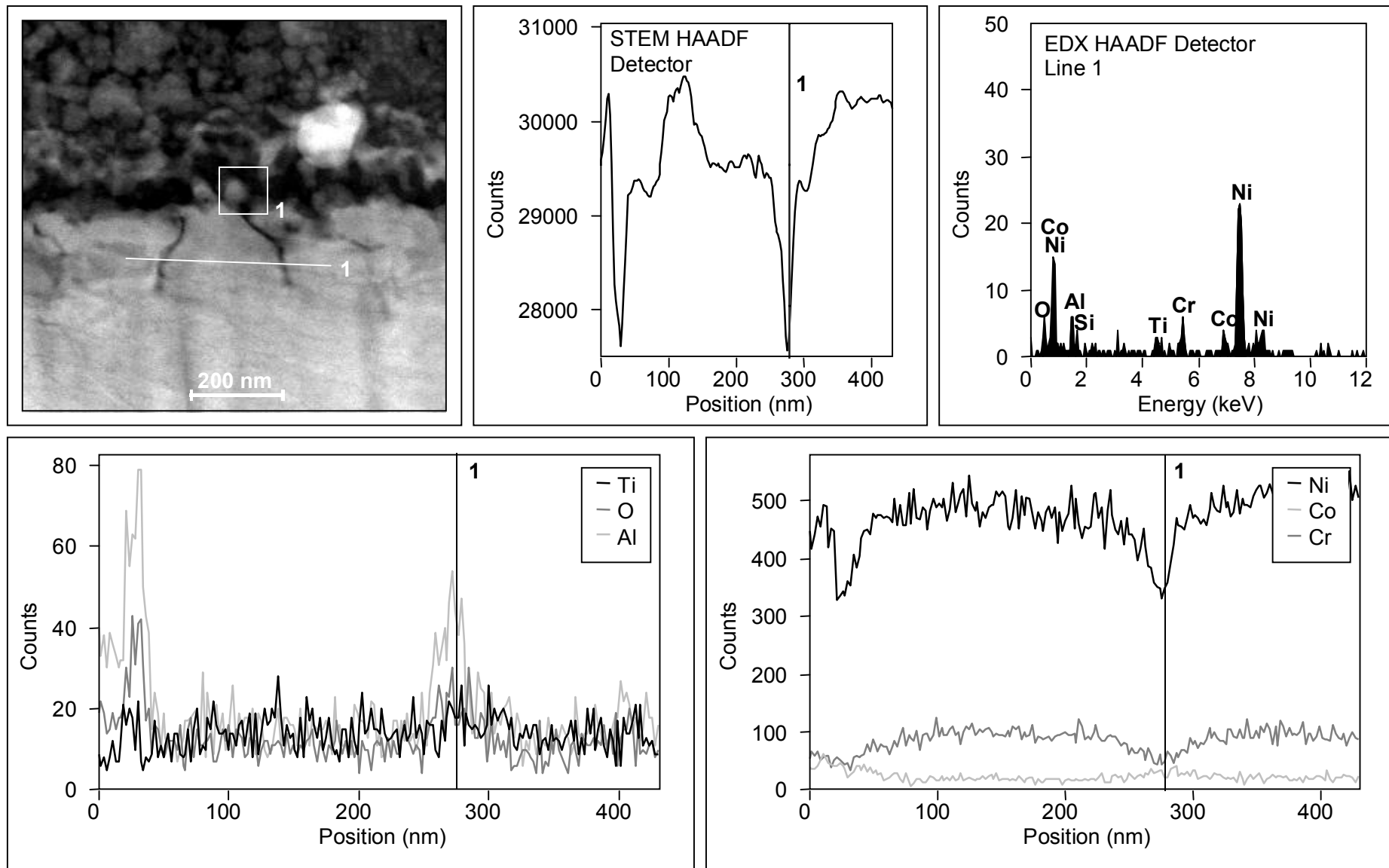


**Fig. 38: HAADF-STEM (50 mm camera length) overview and EDX line trace revealing the aluminium (oxide) segregation at the top of the Nimonic 80A phase (Nimonic 80A versus Stellite 6,  $0.314 \text{ m.s}^{-1}$ ,  $20^\circ\text{C}$ , load 7N, sliding distance 4,522 m); the line trace was performed with a 1 nm probe size and spectra collected every 2 nm [113]**

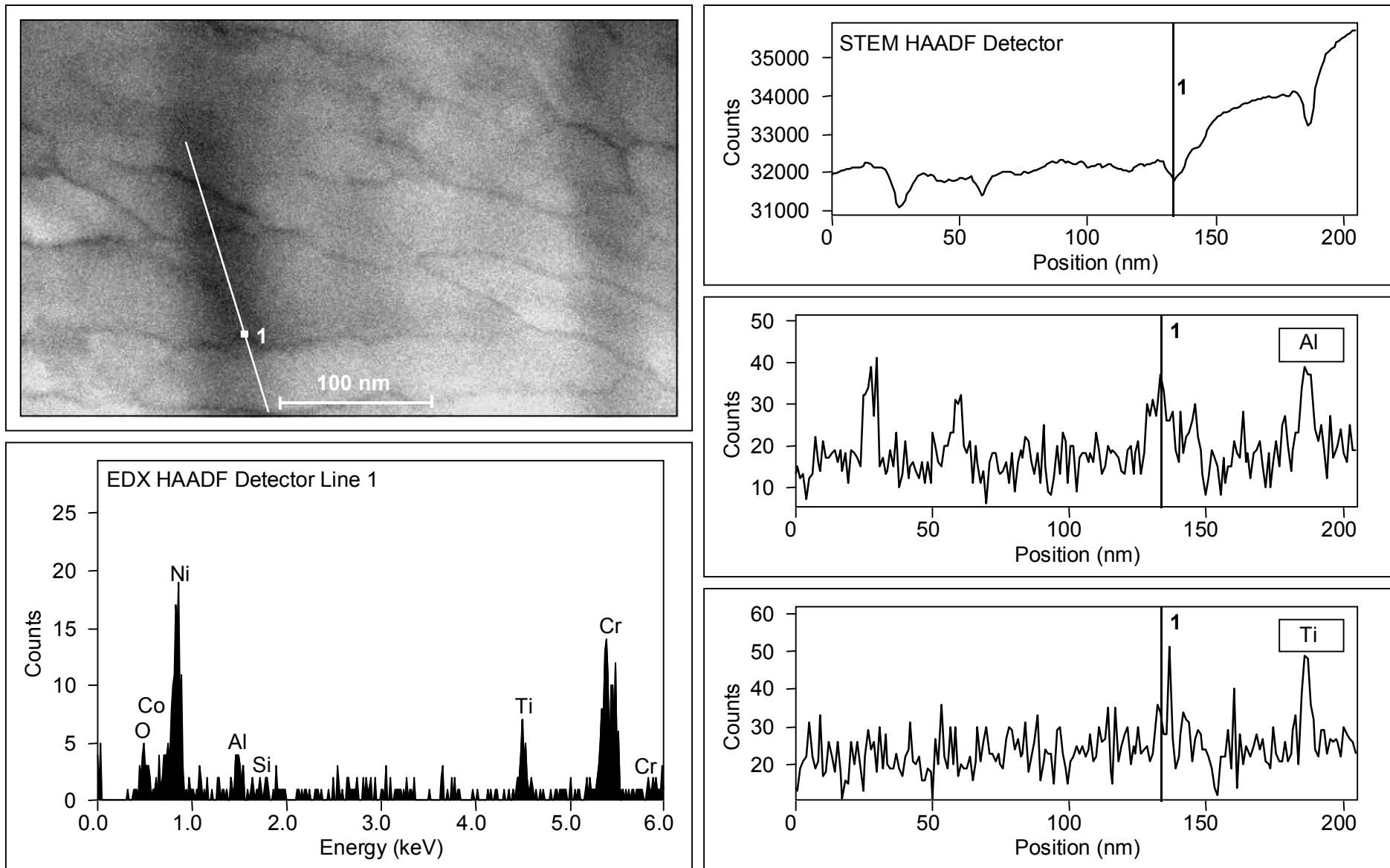


**Fig. 39: HAADF-STEM (50 mm camera length) overview and EDX line trace revealing the precipitation of light elements (aluminium and titanium) in the Nimonic 80A close to the wear interface (Nimonic 80A versus Stellite 6,  $0.314 \text{ m}\cdot\text{s}^{-1}$ ,  $20^\circ\text{C}$ , load 7N, sliding distance 4,522 m) [113]**

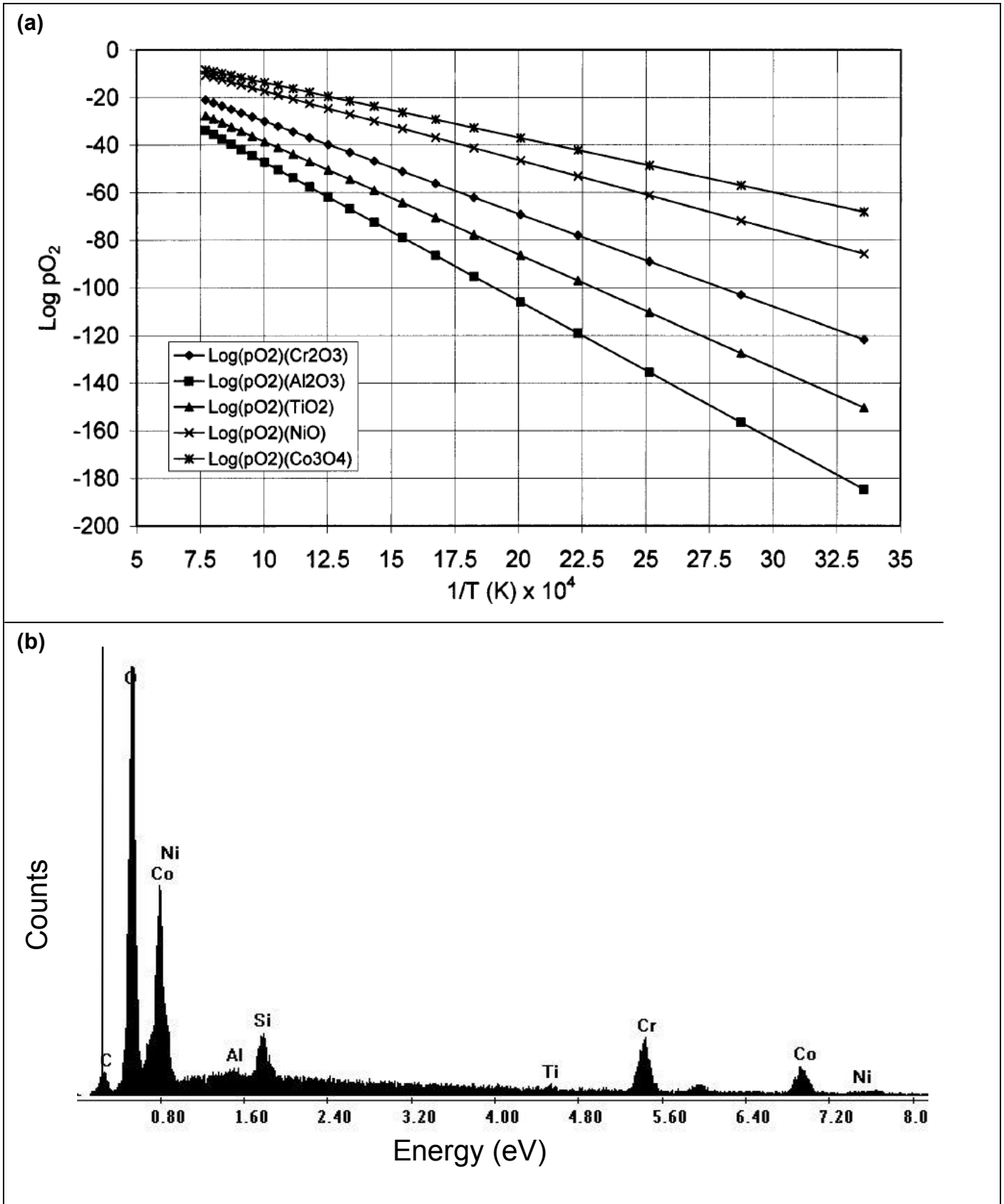
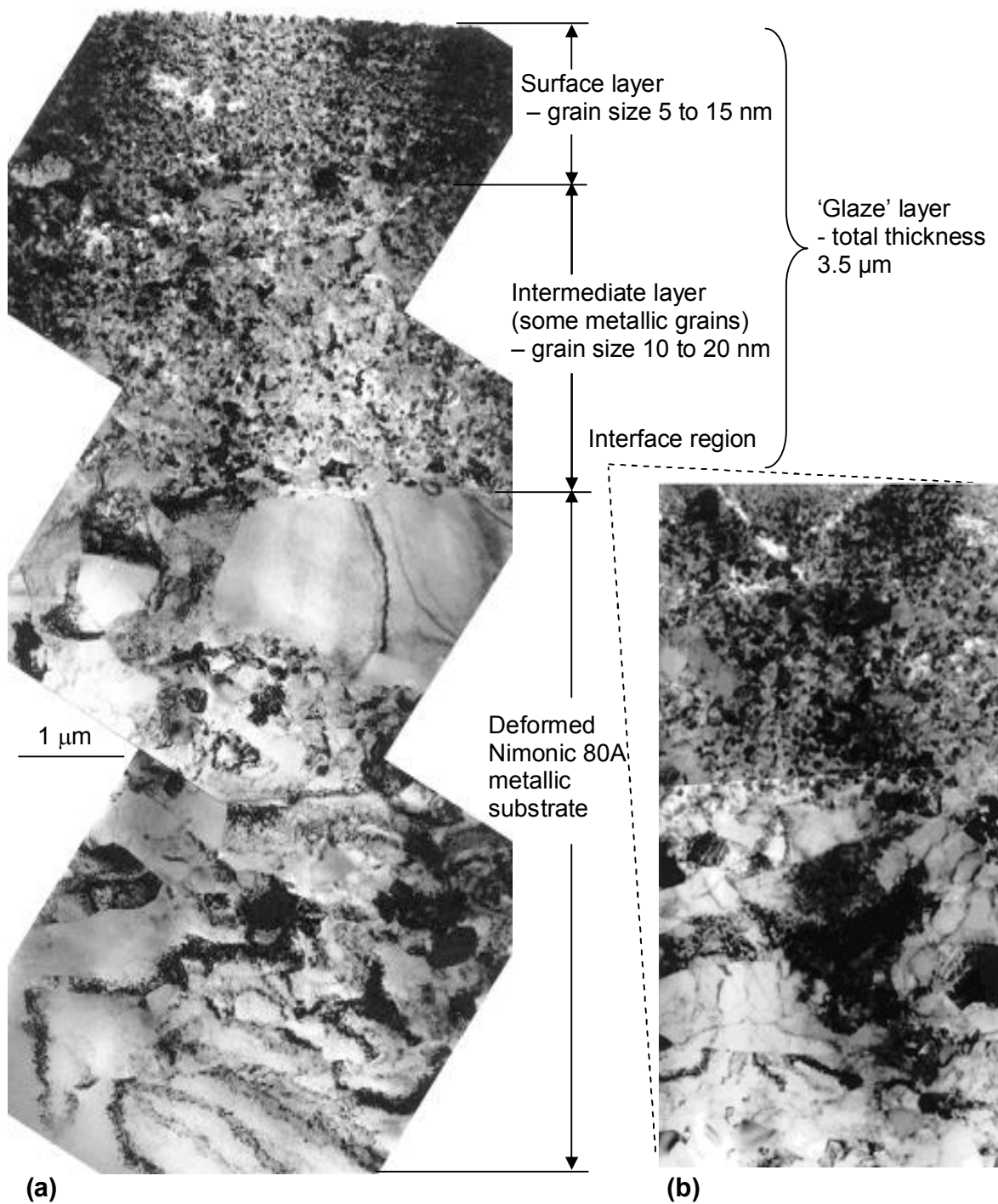
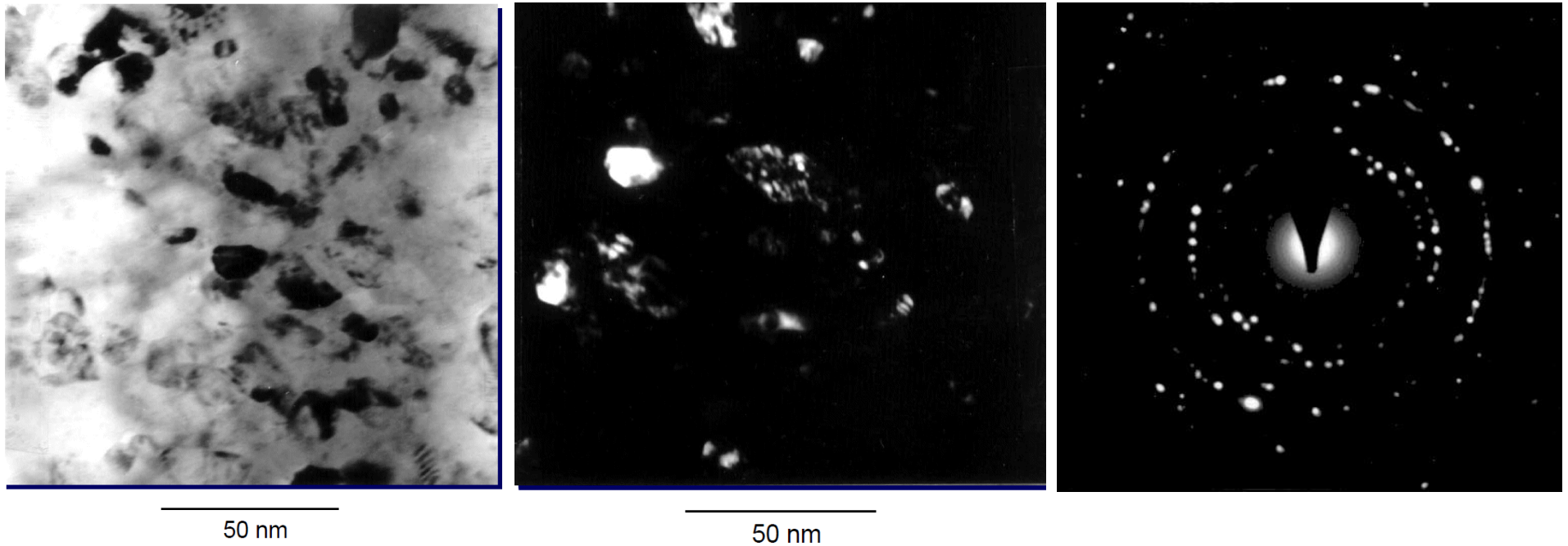


Fig. 40: Plots showing (a) dissociation partial pressures of  $\text{Al}_2\text{O}_3$ ,  $\text{TiO}_2$ ,  $\text{Cr}_2\text{O}_3$ ,  $\text{NiO}$  and  $\text{Co}_3\text{O}_4$  versus reciprocals of temperatures [19] and (b) EDX surface spectrum for Nimonic 80A vs. Stellite 6 ( $0.314 \text{ m}\cdot\text{s}^{-1}$ ,  $750^\circ\text{C}$ , load 7N, sliding distance 4,522 m) [19, 24]





**Fig. 41: Nano-scale characterisation of 'glaze' layers formed (Nimonic 80A versus Stellite 6,  $0.314 \text{ m.s}^{-1}$ ,  $750^\circ\text{C}$ , load 7N, sliding distance 4,522 m) showing TEM bright field images of (a) a wear-induced polycrystalline 'glaze' layer plus substrate deformation and (b) the interface of the 'glaze' layer and deformed substrate [3,19,20,24]**



**Fig. 42: TEM morphological and structural details of the 'glaze' layer formed (Nimonic 80A versus Stellite 6,  $0.314 \text{ m.s}^{-1}$ ,  $750^\circ\text{C}$ , load 7N, sliding distance 4,522 m) [19,24]**

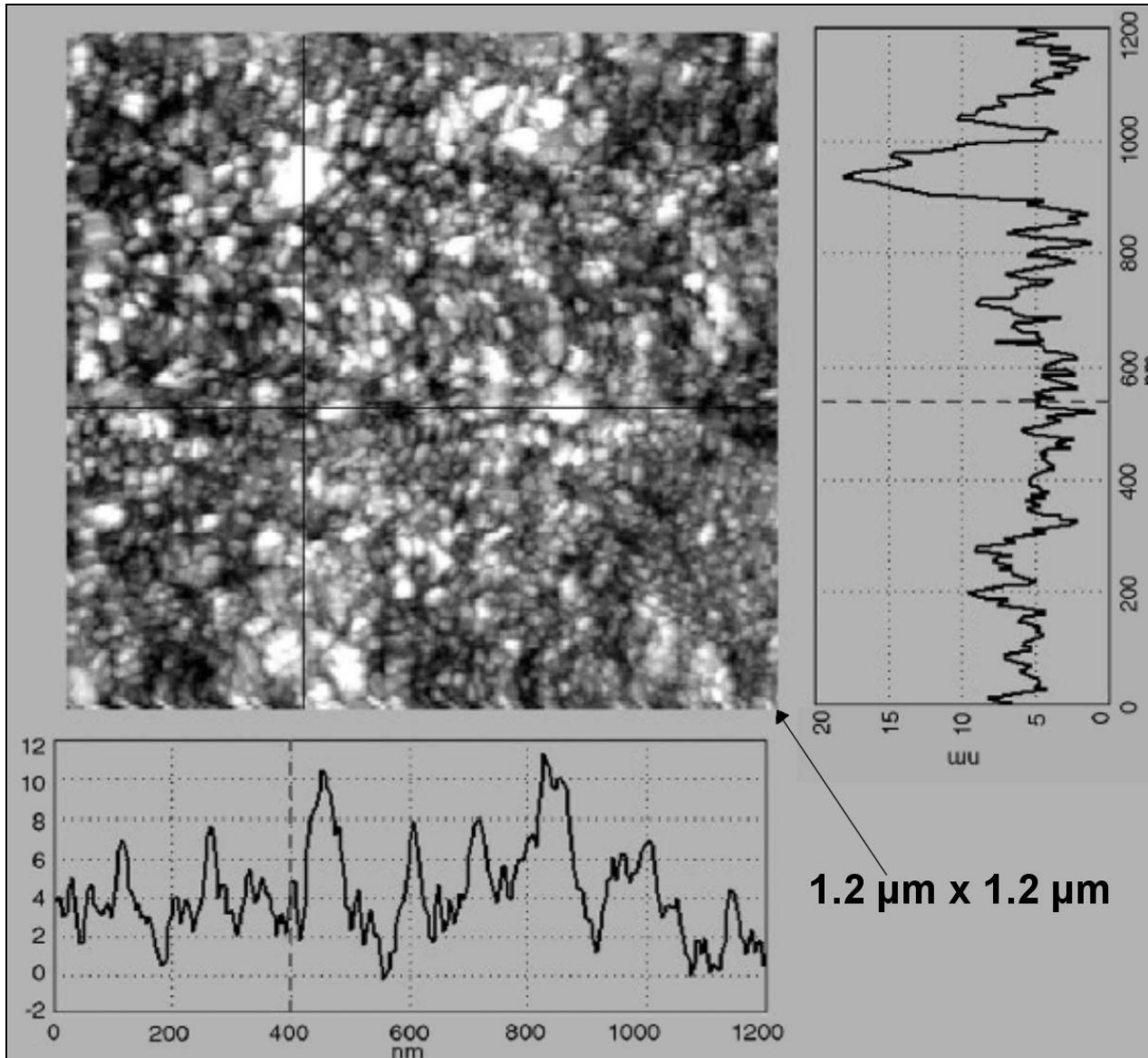
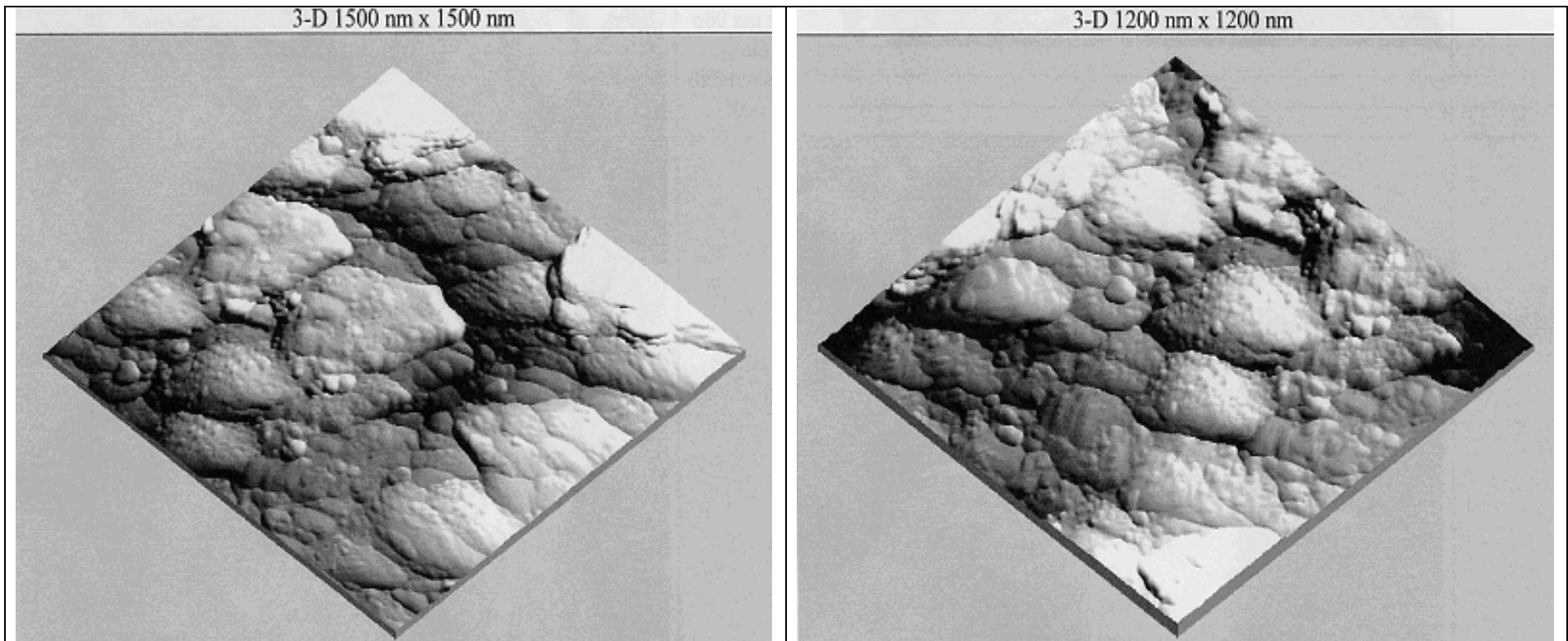


Fig. 43: STM surface line profile results on the 'glaze' layer formed on Nimonic 80A (Stellite 6 counterface,  $0.314 \text{ m}\cdot\text{s}^{-1}$ ,  $750^\circ\text{C}$ , load 7N, sliding distance 4,522 m) [3,19,20,24]



**Fig. 44: AFM image of 'glaze' layer surfaces produced on Incoloy MA956 (slid against Incoloy 800HT) at 750°C and sliding speeds of (a)  $0.314 \text{ m.s}^{-1}$  and (b)  $0.905 \text{ m.s}^{-1}$  [123]**

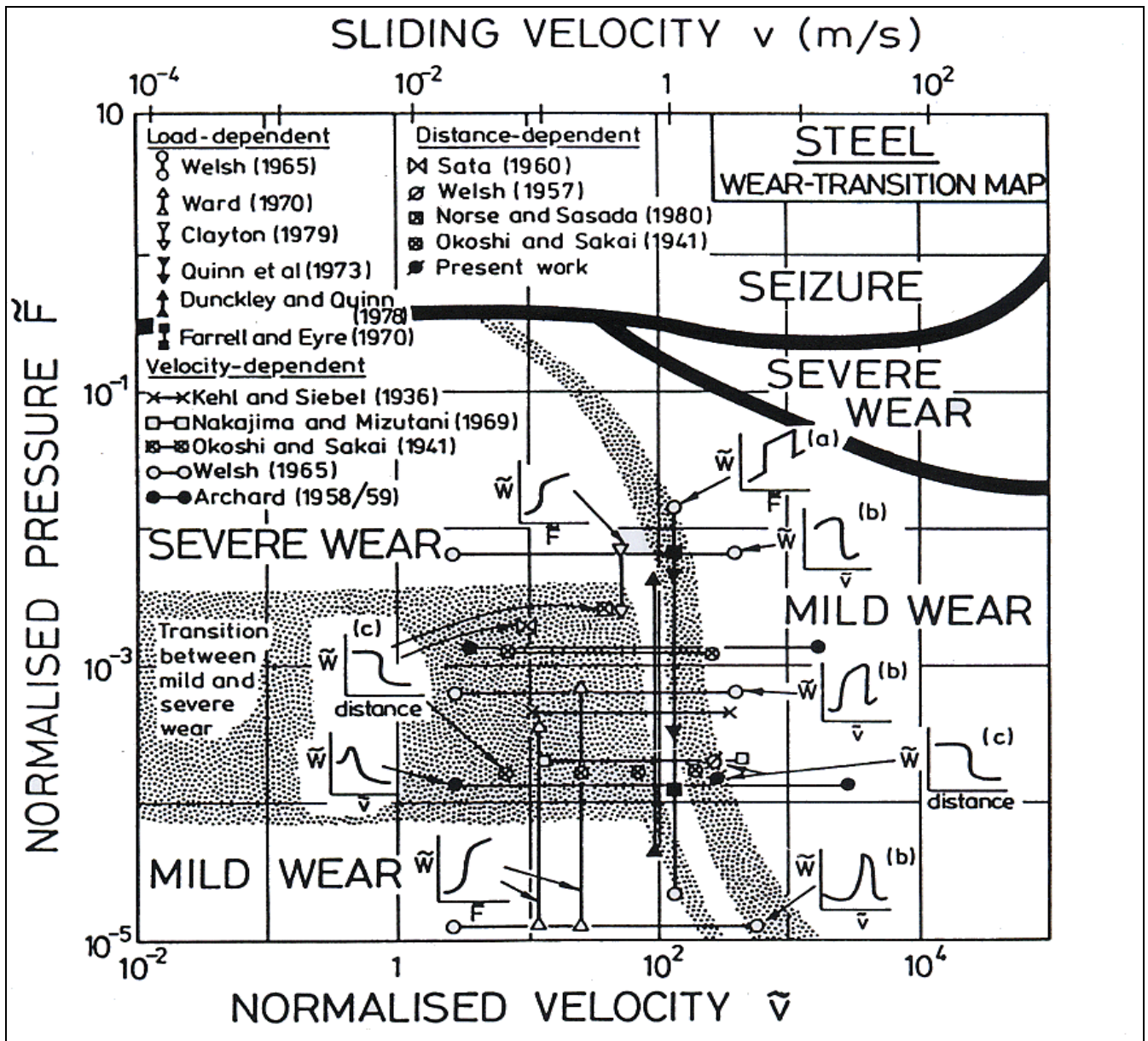


Fig. 45: Wear transition map for steels showing regions of mild and severe wear – sliding conditions corresponding to different types of wear transitions observed are also indicated [124]

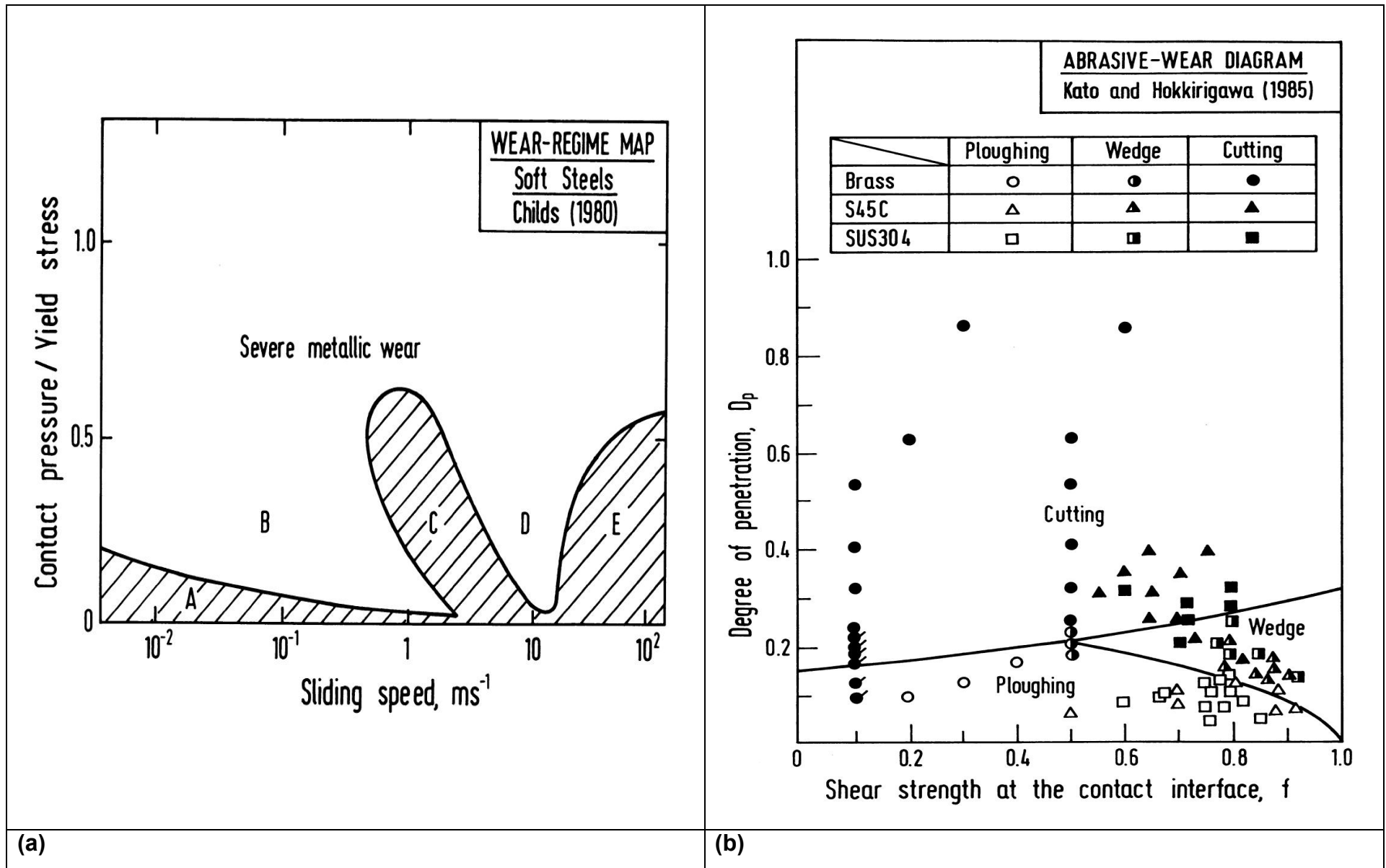


Fig. 46: Examples of 'Alternative Parameter' Wear Maps: (a) Childs soft steels wear-regime map [126]; and (b) Kato and Hokkirigawa's abrasive-wear diagram for Brass, S45C medium carbon steel and SUS304 stainless steel [133]

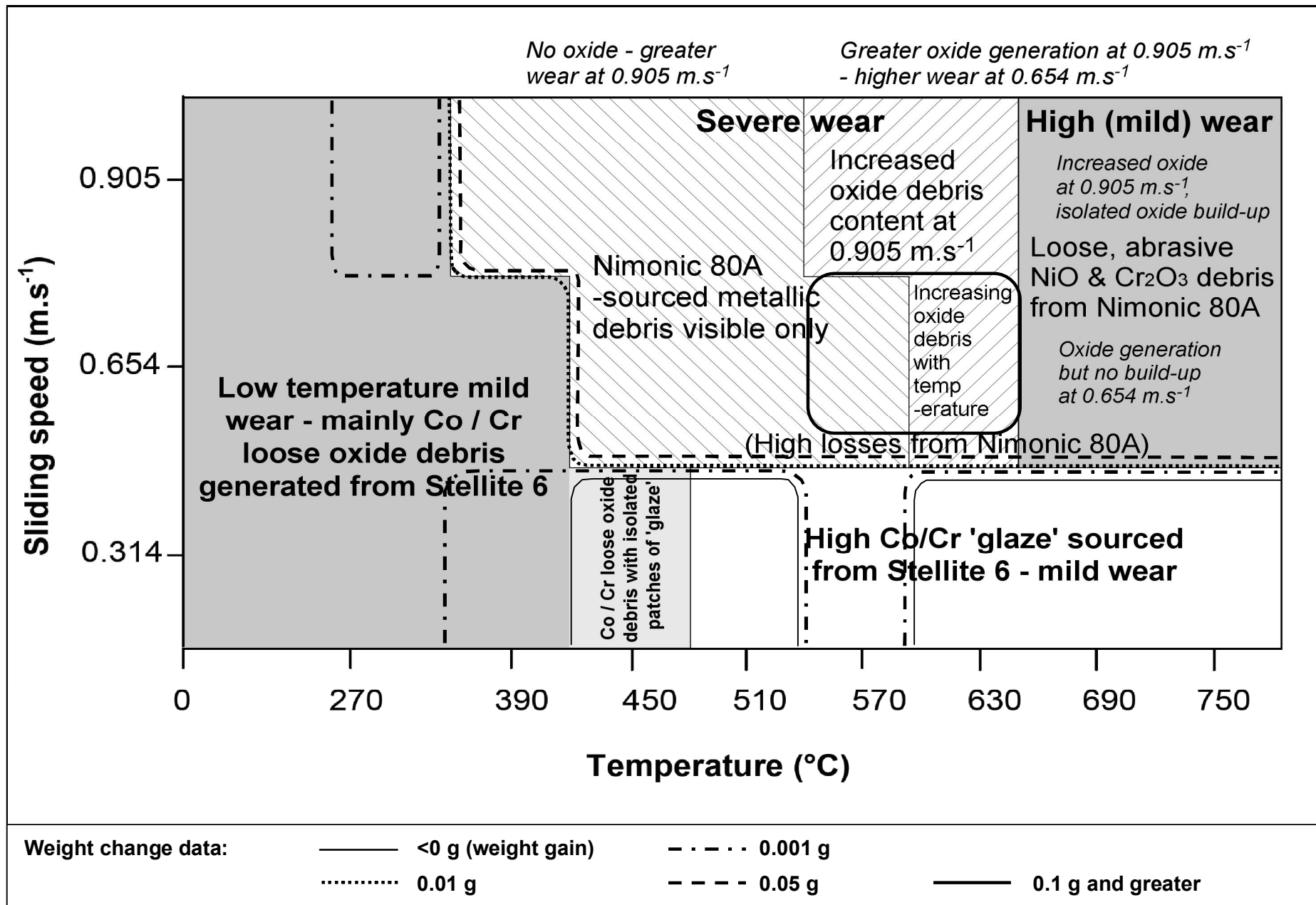


Fig. 47: Wear map for Nimonic 80A versus Stellite 6 (load 7N, sliding distance 4,522 m), with weight loss (contour) data superimposed [21]

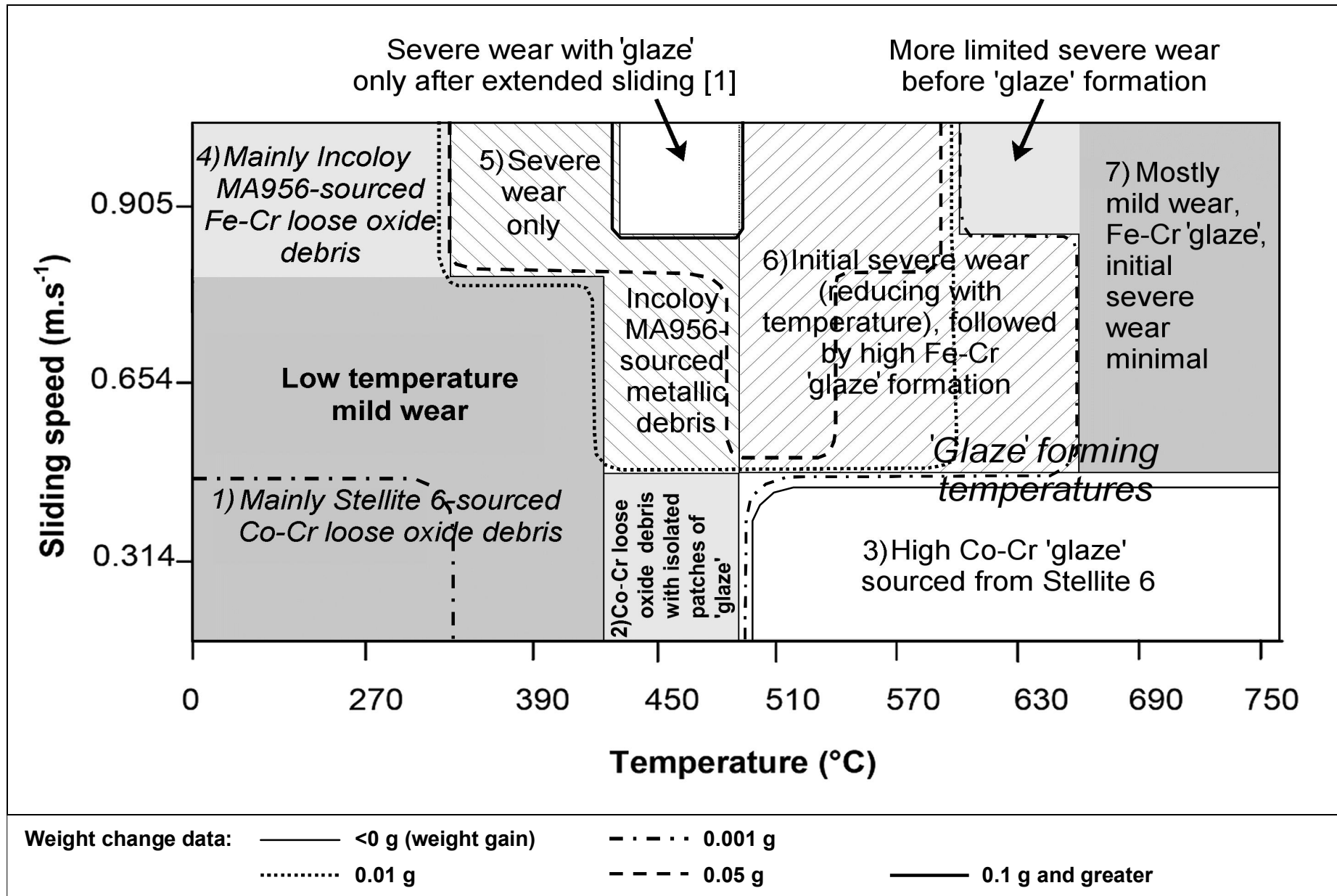
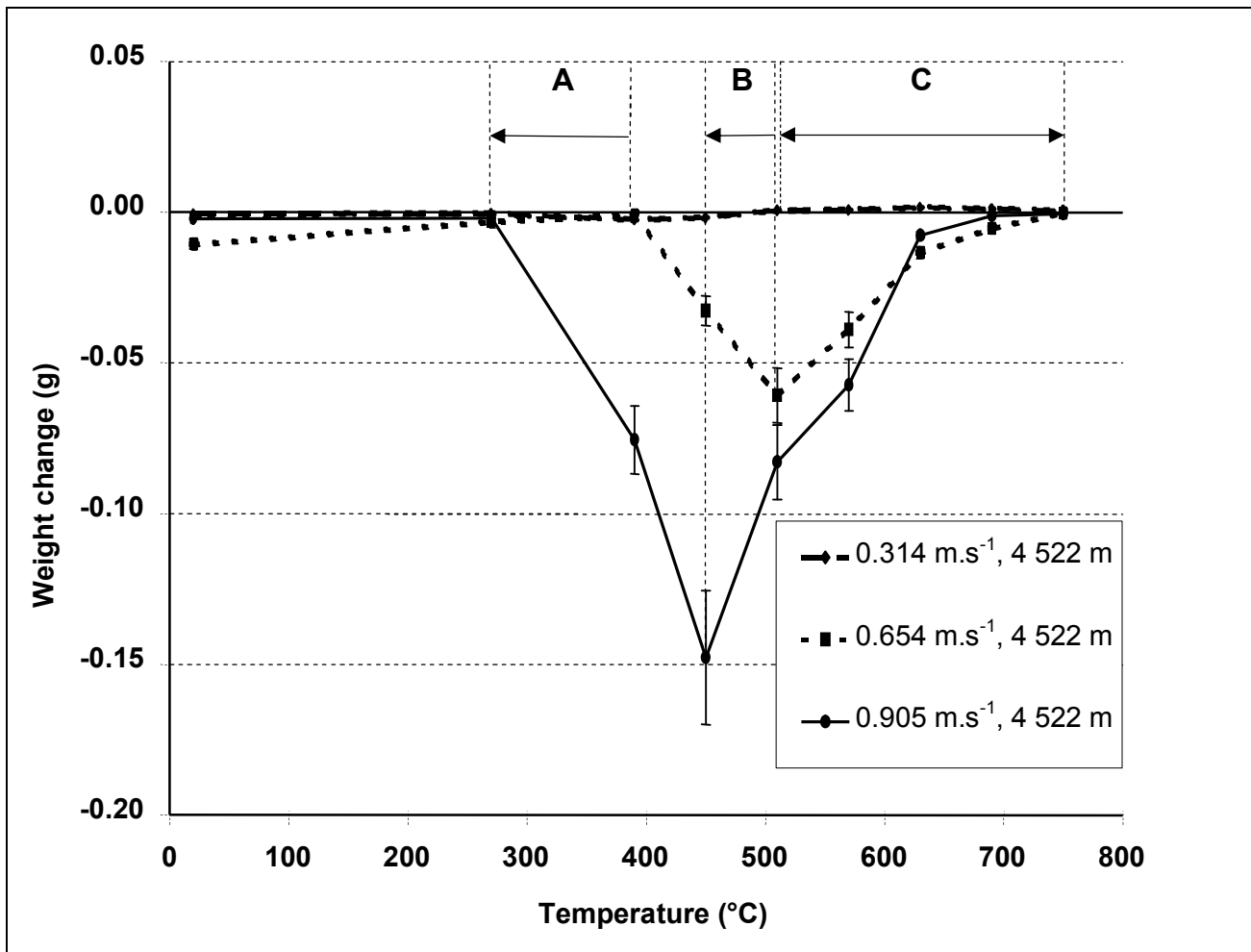


Fig. 48: Wear map for Incoloy MA956 slid against a Stellite 6 counterface (load 7N), with weight loss (contour) data superimposed [22]





- A. Decrease in low temperature mild to severe wear transition from 390°C at 0.654 m.s<sup>-1</sup> to 270°C at 0.905 m.s<sup>-1</sup>
- B. Decrease in temperature of first appearance of 'glaze' from 510°C at 0.654 m.s<sup>-1</sup> to 450°C after extended sliding at 0.905 m.s<sup>-1</sup>
- C. More rapid 'glaze' formation at 0.905 m.s<sup>-1</sup>

**Fig. 49: Weight change versus temperature for Incoloy MA956 slid against Stellite 6 at 0.314, 0.654 and 0.905 m.s<sup>-1</sup> (load 7N, sliding distance 4,522 m) – effect on transition temperatures on increasing sliding speed from 0.654 m.s<sup>-1</sup> to 0.905 m.s<sup>-1</sup> are indicated [22]**

**Withdrawn Data**

## APPENDIX 1: Withdrawn Data

### A1.1 Second Phases in Some Key Alloys in This Study

The four key alloys in the current study are examples where second phases exist, viz.:

1. Incoloy MA956 is an oxide dispersion strengthened (ODS) alloy in a body-centred cubic matrix of iron, chromium and some aluminium. The dispersoids [70] have been shown to consist of mixed yttrium and aluminium oxides in monoclinic ( $3Y_2O_3.5Al_2O_3$ ) and tetragonal ( $2Y_2O_3.Al_2O_3$ ) form, measured in this case as having diameters between 3 nm and 60 nm, the mean diameter being 9 nm. Elsewhere [96], an average diameter of 24 nm is quoted.
2. Nimonic 80A contains what is termed the  $\gamma'$  phase, normally very fine precipitates of the intermetallic  $Ni_3AlTi$  in a face-centred cubic matrix. The size of these precipitates can vary with heat treatment, with Fujita *et. al* [71] demonstrating an increase in size from 30 nm after 24 hours at 720°C to 125 nm after the same period at 875°C with Nimonic 80A. Precipitation can also occur on the grain boundaries, with precipitates apparent in the work of Fujita *et. al* [71] of up to 700 nm.
3. As already discussed, Stellite 6 consists of chromium carbides of the form  $M_7C_3$  and  $M_{23}C_6$  [68] in what is normally a cobalt-chromium hexagonal close-packed matrix. These should also form fine precipitates, however, grain boundary precipitates are observable in Fig. 12, up to 30  $\mu m$  across.
4. The Incoloy 800HT matrix [137] also contains a fine dispersion of titanium nitrides, titanium carbides and chromium carbides of between 1  $\mu m$  and 3  $\mu m$  in size, in an austenitic face-centred cubic matrix. These are very few in number and concentration.

'Glaze' layers at most are only a few microns thick, however, with Incoloy MA956 and Nimonic 80A, comparisons with the studies of Vardavoulias [94] indicates that the second phase in each case is too small to affect the 'glaze' forming process.

The size of the Incoloy 800HT carbide precipitates suggests it is borderline whether or not their presence will have any effect on 'glaze' formation – their scarcity may limit any effect they may have. The continued formation of 'glaze' on the sliding

wear of either Incoloy MA956 or Nimonic 80A against Incoloy 800HT at and above 630°C [2,3] and also the like-on-like sliding of Incoloy 800HT at 750°C [2] suggests no significant effect on ‘glaze’ formation. In each case, there were no sudden changes in friction that might indicate failure of the ‘glaze’ layer.

However, the greatly enlarged grain boundary carbide precipitates within the Stellite 6 at up to 30 µm across should easily exceed the maximum thickness of the ‘glaze’ layer at a few micrometers at most. Any material worn against the Stellite 6 should show poor relative wear properties. The work of Wood [1], Rose [2] and Inman *et al.* [3,19-24] has given mixed results in this respect. Incoloy MA956 readily formed a ‘glaze’ layer irrespective of sliding speed (0.314 m.s<sup>-1</sup>, 0.654 m.s<sup>-1</sup> and 0.905 m.s<sup>-1</sup>, 7N load, ‘block-on-cylinder’ configuration) at high temperature [2,3], but Nimonic 80A only forms ‘glaze’ at 0.314 m.s<sup>-1</sup>, showing high levels of wear at 0.654 and 0.905 m.s<sup>-1</sup>.

Rose attributed the poor wear of the Nimonic 80A he observed (and the absence of ‘glaze’ formation) at 0.654 m.s<sup>-1</sup> (690 to 750°C, 7N load) to the carbides in the Stellite 6 [2]. However, if this were the case, ‘glaze’ would not have been observed when Inman *et al.* tested under the same conditions at 0.314 m.s<sup>-1</sup> [3,19-24] or when Incoloy MA956 was slid against Stellite 6 (Inman showed that Rose’s observations with Nimonic 80A versus Stellite 6 were instead due to failure of the oxides produced to sinter and form ‘glaze’ [3, 20, 21] – see Section 5.3). Inman [3] proposed that despite their size, the carbides were not as hard as the oxides in the ‘glaze’ layers and were thus worn in preference to the ‘glaze’ layer oxides, hence there was no ‘glaze’ layer break-up. It is suggested that for a hard second phase of large particle or precipitate size to disrupt ‘glaze’ formation as proposed by Vardavoulias [90], the hardness of these second phase particles must exceed that of the oxide ‘glaze’ layer on the opposing sliding surface.

### **A1.2 Alternative Wear-resistant Alloys**

Also of interest are the Tribaloy<sup>TM</sup> alloys [138-140], consisting of a Co-based (T400, T800 and T900) or Ni-based (T400 and T475) matrix with a substantial proportion of Laves phase. This C-14 (MgZn<sub>2</sub>) type intermetallic Laves phase, roughly of ternary composition Co<sub>3</sub>Mo<sub>2</sub>Si or Co-Mo-Si in Co-based Tribaloy<sup>TM</sup> alloys [139], imparts a

high level of wear resistance and remains stable to high temperatures. Carbon in these alloys is kept to a minimum ( $\leq 0.08\%$  [138]) in order to promote Laves phase development ahead of carbide precipitation [139,140].

Whilst Co-based alloys show high wear resistance with good anti-galling properties [69,87-90], one disadvantage is their susceptibility to nuclear activation [88,89]. One examined alternative is Fe-based Norem 02 [88,89] with a microstructure of carbides in an austenitic matrix; this alloy exhibits low temperature, low wear properties due to a strain induced austenitic-martensitic transformation at  $< 180^\circ\text{C}$ . However, materials used in nuclear applications need good wear resistance well in excess of this; a target temperature  $> 350^\circ\text{C}$  is suggested for this transformation. The Ni-based Tribaloy<sup>TM</sup> alloys (T400 and T475) offer another potential approach [138].

### **A1.3 Hall-Petch Effects**

The superior wear resistance of this nano-structured 'glaze' layer can be ascribed to several factors. The nano-structured 'glaze' layer generated did not suffer Hall-Petch softening, with micro-hardness for the 'glaze' layers measured at up to 6.06 GPa [3,24]. However, there has also not been a significant degree of work-hardening believed to be associated with the difficulties in generating dislocations in nano-sized grains [121,122]. These two factors together with improved fracture toughness, expected to be conferred by the presence of nano-polycrystalline structure, have made debris generation an inefficient process.

However, the microhardness data [3,24] does not indicate any significant hardening of the surface layers either (the undeformed Nimonic 80A gave hardness values of between 3.9 GPa and 5.3 GPa). During 'glaze' layer micro-hardness testing, even at low loads, the indenter would at times readily penetrate or break up the 'glaze' [3] – this implies higher 'glaze' hardness levels than were measured during testing. Further investigation using nano-indentation indicated some potential for hardening (Table 6 – mean hardness 22.62 GPa) [3,20], however, the use of nano-hardness data to interpret results needs to be treated with caution, due to vulnerability to localised variations in the 'glaze' layer brought about by the extremely localised nature of nano-indentation. Values were, however, consistently higher than those obtained for micro-indentation.

## Withdrawn Tables

	Sample 1	Sample 2	Sample 3	Sample 4	Mean
<b>Nominal load (<math>\mu\text{N}</math>)</b>	5,000	5,000	5,000	1,000	-
<b>Actual load (<math>\mu\text{N}</math>)</b>	4,968.4	4,967.8	4,964.1	996.4	-
<b>Hardness (GPa)</b>	24.50	27.34	16.62	22.01	22.62
<b>Modulus (GPa)</b>	130.2	131.1	110.4	147.1	129.7

**Table W1: Nano-indentation data for ‘glaze’ layers formed on Nimonic 80A slid against Stellite 6 at  $0.314 \text{ m.s}^{-1}$  and  $750^\circ\text{C}$  (all measurements in GPa) [20]**

	<b><math>0.314 \text{ m.s}^{-1}</math></b>			<b><math>0.905 \text{ m.s}^{-1}</math></b>		
	<b>Mean</b>	<b>Max.</b>	<b>Min.</b>	<b>Mean</b>	<b>Max.</b>	<b>Min.</b>
<b><math>510^\circ\text{C}</math></b>	12.72	16.54	6.90	17.51	23.82	12.28
<b><math>750^\circ\text{C}</math></b>	21.97	28.39	17.51	15.45	22.65	6.74

**Table W2: Nano-indentation data for ‘glaze’ layers formed on Incoloy MA956 slid against Stellite 6 at sliding speeds of  $0.314$  and  $0.905 \text{ m.s}^{-1}$  and temperatures of  $510$  and  $750^\circ\text{C}$  (all measurements in GPa) [22]**

## Withdrawn Figures

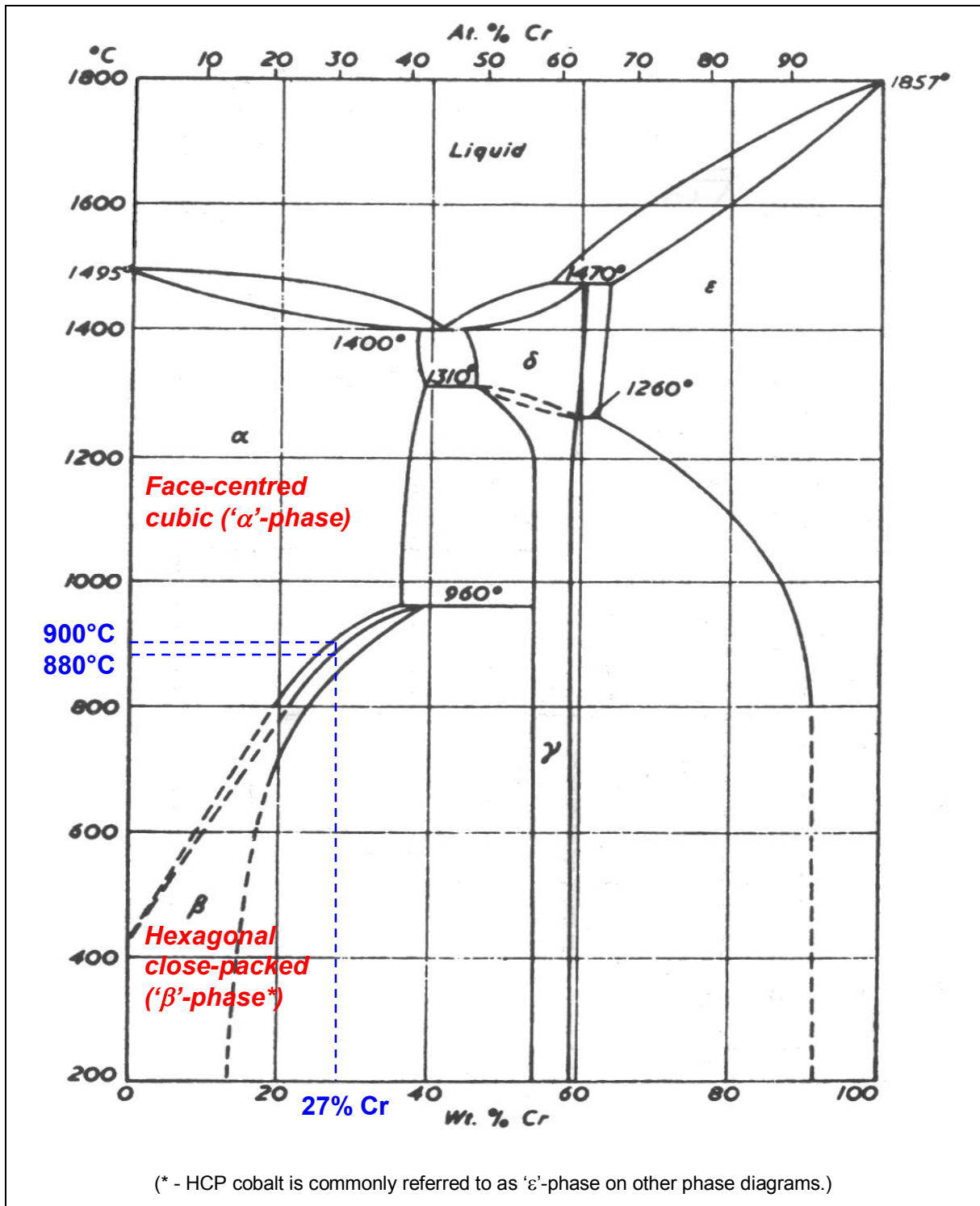
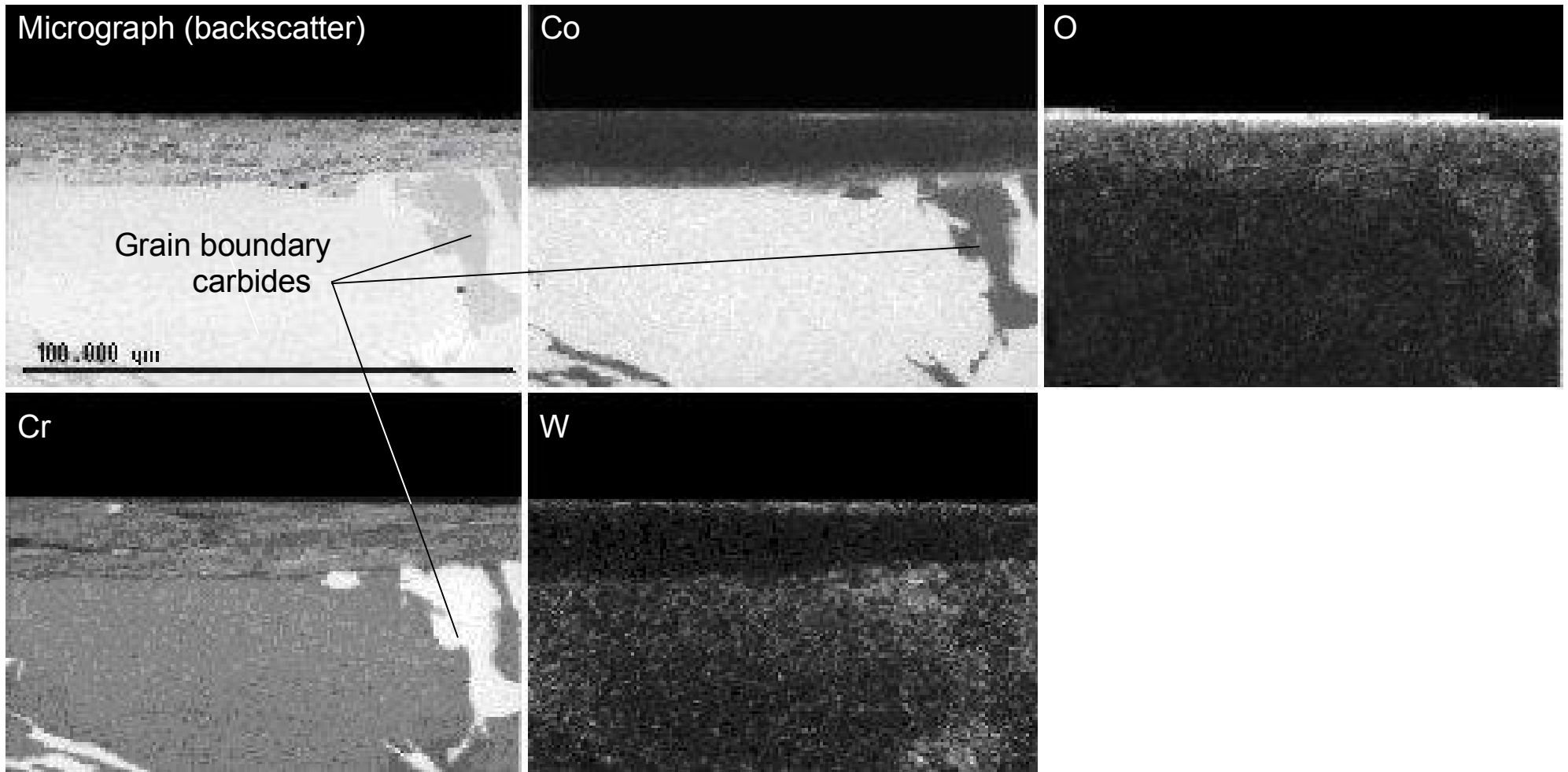


Fig. W1: Binary phase diagram for cobalt and chromium, showing the transition temperature for 27% chromium [92]



**Fig. W2: Identification of grain boundary carbides by changes in distribution of cobalt and chromium in the Stellite 6 substrate [2,3]**



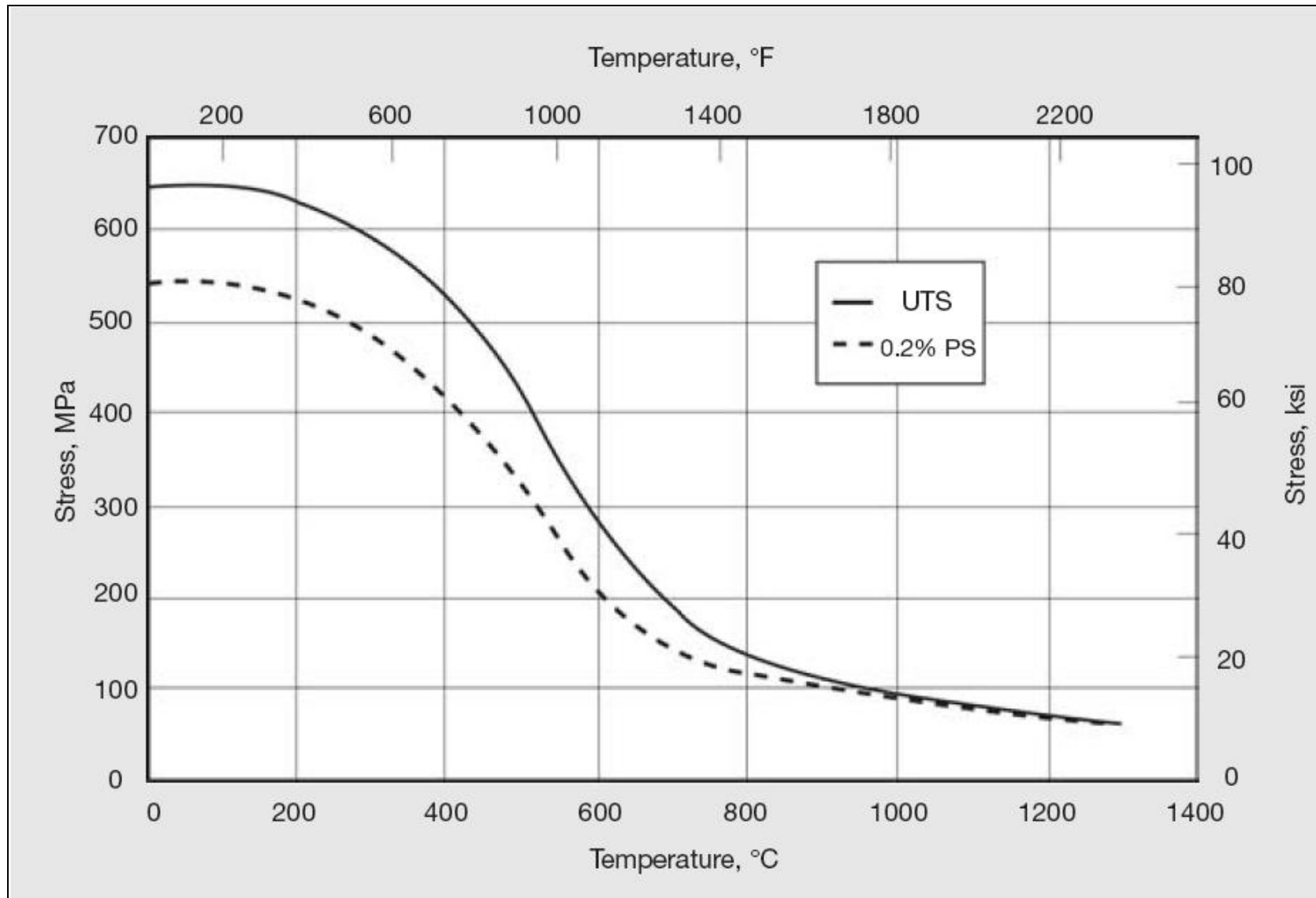


Fig. W3: Tensile Strength versus Temperature – Cold Rolled Incoloy MA956 Sheet [96]

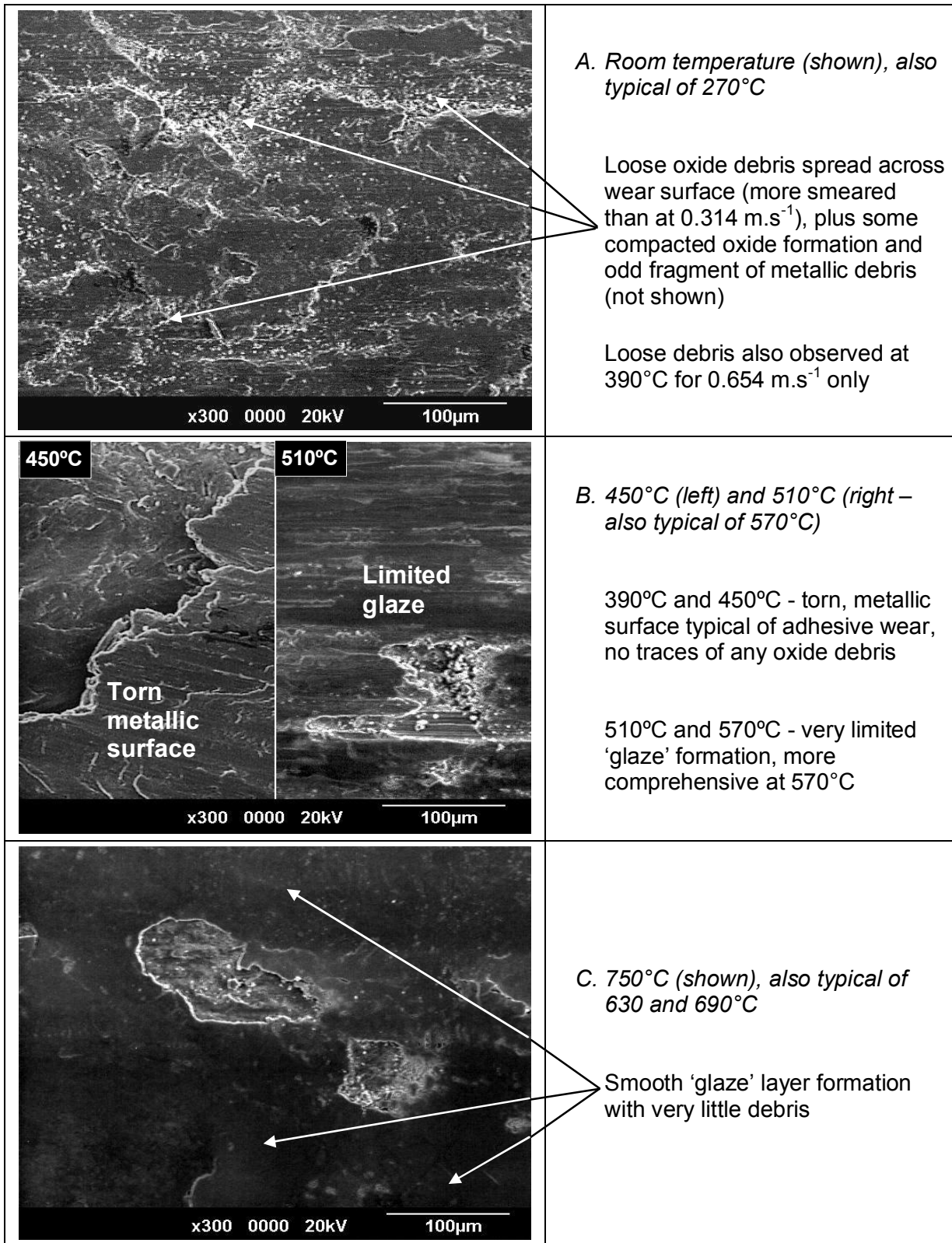


Fig. W4: SEM micrographs of Incoloy MA956 wear surfaces after sliding at 0.905 m.s<sup>-1</sup> against a Stellite 6 counterface at room temperature, 450, 510 and 750°C [22]

	<p>A. Room temperature and 270°C</p> <p>Loose oxide separating wear surfaces</p>
	<p>B. 390°C (shown), also typical of 450, 510, 570 and 630°C</p> <p>390, 450 and 510°C - torn, metallic surface typical of adhesive wear, no traces of any oxide debris</p> <p>570 and 630°C – adhesive wear persists, however, some oxide present and assisting wear by abrasion (not shown)</p>
	<p>C. 750°C (shown), also typical of 690°C</p> <p>Limited oxide build-up</p> <p>Loose oxide</p> <p>Parallel grooves due to abrasion (holding some loose oxide debris)</p>

**Fig. W5: SEM micrographs of Nimonic 80A wear surfaces after sliding at 0.905 m.s<sup>-1</sup> (load 7N, sliding distance 4,522 m) against a Stellite 6 counterface at room temperature, 270, 390 and 750°C [21]**

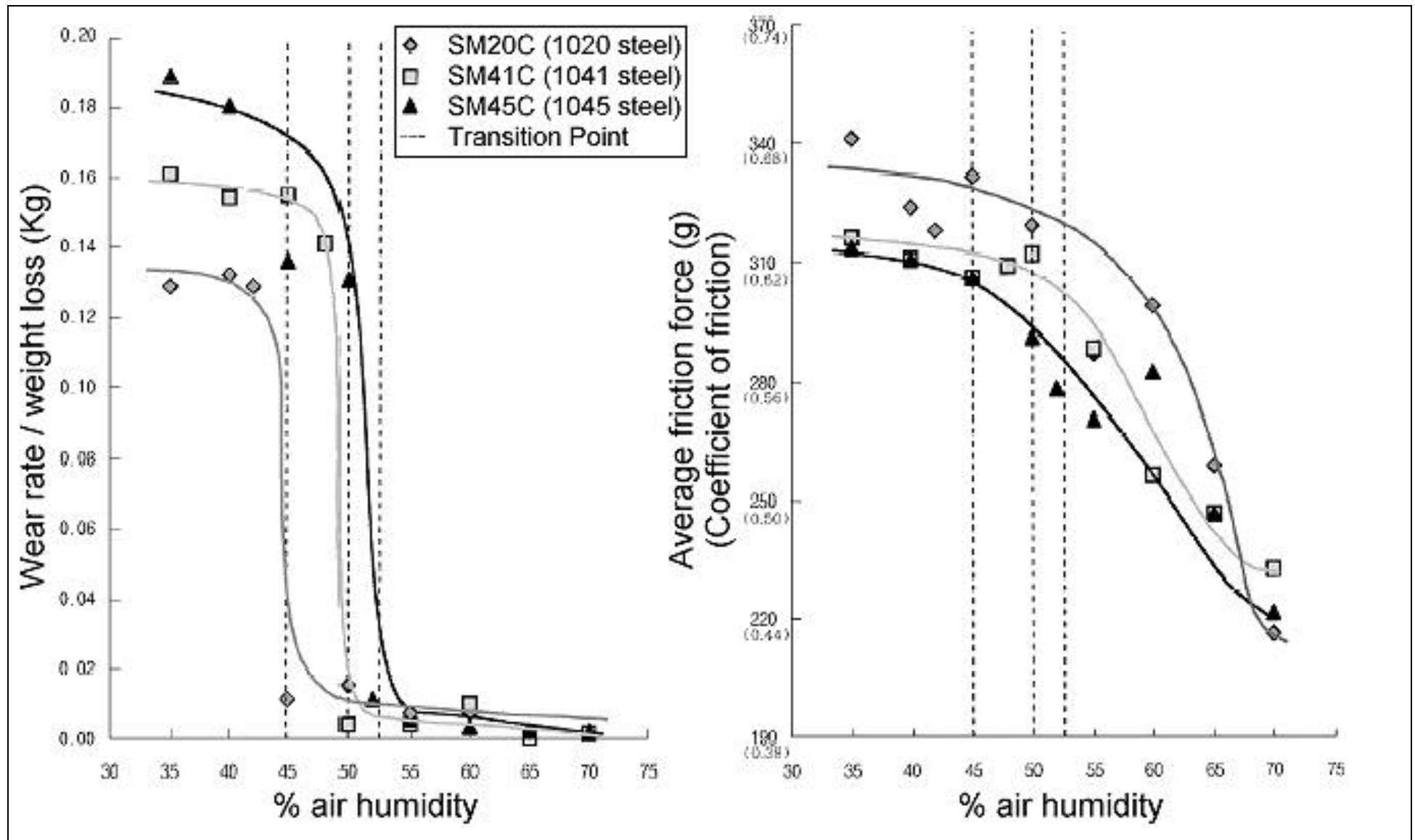


Fig. W6: Variation of wear and coefficient of friction as a function of relative humidity [30]

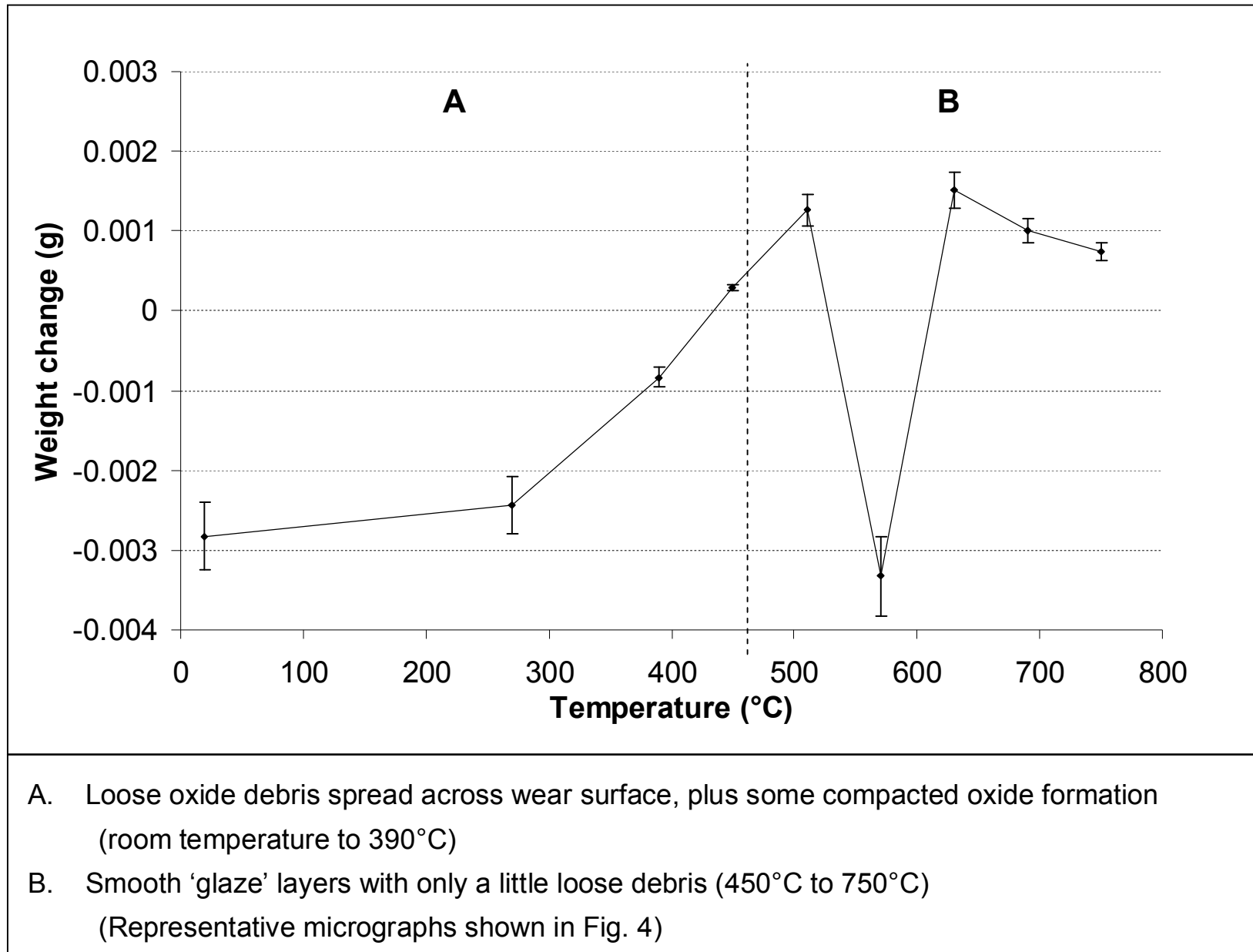
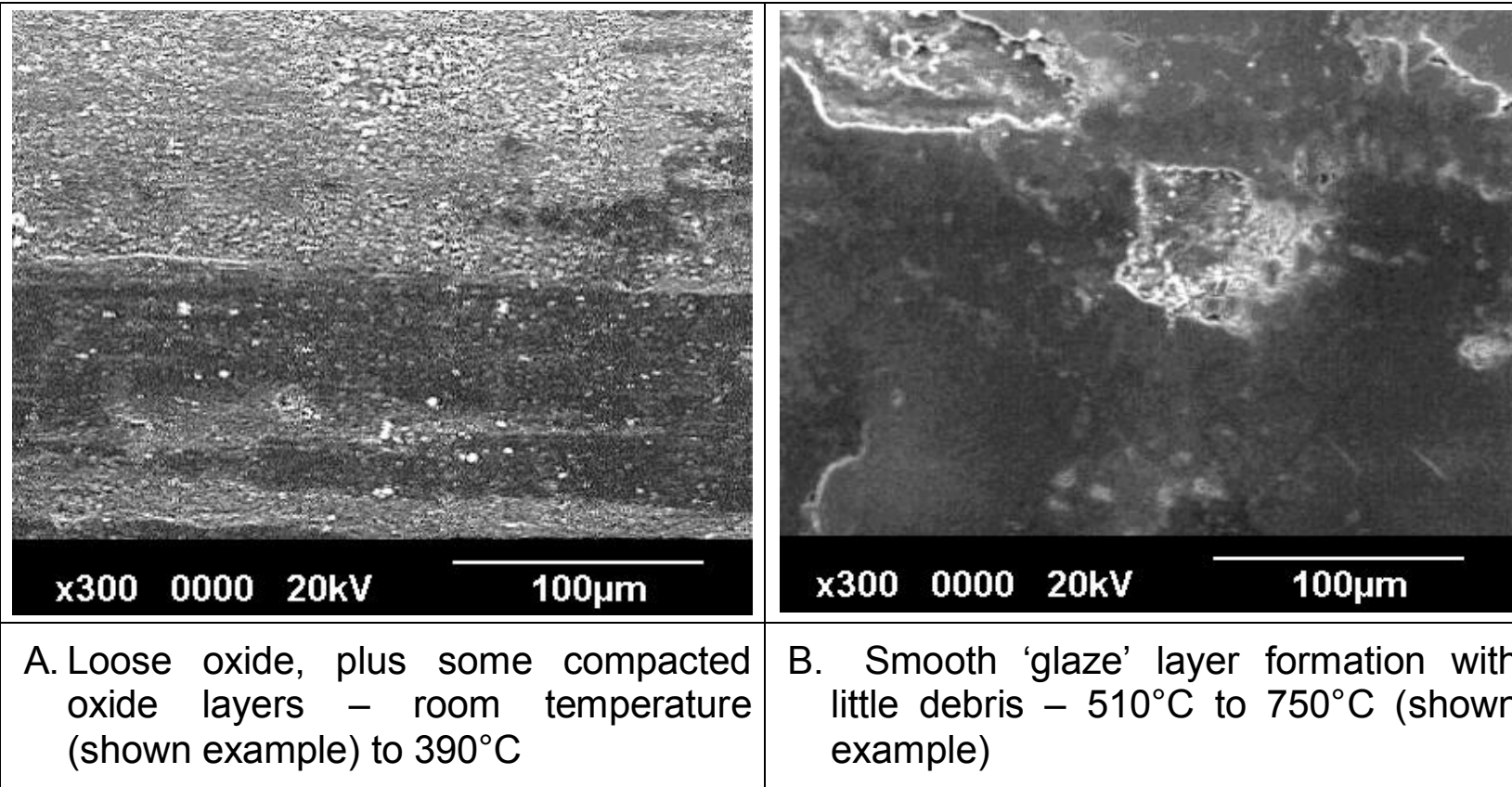


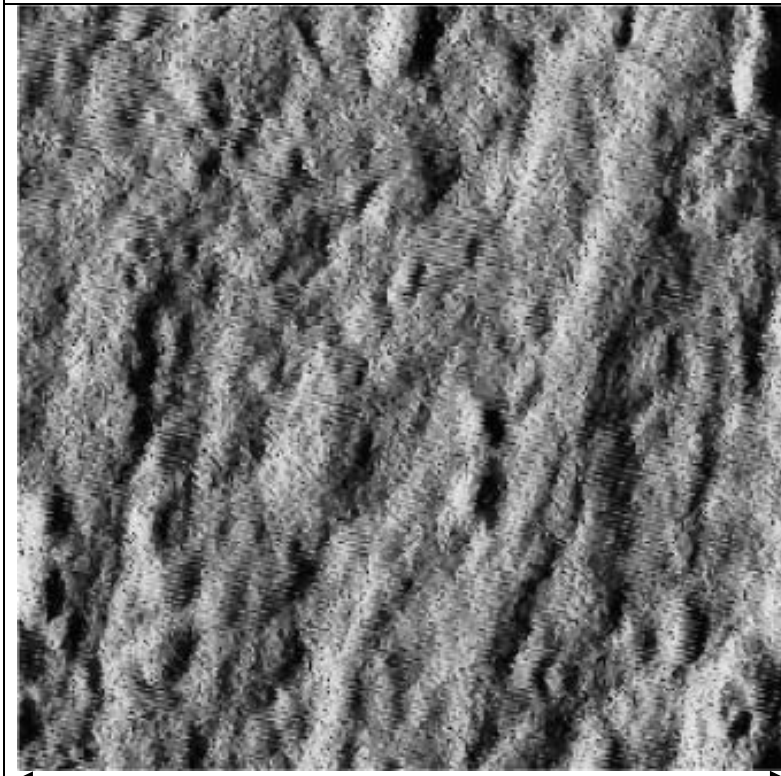
Fig. W7: Weight change versus temperature for Nimonic 80A slid against Stellite 6 at 0.314 m.s<sup>-1</sup> [3, 20, 24]



**Fig. W8: SEM images of Nimonic 80A wear surfaces after sliding at  $0.314 \text{ m.s}^{-1}$  against a Stellite 6 counterface at room temperature and 750°C [3,20]**



(a)  $0.314 \text{ m.s}^{-1}$



(b)  $0.905 \text{ m.s}^{-1}$

**Fig. W9: Top-down AFM image of ‘glaze’ layer surfaces produced on Incoloy MA956 (slid against Stellite 6) at 750°C and sliding speeds of (a)  $0.314 \text{ m.s}^{-1}$  and (b)  $0.905 \text{ m.s}^{-1}$  [22]**